AN EFFICIENT HEMODYNAMIC WORKFLOW IN COMPUTATIONAL SURGERY

A Dissertation

Presented to

the Faculty of the Department of Computer Science

University of Houston

In Partial Fulfillment

of the Requirements for the Degree

Doctor of Philosophy

By

Guillaume Tran-Son-Tay

August 2013

AN EFFICIENT HEMODYNAMIC WORKFLOW IN COMPUTATIONAL SURGERY

Guillaume Tran-Son-Tay

APPROVED:

Dr. Marc Garbey
Dept. of Computer Science, University of Houston

Dr. Scott A. Berceli
Dept. of Surgery, University of Florida

Dr. Mark G. Davies
Dept. of Surgery, The Methodist Hospital

Dr. Victoria Hilford
Dept. of Computer Science, University of Houston

Dr. Nikolaos V. Tsekos
Dept. of Computer Science, University of Houston

Dean, College of Natural Sciences and Mathematics

Acknowledgements

First, I would like to thank Pr. Marc Garbey for giving me the opportunity to do this work, spending the time and effort in helping me and pushing me forward.

I am thankful to the members of the supervisory committee: to Dr. Scott Berceli, Dr. Mark Davies, Dr. Victoria Hilford, and Dr. Nikolaos Tsekos for their collaboration and technical assistance in their fields of expertise.

Special thanks to all my friends, here in Houston and back home, who have always been there for me. A big thanks to the members and alumni of Modeling and Computational Science Laboratory at the University of Houston.

Finally, I wish to thank my whole family for their moral support.

AN EFFICIENT HEMODYNAMIC WORKFLOW IN COMPUTATIONAL SURGERY

An Abstract of a Dissertation

Presented to

the Faculty of the Department of Computer Science

University of Houston

In Partial Fulfillment

of the Requirements for the Degree

Doctor of Philosophy

By

Guillaume Tran-Son-Tay

August 2013

Abstract

For few decades, it has been shown that atherosclerosis is the cause of the majority of clinical cardiovascular diseases including peripheral arterial diseases. The diagnosis and treatment for vascular disease has evolved significantly over the past years considering the rapid advances in imaging technologies. In recent years, computational fluid dynamics has been increasingly used as a simulation tool for blood flows. Numerous researches connect wall shear stress quantities to endovascular diseases such as stenosis, aneurism, and atherosclerosis. A thorough knowledge of vascular anatomy and hemodynamic would be beneficial for understanding the development and progression of the disease, the therapeutic decision process and follow up.
The objective of this dissertation is to propose a computational fluid dynamic framework that includes:

- Understanding how streamline efficiently hemodynamic simulation for main arteries to produce database for clinical study.
- Providing some confidence estimate on numerical results.
- Extending the state of the art of clinical study by including motion and particles analysis.

Contents

List of Figures

List of Tables

Part I

Motivation and Background

Chapter 1

Introduction

Cardiovascular diseases remain the leading cause of death worldwide. According to the World Health Organization, an estimated 17.3 million people died from cardiovascular diseases in 2008, which represents 30% of all global deaths [105]. According to the National Heart, Lung, and Blood Institute, peripheral arterial disease affects 8 to 12 million people in the United States, which is around 12% of the adult population [71]. These diseases are associated to atherosclerosis and plaque formation. The study of the development and evolution of these diseases involve many disciplines such as medicine, biology, and mechanics. It has been notably shown that endothelial dysfunction was one of the main factors for the development of atherosclerosis. In recent years, computational fluid dynamics has proven to be a convenient and reliable tool to study the characteristics of 3D blood flow, as well as its temporal variations, in complex arterial geometries, but often idealized.

Our work in this dissertation has been focused on the computation of the wall shear

stress. The objectives are to understand the factors influencing the accuracy on hemodynamic simulation and to observe the impact of the body motion and particle deposition on the computation of flow variables.

1.1 Dissertation Overview and Contributions

The work in this dissertation focuses on the development of a computational framework for hemodynamic simulation applied on clinical data. This work addresses three different areas of hemodynamic: the accuracy assessment during the simulation process, the dynamic simulation via moving meshes, and the study of particles trajectories.

This dissertation is divided into five major parts, each consisting of a set of chapters focused on a specific area of work. An overview of the parts and chapters in this dissertation are provided here, highlighting the contributions made by this research to the field of hemodynamic.

Part I: Motivation and Background

Part I provides an introduction and background information to the work in this dissertation.

Chapter 2 provides background information on the anatomy of the blood vessels, the mechanics theory for computational fluid dynamics including dynamic simulation and particle tracking.

Part II: Accuracy Assessment

Part II describes the work done on error estimation during CFD simulation.

Chapter 3 outlines the different steps of hemodynamic simulations: data acquisition, 3D reconstruction, boundary conditions, etc. We detail the various sources of uncertainties encountered and establish an error estimation study.

Part III: Dynamic Blood Flow Simulation

Part III describes the work accomplished to simulate blood flow in moving models.

Chapter 4 describes the two kinds of motion that we used. First, we presented the problem of the wall displacement due to the blood pressure. Secondly, we studied the influence of the bending motion of the knee on the wall shear stress computation.

Part IV: Motivation and Background

Part IV describes the work accomplished to simulate hemodynamic simulation with particle tracking.

Chapter 5 describes the study done on vein grafts where we performed a statistical analysis in order to provide additional information on the correlation between wall shear stress and endovascular diseases.

Part V: Dissertation Review

Chapter 6 summarizes the body of work presented in this dissertation, the limitation of our work, and outlines the future directions.

Chapter 2

Background

2.1 Blood Vessels

An understanding of the blood vessels anatomy, the biological specificity of the atherosclerosis, as well as the treatment for peripheral arterial diseases, is important for the development of our hemodynamic workflow. We will take time to describe these in the following sections. Subsection 2.1.1 provides a precise description of the carotid artery and superficial femoral artery. This is followed by a description of the biology mechanism of atherosclerosis and thorough description of the arterial wall and the endothelial cells (Subsection 2.1.2). This section concludes with a description of the tools and methods available to detect and treat plaque formation (Subsection 2.1.3).

2.1.1 Carotid Bifurcation and Superficial Femoral Artery Anatomy

In the human body, the blood vessels are part of the cardiovascular system that transports blood throughout the body. There are three kinds of blood vessels: arteries, capillaries, and veins.

- The arteries carry blood away from the heart.
- The capillaries are the smallest blood vessels and are where the blood and tissues exchange oxygen, nutrients, and wastes.
- The veins transport blood from the capillaries toward the heart.

The walls of veins and arteries are constituted of three layers.

- The tunica intima or tunica interna.
- The tunica media.
- The tunica externa or adventitia.

The tunica intima is the innermost layer that is in contact with blood. It is composed of endothelium surrounded by connective tissues. It ensures the permeability of the vessel and prevents the coagulation of the blood.
Beneath the intima, there are smooth muscles with elastic tissues called the tunica media. The elastic fibers prolong the effect of the heartbeat allowing progress of the blood. Smooth muscle fibers promote vasodilation or vasoconstriction.

Finally, outside of these two layers, there is the intima externa or adventitia which is a layer of connective tissues. This tunica has nervous fibers that control smooth muscle cells of the media and vessels providing nutrition known as vasa vasorum.

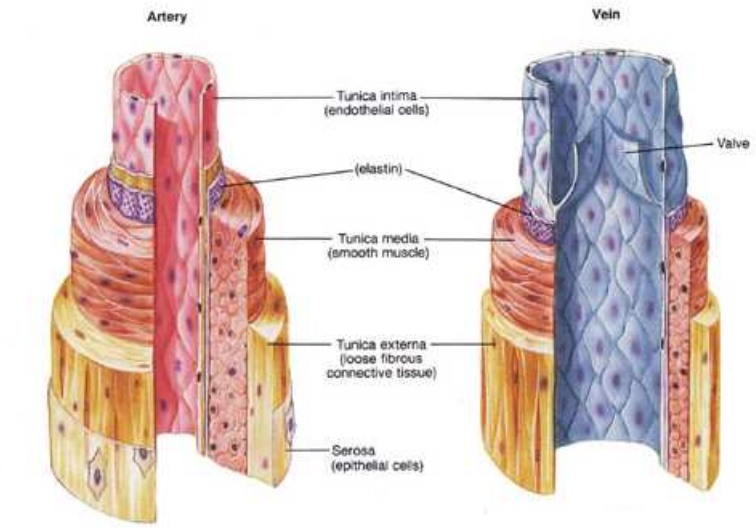

Figure 2.1: Structures of blood vessels given by [34]

The endothelium helps prevent blood clotting and may also help in regulating blood flow. Endothelial cells are very sensitive to mechanical stimuli imposed by blood flow, especially to variations in shear stress. The physiology of the endothelium is explained in the next subsection.

In this dissertation, there are two common regions where atherosclerosis develops that we are interested in: the carotid bifurcation and the superficial femoral artery (SFA).

The carotid arteries begin at the aorta as common carotid arteries and run through the neck to the head. Each common carotid artery divides into 2 branches: the external and internal carotid artery. The external carotid artery supplies blood to the face and neck and the internal carotid artery goes up and provides blood to the brain and orbital cavities [8]. Figure 2.2 depicts the anatomy of the network of arteries around the neck.

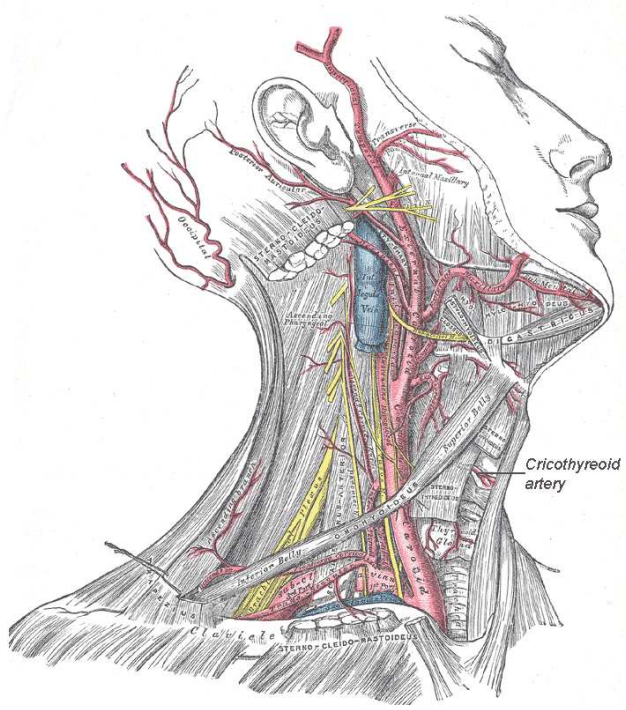

Figure 2.2: Network of arteries of the neck given by [8]

Femoral arteries are systemic arteries supplying blood to the lower limbs and pelvis. A femoral artery divides in two: the deep femoral artery, which provides blood to the thigh, and the SFA which provides blood to the arteries that circulate the knee and foot. The SFA connects the popliteal artery behind the knee joint.

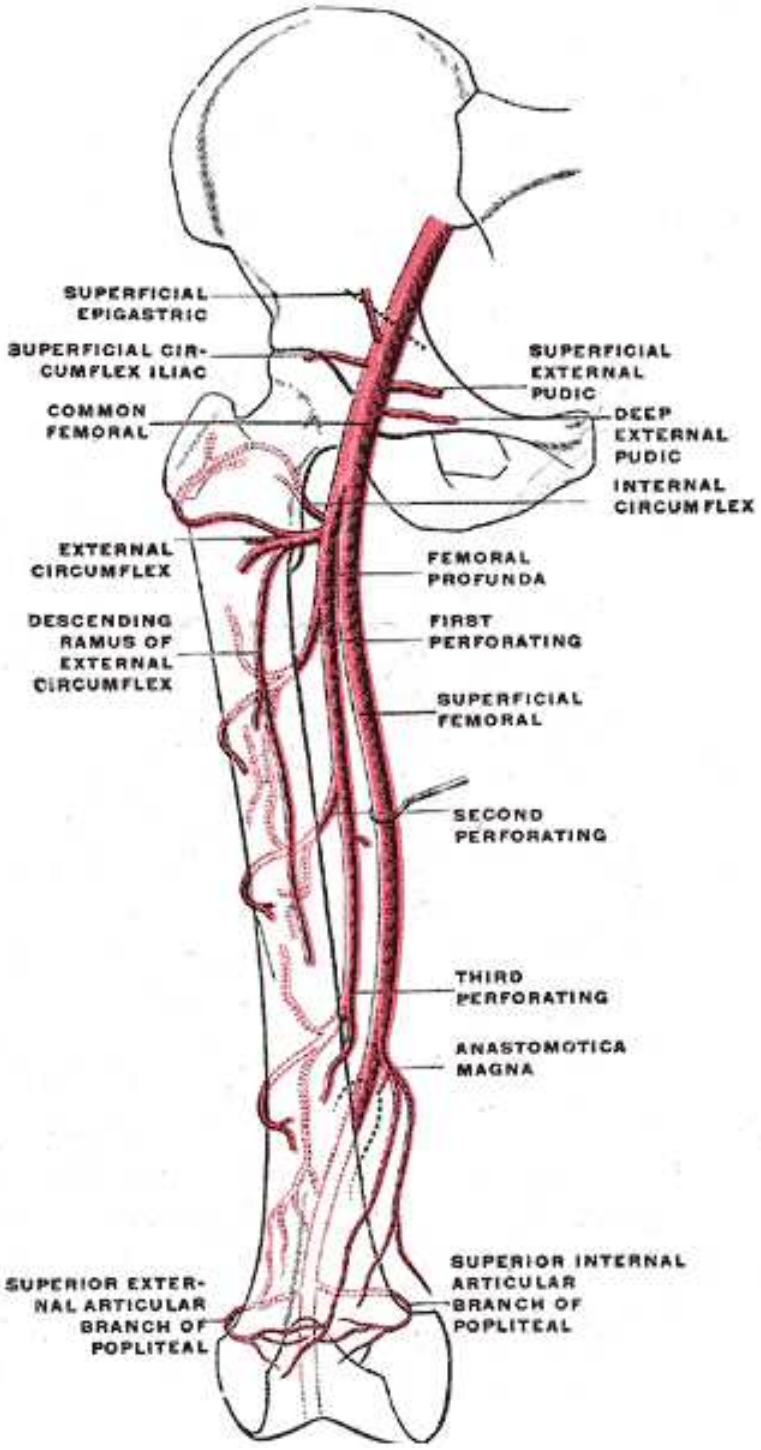

Figure 2.3: Femoral artery anatomy given by [8]

2.1.2 Atherosclerosis and Plaque Formation Process, Endothelial Cells

Atherosclerosis or hardening of the arteries is a common health problem. It occurs when substances such as calcium, fat, or cholesterol accumulate inside the artery wall and form hard structures called plaques. Over time, plaque narrows arteries and therefore limits blood flow to organs and other parts of the body. Atherosclerosis can lead to serious problems, including heart attack, stroke, or even death. The prevalent sites where atherosclerosis develops are the vessels branching, curvatures, zones of low wall shear stress, regions where external forces occur, etc. Figure 2.4 shows the common sites where plaque formation occurs such as the coronary arterial tree, the carotid bifurcation, the femoral artery, etc.

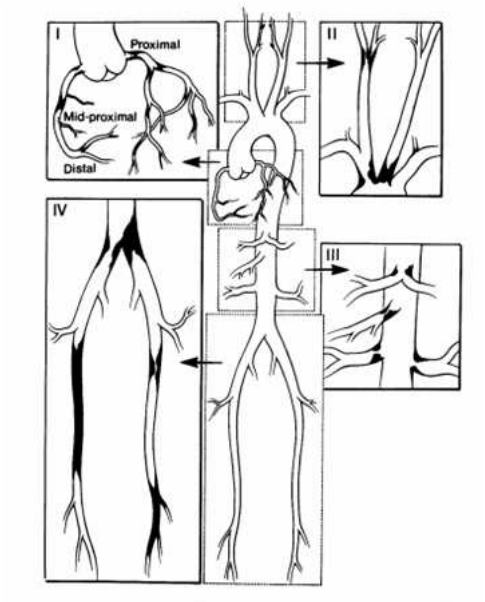

Figure 2.4: Prevalent sites of plaque formation given by [26]

During the past few decades, it has been showed that endothelial dysfunction is an early marker for atherosclerosis [56, 13]. Atherosclerosis is linked to multiple risk factors such as hypertension, elevated cholesterol, smoking, diabetes, obesity, etc. These risk factors are related to the dysfunction of the endothelium. Figure 2.5 represents the earliest changes that precede the formation of lesions of atherosclerosis that take place in the endothelium.

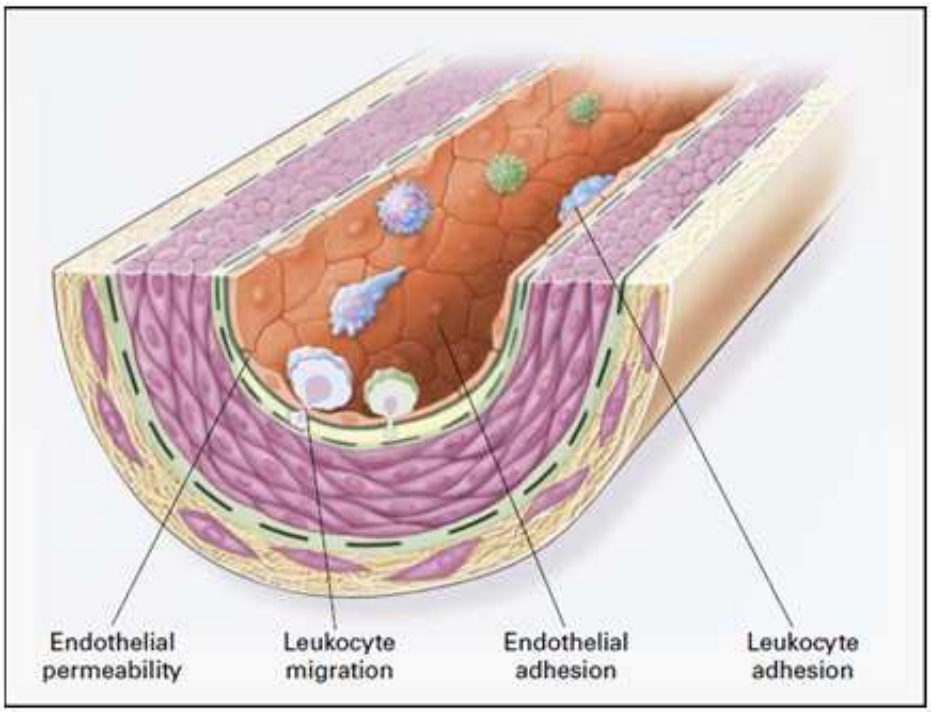

Figure 2.5: Early stage of atherosclerosis formation in the endothelium given by [88]

One major factor that is involved in the pathogenesis of the endothelial dysfunction is Nitric Oxide (NO). This molecule is produced by the endothelial cells and its production is extremely important to the physiology of the vessels. As seen before, the vascular endothelium lines the inner surface of the cardiovascular system

and especially of the vessels. Its function contributes to the vascular homeostasis by modulating hemostasis, inflammation, cell growth and proliferation, and vascular smooth muscle tone and growth. The vascular tone modulates the perfusion of organs and muscles by adapting the vessel diameter to the body needs. Hence, the endothelium maintains the equilibrium between vasoconstriction and vasodilatation, inhibition and promotion of underlying smooth muscle cells proliferation and migration.

Nowadays the role of NO has been widely reported to be a factor that inhibits platelet aggregation and thrombosis, monocyte and macrophage adhesion, inflammation, and vascular permeability [36, 99, 59, 18]. Therefore, abnormalities in NO production result in endothelial dysfunction and contribute to atherosclerosis [25]. The enzyme called Nitric oxide synthase (eNOS) converts its substrates L-arginine and O2 into NO and L-citrulline [29]. Dysfunctional eNOS is closely implicated in the endothelial dysfunction represented by impaired endothelium dependent relaxation in atherosclerotic vessels. It seems to be widely accepted that eNOS with normal function inhibits atherogenesis by producing NO [48]. Nevertheless, the release of NO can be also stimulated by physical reaction such as shear stress, flow pattern, etc [98, 91].

Numerous research have correlated wall shear stress quantities to endovascular diseases such as stenosis, aneurism and atherosclerosis, for the reason that variations in shear stress; especially low and oscillating shear stress and zone of flow reversal, play an important role on dysfunctional endothelium. The exposure of vascular endothelium to shear forces in the normal value range stimulates endothelial cells to

release vasoactive substances [77].

In fluid mechanics, for any fluid that has a viscosity, there is shear stress. Indeed, even if a fluid is in motion, it must have a zero velocity in the region of contact with the solids. And any difference in speed in a viscous fluid causes shear stress. Therefore the fluid particles moving faster are constrained by those going slower. In the vascular system, the shear stress is defined as the tangential force from the friction of the blood flowing on the endothelial surface of the artery wall. The shear stress depends on the viscosity of blood and the spatial gradient of the velocity of blood from the artery wall

$$\tau(y) = \mu \frac{\partial u}{\partial y} \tag{2.1}$$

where μ is the dynamic viscosity, u is the velocity of the fluid at a height y and y is the spatial coordinate of the fluid position.

To maintain normal functioning of the vascular system, arteries adapt to long-term increases and decreases in wall shear stress (WSS). That is, arteries attempt to reestablish a normal WSS by dilating and subsequently remodeling to a larger diameter in the presence of increased WSS and thickening the intimal layer or remodeling to a smaller diameter in the presence of decreased WSS [53]. If local disturbed flow patterns, such as zones of low WSS, persist, an excessive and uncontrolled intimal thickening response may occur [54].

Steady laminar shear stress promotes release of factors from endothelial cells that inhibit coagulation, migration of leukocytes, and smooth muscle proliferation while simultaneously promoting endothelial cell survival [99]. On the contrary, if the flow tends to depart from a laminar pattern and that low shear stress and oscillating shear

stress occur, it will favor the opposite effects. Consequently it will contribute to the development of atherosclerosis. Figure 2.6 illustrates the behavior of the endothelial cells depending on the flow pattern.

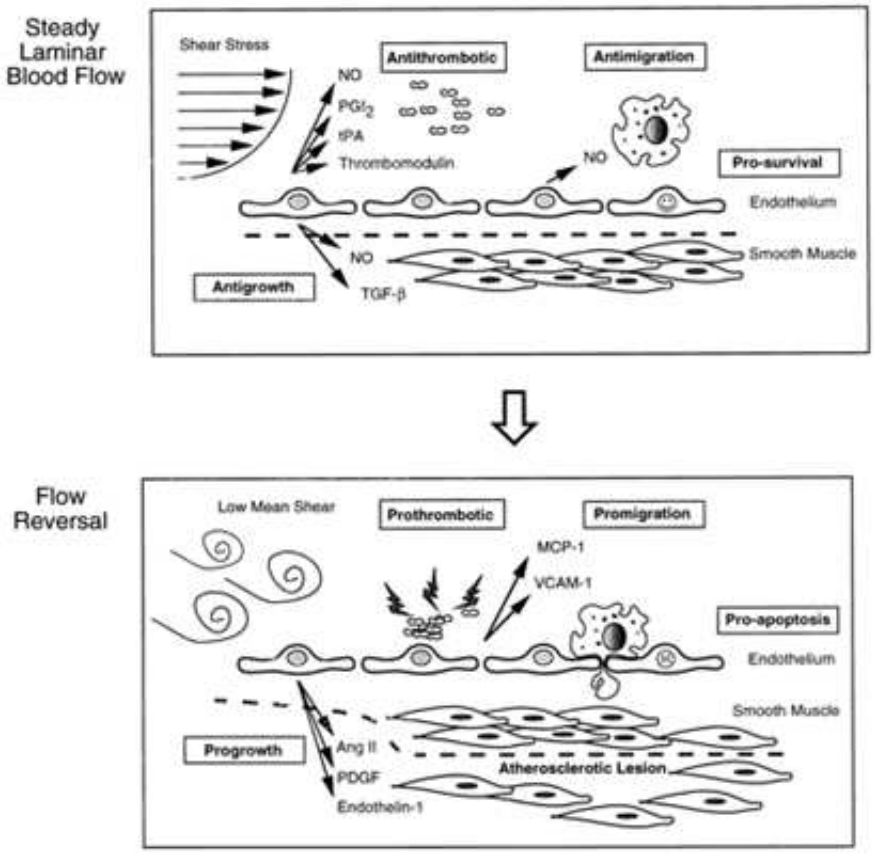

Figure 2.6: Flow pattern influencing the behavior of endothelial cells given by [99]

Atherosclerosis involves a deformation of the main arteries like the carotid artery, the abdominal aorta, or the femoral artery. Blood vessel deformations result in an increase of the mechanical stress on the vessels' walls but also create some perturbations in the blood flow. Theodore G. Papaioannou et al. presented that variations

in the shear stress appear in the vasculature, notably when unstable flow conditions occurs, such as turbulent flows or zone of blood recirculation [76].

2.1.3 Atherosclerosis Diagnosis and Treatment

In the previous subsection, we saw that atherosclerosis develops because of endothelial dysfunction that leads to an abnormal production of NO. If the production is blocked by risk factors, the vascular muscles do not relax to the appropriate degree and vasoconstriction ensues. Vasoconstriction increases blood pressure, and decreases flow, and is responsible for hypertension. Endovascular therapy aims to regulate the blood flow and the wall shear stress (WSS) as well as the normal production of NO.

A doctor will give a physical exam to a patient in order to diagnose atherosclerosis. He will listen to the arteries or check to see whether any of the pulses are weak or absent, in order to find signs of narrowed, enlarged, or hardened arteries. Depending on the physical exam, the doctor may recommend more diagnostic tests. These complementary tests can be blood tests, medical imaging tests, angiography, etc.

Blood tests can detect the level of cholesterol and blood sugar. If these levels are abnormal, it may be a sign that the patient is at risk for atherosclerosis.

Medical imaging modalities, such as ultrasound, computed tomography, or magnetic resonance imaging, can also be used to evaluate and quantify atherosclerosis [74]. These tests can often show stenoses and the hardening of large arteries.

Angiography has become the first modality to detect atherosclerosis in the coronary

arteries. This is an invasive technique where the doctor injects an iodinated contrast agent through a catheter placed at the ostium of the coronaries. The contrast agent is visible through x-ray fluoroscopic examination of the heart. Coronary angiography depicts "only" a luminogram of the vessel [43]. Nevertheless, this technique does not give information on the volume of plaque built in the arterial walls.

The main treatments for atherosclerosis are lifestyle changes, medications, and medical procedures. Lifestyle changes consist mainly on weight management, physical activity, healthy diet, and quitting smoking. Maintaining a healthy weight can lower the risk for atherosclerosis. A healthy diet is an important part of a healthy lifestyle. Following a healthy diet can prevent or reduce high blood pressure and high blood cholesterol and help you maintain a healthy weight. Regular physical activity can lower many atherosclerosis risk factors, cholesterol, high blood pressure, and excess weight [71]. Numerous researches have demonstrated that physical exercise is beneficial to health conditions [12, 79] and especially to cardiovascular health [70, 16]. Taylor et al. [94] have shown that moderate levels of lower limb exercise are necessary to eliminate the flow reversal and regions of low wall shear stress in the abdominal aorta that exist under resting conditions.

If the diagnostic tests are positive to atherosclerosis, the doctor can prescribe medications to a patient in order to slow the progress of plaque buildup.

Antiplatelet agents, for example aspirin, and anticoagulant drugs, such as heparin or warfarin, prevent blood clots or prevent existing clots from getting larger. These drugs prevent the accumulation of plaque. Another use of medications against atherosclerosis is to regulate the abnormalities of the NO's production. Huige Li

[57] stated that pharmacological approaches to improve eNOS functionality may be useful for the prevention and therapy of atherosclerosis.

If lifestyle changes are not enough to lower the levels of cholesterol, doctors can prescribe cholesterol medications. These drugs, such as statins, niacin or cholesterol absorption inhibitors, help to control cholesterol and blood pressure levels. Most of these drugs have the effect of decreasing low-density lipoprotein (LDL), which is the "bad" cholesterol that increases the risk of heart disease while increasing the high-density lipoprotein (HDL) cholesterol, the "good" cholesterol.

For severe cases of atherosclerosis, doctors may suggest surgical procedures to treat the disease. The medical interventions available are endarterectomy, angioplasty, and vascular bypass grafting.

Endarterectomy is an invasive procedure where surgeons make an incision in an artery that has been narrowed or blocked. From there, they remove the plaque that built up in the arterial wall. Therefore the artery remains open and blood flow is restored.

Angioplasty is a procedure where surgeons insert a small balloon inside a constricted blood vessel. The balloon is then inflated in order to widen the blood vessel and improve blood flow. Once the vessel is enlarged with angioplasty, surgeons sometimes place a stent depending upon the situation. A stent is a small mesh tube that helps to support the inner wall of the blood vessel and to keep the vessel wide open. The following figure 2.7 describes the carotid artery angioplasty procedure.

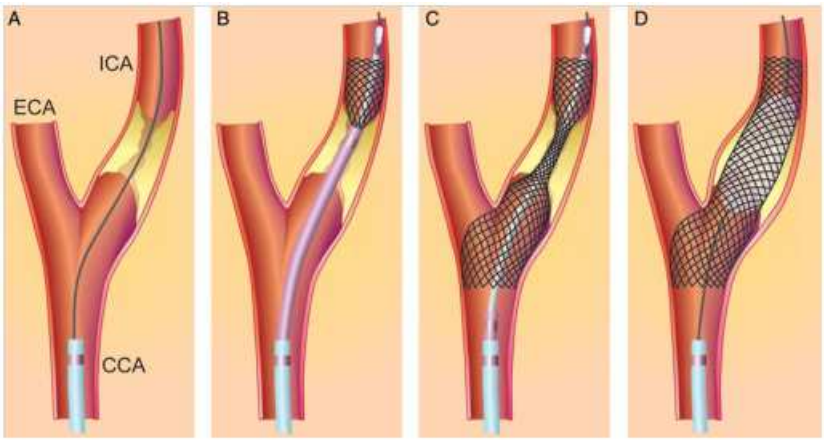

Figure 2.7: Different steps of the carotid artery stenting procedure given by [87]

In carotid disease, atherosclerosis usually develops around the bifurcation of the external and internal branches. If the narrowing of the carotid also called carotid stenosis is significant and that the disease is not treated in a timely manner, it can cause a stroke and lead to brain damage.

Vascular bypass grafting treats the narrowed arteries by giving to the patient an alternate or additional route for blood flow, created during bypass surgery. During a bypass procedure, vascular surgeons create a new pathway for blood flow using a graft. A graft can be a portion of one of the patient's veins or a man-made synthetic tube that surgeons connect above and below a blockage to allow blood to pass through it and around the blockage [87]. Bypass grafting is commonly used to treat peripheral arterial occlusive disease (PAD), for example leg artery disease. The following figure 2.8 illustrates a vein graft procedure when a blockage occurs in the femoral artery.

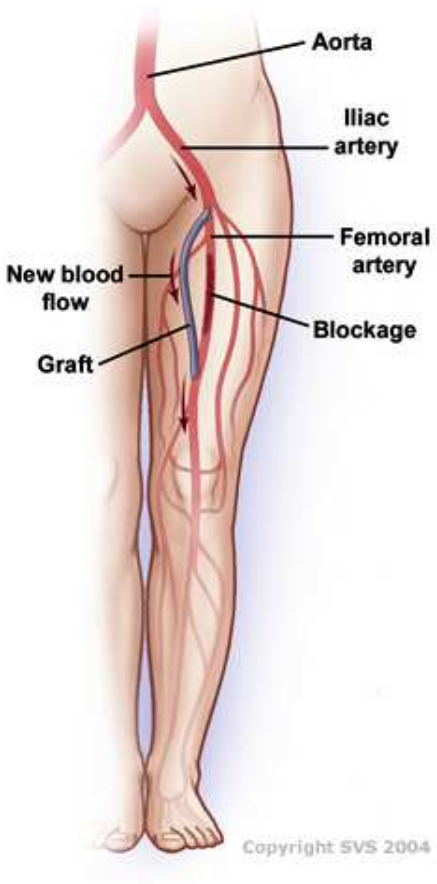

Figure 2.8: Bypass vein grafting procedure for the femoral artery given by [100]

Femoral arteries diseases are part of the peripheral arterial occlusive diseases that affect 8 to 10 million Americans. In extreme cases of PAD, when the patient condition cannot be improved by any of the methods already discussed, the affected leg or foot may need to be amputated. The amputation risk is about 1% per year and the risk of death is about 5% to 10% per year [62].

2.2 Elements of Computational Fluid Dynamics

This section presents an introduction for the field of computational fluid dynamics. To deal with a fluid dynamics problem, there are three different types of approaches to resolve it:

- The analytical approach has a great advantage to allow for exact solutions. However, it is limited to very simple cases by making a certain number of assumptions.
- The experimental approach is probably the approach that best represents reality. In return, it is often difficult to implement and requires some time to resolve any problems that may be encountered. Not to mention that it can quickly become very expensive.
- The basic principle of Computational Fluid Dynamics (CFD) is to use numerical methods and algorithms in order to solve and analyze problems that involve fluid flows. This approach is the subject of a major effort because it allows the access to all the instant information (velocity, pressure, concentration) for each point of the computational domain, for a total cost generally modest compared to experimental techniques.

Generally speaking, solving a CFD problem involves three main phases:

- The preparation of the problem: this requires the definition of a geometry, the construction of a mesh that discretize the computational domain and the choice of numerical methods to be used.

- Solving numerically the problem by the means of software. With high-speed supercomputers, better solutions can be achieved.
- Analysis of results: we first check their consistency, and then we investigate the results to provide answers to questions posed by the CFD problem.

In the first subsection, we present the governing equations for fluid flow. The second subsection outlines the discretization methods commonly used in computation fluid dynamics.

2.2.1 Navier-Stokes Equations

The very first step in fluid dynamics is to find a mathematical model according to a specific physical problem. The Navier-Stokes equations form a mathematical model derived from conservation laws which describes the flow of a fluid. The Navier-Stokes equations express the law of conservation of mass and the law of conservation of momentum or second Newton's law.

On one hand, the conservation of mass is given by 2.2:

$$\frac{\partial \rho}{\partial t} + \nabla \cdot (\rho u) = 0 \tag{2.2}$$

where u is the flow velocity, and ρ is the density of the fluid.

The conservation of momentum is on the other hand given by the following equation 2.3:

$$\frac{\partial}{\partial t}(\rho u) + (\rho u \cdot \nabla)u = f - \nabla p + \nabla \cdot \underline{\tau} \tag{2.3}$$

where u is the flow velocity, ρ is the density of the fluid, f is the other body forces, p is the pressure and $\underline{\tau}$ is the component of the total stress tensor.

The Cauchy stress tensor is defined by 2.4:

$$\underline{\sigma} = -pI + \underline{\tau} \tag{2.4}$$

where I is a 3x3 tensor identity matrix.

On the basis of the so-called Stokes' postulates, it is possible to derive the dependence of the stress tensor on the thermodynamic variables [28]. Therefore the velocity deformation tensor can be expressed by 2.5:

$$\underline{d} = \frac{1}{2}(\nabla u + (\nabla u)^T) \tag{2.5}$$

From 2.4 and 2.5, we can write the stress tensor in the form 2.6:

$$\underline{\tau} = (-p + \lambda div(u))I + 2\mu\underline{d} \tag{2.6}$$

where λ and μ are the Lam*é* parameters. μ is the dynamic viscosity of the fluid.

We obtain the general Navier-Stokes equations 2.7 and 2.8 by injecting 2.6 in 2.3:

$$\frac{\partial \rho}{\partial t} + \nabla \cdot (\rho u) = 0 \tag{2.7}$$

$$\frac{\partial}{\partial t}(\rho u) + (\rho u \cdot \nabla)u = f - \nabla p + \nabla(\lambda \nabla \cdot u) + 2\nabla \cdot (\mu \underline{d}) \tag{2.8}$$

If we consider an incompressible flow of a Newtonian fluid, we can simplify the Navier-Stokes equations. In reality, all fluids are more or less compressible. However, in order to simplify the equations of fluid dynamics, one often considers that fluids are incompressible when the flow velocity is not too high. The incompressibility condition is usually a sufficient hypothesis and it is written $\nabla \cdot u = 0$. The conservation of

mass and the fluid homogeneity ensure that the density is constant. We then obtain the following set of Navier-Stokes equations 2.9 and 2.10:

$$\rho(\frac{\partial u}{\partial t} + u \cdot \nabla u) = f - \nabla p + \mu \nabla^2 u \tag{2.9}$$

$$\nabla \cdot u = 0 \tag{2.10}$$

2.2.2 Discretization

By observing into details the Navier-Stokes equation 2.9, we can give the meaning of each term: $\frac{\partial u}{\partial t}$ corresponds to the unsteady velocity, $u \cdot \nabla u$ is the convective acceleration, $-\nabla p$ is the pressure gradient, f represents the other body forces and $\mu \nabla^2 u$ is the viscosity term. In the incompressible Navier-Stokes equations, the convective acceleration $u \cdot \nabla u$ is a non-linear term. In general, there is no analytical solution that exists for non-linear models. Therefore solution techniques aim to approximate the solutions using numerical methods such as iterative methods. A mathematical problem on a continuous domain (space and time) is not resolvable as such by a computer, which can handle only a finite number of unknowns. To be able to work from a infinite dimensional problem to a finite dimensional problem, we discretize space and time. The goal of discretization methods is to divide up a very complex problem into small elements that can be solved in relation to each other.

Nowadays, there exist many computational fluid dynamics techniques. Several discretization methods are now available, choosing one or the other of these methods is generally dictated by the physical application. The most common technique in commercially available CFD programs is the Finite Volume method that has the

broadest applicability ($\sim 80\%$) and then comes the Finite Element method ($\sim 15\%$) [94, 6]. Other approaches can be found such as the Finite Difference method, Spectral methods, Boundary Element method, Lattice Boltzmann methods, and many more. In this subsection, we explain the Finite Volume method where the solution domain is subdivided into a finite number of contiguous control volumes and where the conservation equations are applied to each control volume. Although we focus on the Finite Volume method, we give a short description of few other approaches such as the Finite Difference method and the Finite Element method.

In numerical analysis, the Finite Difference method is a common technique that consists in replacing the partial derivatives by divided differences or combinations of point values of the function at a finite number of discrete points or nodes of the mesh. In appearance, this method appears to be the easiest to implement because it proceeds in two steps: on one hand the Finite Difference discretization of the derivation and differentiation operators, on the other hand the convergence of the numerical scheme obtained when the distance between points decreases. The derivatives of the governing equations are obtained by the Taylor's theorem. The advantages of this method are that there are a great simplicity of writing the method and low computational cost. Its disadvantages are that it is limited to simple geometries, and that there are difficulties of taking into account the boundary conditions of the Neumann type.

The Finite Element method is a spatial discretization method that is currently applied in virtually all areas of physics using the numerical discretization techniques. Courant [21] introduced the concept of variational formulation, which is the basis of

any method of finite elements. By using a Finite Element method, the problem becomes generally much easier to solve. The Finite Element method is based on a very simple idea: split or discretize a complex shape into a large number of elementary subdomains of simple geometric shape or finite elements interconnected at points called nodes. One considers the mechanical behavior of each element separately, and then assembles these elements so that the balance of forces and compatibility of displacements are met in each node. The Finite Element method uses simple approximations of the unknown variables in each element to transform the partial differential equations (PDE) into algebraic equations. Nodes and elements do not necessarily have specific physical meaning, but are based on considerations of accuracy of the approximation. One of the main advantages of the Finite Element method is its systematic development on unstructured meshes. Its drawback is that it is not well adapted to the numerical resolution of nonlinear equations.

In this dissertation, the hemodynamic simulations have been mostly performed by the commercial software FLUENT developed and marketed by ANSYS Inc [6]. The discretization method used by that software is the Finite Volume method. This method is used to solve numerically PDE, such as the Finite Difference method and the Finite Element method. Unlike the Finite Difference method that involves approximations of derivatives, the Finite Volume method and the Finite Element method operate on approximations of integrals. However, the Finite Volume method is based directly on the integral form of the equation to be solved, while the Finite Element method is based on a variational formulation of the equation. The domain is subdivided into a finite number of contiguous control volumes by a grid. The principle of this method

is to apply the conservation equations to each control volume. The partial differential equations, that govern the fluid flow, contain terms of divergence. Using the Divergence theorem, the volume integrals of a divergence term are converted into surface integrals and these flow terms are subsequently measured at interfaces between finite volumes. A numerical flow function is used to establish an approximation of the flow at the interfaces. Since the flow entering a given volume is equal to the flow leaving the adjacent volume, these methods are conservative and therefore ideally suited to solving conservation laws. In order to solve the governing equations of flow fluids using the Finite Volume method, it is necessary to define the numerical scheme. It consists on finding a relationship that provides step by step the following terms when a solution is given. Numerical scheme are computation algorithms that permit to solve numerically partial differential equations. The goal of numerical schemes is to transform all mathematical operators ($\frac{\partial}{\partial x}, \frac{\partial}{\partial t}, ...$) into arithmetic operations on grid points. When the PDE that one seeks to solve involves more than one direction in space, there are many options to discretize it. We present two numerical schemes that are commonly used in CFD known as first-order upwind scheme and second-order upwind scheme. However numerous schemes exist.

Upwind schemes are based on an adaptive Finite Difference method to numerically simulate the direction of propagation of information in a flow field.

First-order upwind scheme for a 1D problem can be written as follows:

$$\frac{\partial u_x}{\partial x} = \frac{u_i^n - u_i^{n-1}}{\Delta x} \tag{2.11}$$

The following equation describes a second-order upwind scheme for 1D problem:

$$\frac{\partial^2 u_x}{\partial x^2} = \frac{u_{i-1}^n - 2u_i^n + u_{i+1}^n}{\Delta x^2} \tag{2.12}$$

The discretization in time used the same concept than the spatial discretization. We replace the partial differential operators for the time derivative with the difference expressions.

All numerical schemes must satisfy certain conditions to be accepted: consistency, stability and convergence.

As a result, a set of linear algebraic equations can be found for each control volume. Hence iterative methods are generally used to solve this system of equations.

2.3 Dynamic Simulation and Particle Tracking

This section presents an introduction for the computational fluid dynamics simulations in moving objects and for the CFD simulations coupled with particle tracking. The first subsection presents the necessary fluid kinematics to describe a fluid flow. Then we outline different methods to simulate multiphase flow. The next subsection explains the techniques to run CFD simulations when the fluid domain is not static. Finally, we introduce the immersed boundary method, an approach to simulate fluid-structure interaction, which can handle motion during simulations.

2.3.1 Kinematics

In fluid kinematics, there are two techniques to characterize a flow known as Eulerian description and Langrangian description. The Eulerian approach describes the

velocity field which associates each point a velocity vector, while the Lagrangian approach is to follow in time the fluid particles along their trajectories: it is an intuitive description of their movement. The first is more suited to the fluid dynamics, and the second to solid mechanics, but this distinction between the two is not settled. In reality, each of these descriptions provides tools that simplify more or less the definition and problem to be solved based on a given context. Therefore, it is important to have an understanding of the two descriptions.

The Lagrangian description consists of following a physical particle (represented by a point M) in its movement from an original position. Individual particles can be followed over time, which means that at every instant their position is known.

Figure 2.9: Particle movement in Lagrangian description

Consider $M(t)$ the position of the particle at the instant t, of coordinates $x_M(t)$,$y_M(t)$,$z_M(t)$, the particle velocity has the components:

$$u_M = \frac{dx_M}{dt}, v_M = \frac{dy_M}{dt}, w_M = \frac{dz_M}{dt} \tag{2.13}$$

Over time, the particle will be at different points M, the set of points M is then the path of the particle. This description, although simple and natural, studies only one fluid particle, so if the problem considered few particles, this approach would be acceptable. However, it is not possible to track each particle in a complex flow field.

Lagrangian description is rarely used in fluid dynamics.

The Eulerian description is radically different from the Lagrangian approach. We do not consider the initial time anymore and we do not choose to follow the fluid particles in their movement. The observation of the fluid flow is made from a fixed position. The Eulerian description of the fluid flow movement consists then of defining the velocity field of particles occupying a given position at a given time. For a small cell or control volume $dxdydz$, whose position (x,y,z) is fixed in the Eulerian frame of reference, we determine the velocity of the fluid particles which pass through this element of volume. The measured velocity $\mathbf{U}$ obviously depends on the time and the measurement point (x,y,z):

$$\mathbf{U} = \{u(x, y, z, t), v(x, y, z, t), w(x, y, z, t)\} \tag{2.14}$$

This approach is usually preferred to the Lagrangian description, the understanding of the velocity field is sufficient for the description of fluid motion but also because there are too many particles to keep track of in a Lagrangian description.

2.3.2 Multiphase Model

Multiphase fluid dynamics is the field of fluid dynamics that study what happens when dealing with multiple fluids flowing together: it can be the same fluid present in two phases different (e.g. water vapor), two different liquids in the same phase (liquid water and oil), or two different fluids in different phases (water and air)... The flow behavior in the presence of two different fluids is strongly modified compared to one-phase case, which is why it is now becoming one of the sub domains the more

active in terms of research of fluid dynamics [20, 27, 107, 33].

The commercial package FLUENT offers various numerical models to simulate two-phase flows. We discuss two different methods; the first one is based on an Euler-Lagrange approach, while the second one is related to an Euler-Euler approach. These two methods have been thoroughly detailed in [52, 93, 92, 10].

The first approach is called the Discrete Phase Model (DPM). The fluid phase is treated as continuous by solving the Navier-Stokes equations, while the discrete phase is calculated in accordance with a large number of particles, bubbles, or droplets through the field. The continuous phase is computed in the Eulerian reference of frame, although FLUENT allows the user to simulate a discrete second phase in a Lagrangian description. The dispersed phase can exchange kinetic energy, heat, and mass with the fluid phase. The strong assumption of this model is that the discrete second phase occupies a low volume fraction. Particle trajectories are calculated individually for the calculation of the continuous fluid phase, making it a suitable model for problem of combustion [10, 11] and flow of certain particles but inappropriate for liquid-liquid mixtures, fluidized beds, or any application for which the volume fraction of the second phase is not negligible (the FLUENT documentation gives the limiting value of 10%). The set of equations that predicts the trajectory of a discrete phase particle are presented in the FLUENT documentation [4]. The standard Lagrangian DPM is based on a translational force balance that is formulated for an individual particle [51]. This force balance represents the particle inertia with the forces acting on the particles can be written as follows:

$$\frac{\partial u_p}{\partial t} = a_1 + a_2 + a_3 \tag{2.15}$$

where u_p is the particle velocity, a_1 is the drag force per unit particle mass, a_2 is the gravitational force and a_3 is any additional acceleration terms resulting from thermophoteric, Brownian or Saffman's lift force for instance. The drawback of the DPM model, in addition to the limitation of the volume fraction of the discrete second phase, is that the interaction between particles is neglected. This method has been widely studied in different fields.

In the Euler-Euler approach, the different phases are treated mathematically as interpenetrating continuous phases. The concept of volume fraction is then introduced to reflect the presence or absence of a certain phase at a given point at a given time. This approach does not attempt to determine the properties of each particle present in the flow but to compute local properties of two-phase flow characteristics. FLUENT presents three Euler-Euler methods to describe the multiphase flow: the Volume of Fluid (VOF), the Mixture Model and the Eulerian Model.

The basic idea of the VOF method is to use a discrete function which represents the volume fraction of one of the fluids in each control volume. This method has been proposed by Hirt and Nichols [40]. The VOF formulation relies on the fact that several fluids or phases are immiscible. It is designed to track the position of the interface between the fluids. The VOF model uses a single equation for the balance of momentum, shared with all the phases, and introduced the concept of phase volume fraction to translate the presence or absence of a phase at a given point in space at a given time.

The second Euler-Euler method available in FLUENT is the Mixture Model. The Mixture Model has been introduced by Ishii in 1975 [44]. The Mixture Model is

a simplified multiphase model to simulate flow where the fluid phases can move at different velocity. Unlike the VOF model, this approach treats the mixing phases as continuous phases occupying all the space and can interpenetrate. The balance equations for calculating the relative velocity can be rigorously derived by combining the momentum equations for the dispersed phase and the mixture [63].

Finally, unlike previous models, using a single set of equations for the conservation of momentum and continuity, the Eulerian model introduces other set of equations. This approach is more complex considering that the conservation equations are calculated for each phase, and an equation ensures the exchange between the different phases by means of an exchange coefficient. It is therefore interesting when there are couplings between the phases, such as transfer of energy or matter. The coupling is carried out through the pressure and interchange coefficients between the phases depending on the nature of the phases involved (granular flow fluid-solid or non-granular-type fluid-fluid). With the Eulerian model, the number of secondary phases is limited only by the capabilities of the tool calculations.

2.3.3 Fluid Structure Interaction

In recent years, numerous researches have studied the correlation between cardiovascular disease and hemodynamics for various cases such as the development of the abdominal aortic aneurism (AAA) [78, 14, 22], the evolution of atherosclerosis in major arteries [54, 60, 50], or the investigation of the restenosis process [46, 19, 35]. Fluid Structure Interaction (FSI) regards the problems where the coupling of fluid

dynamics and solid mechanics occurs. The numerical simulation of coupling problems has grown steady in recent years. This development is due in particular to the precedent success of the numerical simulation in general, but also to the permanent increase in the computational tools performances. FSI involves a structure mobile, rigid or deformable, which interacts with an internal or surrounding fluid flow [41]. It is indeed common in fluid mechanics to consider the surrounding solid as a simple boundary of the fluid studied. Besides, solid mechanics as it is often considered that the fluid has little influence on the dynamics of the solid. Many industrial problems require, yet taking into account, both contributions to be modeled appropriately. These problems are called FSI, because the evolution of each of the two components depends on the other. FSI finds applications in many various fields such as automotive industry, aeronautical or civil engineering, biofluid, and bio-mechanics. The numerical simulations are based mostly on a simplified model of one of the two mediums, or rely on specific coupling procedures used to run all computational codes developed specifically for the fluid on one side, and the structure on the other. Therefore, there are widely two types of approaches for modeling the FSI problems: the monolithic approach and the partitioned approach. The monolithic approach [65] theoretically represents the optimal solution, since the fluid and the solid are treated by the same calculation code. However, when the geometry or the physics of the problem becomes more complex, this type of method is not suitable because each medium (liquid or solid) requires specific numerical procedures. In contrast, by using specialized codes, the partitioned approach [104, 47, 30] can solve the fluid dynamics on one side and the mechanics of the solid on the other. The challenge

of this method is to exchange information from one code to another. Each physical field is separately defined, discretized and numerically solved with coupling procedures applied to transfer the required interface information [104]. Each method has advantages and drawbacks but in practice, the partitioned approach is mostly used. The monolithic approach is generally not feasible to treat complex configurations, notably because the methods used to model fluids and solids are usually different: the Lagrangian description is preferably used to describe the solids, while the fluids are rather treated in an Eulerian approach. The partitioned approach is therefore a good alternative, especially since it allows reusing existing codes to each environment. The difficulty lies in the treatment of the interface location that divides the fluid and the structure domains, which requires the development of efficient coupling algorithms.

With the advances in numerical methods and the rapid improvement in computational tools, and due to the great clinical interest, CFD has been increasingly used as a simulation tool for blood flow. To propose new prevention and diagnosis criteria that are more reliable, many experimental and numerical studies concerning the biomechanics of aneurysms or atherosclerosis as well as the blood flow dynamics have been performed over the last two decades. One of the main objectives of these studies is to better understand and model the fluid-structure interaction, within aneurysms and atherosclerosis. They aim to quantify more precisely: the spatial and temporal distribution of the hemodynamic forces such as pressure and shear applied to the wall; the spatial and temporal distribution of the stresses induced by these forces within the arterial wall.

2.3.4 Immersed Boundary Method

The conventional approach used to simulate the flow around a solid structure is to create an adaptive mesh for the solid, then solve the equations on this mesh with the appropriate boundary conditions. Immersed boundary methods are a class of methods where the calculation is performed on a Cartesian mesh that does not rely on the solid contours in the flow. Obviously, this is an advantage when moving solids are considered. Solving the equations governing the fluid flow is easier and less expensive on a Cartesian grid. The boundary conditions are easy to impose on adapted mesh. In the case of immersed boundary methods, it is not as easy to impose the boundary conditions since there is no mesh point on the surface of the solid, and this is clearly on this point that focuses effort [66, 69].

The immersed boundary method has been introduced and developed in 1972 by Charles S. Peskin [82] in order to study blood flow around heart valves. The physical model describes the interaction of elastic membranes and an incompressible fluid. The immersed boundary method considers the structure as a fiber or fiber bundles. In this context, the formulations for the structure involve the Dirac function. This significantly changes the way in which we consider the structure, since it is simplified in a way to no longer be concerned with the eventual inside of the structure. Thus, the structure then has no thickness. The membrane is represented by a set of Lagrangian particles, of coordinates X_k, that are moving at the velocity of the fluid with the equation:

$$\frac{\partial X_k}{\partial t} = u(X_k, t) \tag{2.16}$$

The governing equations for the interaction are given by the incompressible Navier-Stokes, presented in previous section:

$$\rho(\frac{\partial u}{\partial t} + u \cdot \nabla u) = f - \nabla p + \mu \nabla^2 u \tag{2.17}$$

$$\nabla \cdot u = 0 \tag{2.18}$$

where f represents a vector term that reflects the presence of elastic structure in the fluid. f is given by the following equations:

$$f(x,t) = \sum_k F_k \delta(x - X_k) \tag{2.19}$$

where F_k is the elastic force density and δ is the Dirac function.

Part II

Accuracy Assessment

Cardiovascular diseases such as atherosclerosis and aneurysm are among the leading causes of mortality in the world. World Health Organization reported an estimation of 17.3 million people who had died from cardiovascular diseases in 2008, which represents 30% of all global deaths [105]. According to the National Heart, Lung, and Blood Institute, peripheral arterial disease affects 8 to 12 million people in the United States, which is around 12% of the adult population [62]. In recent years, computational fluid dynamics has been increasingly used as a simulation tool for blood flow. The treatment for vascular disease has evolved significantly over the past years considering the rapid advances in imaging technology. Endovascular surgery is now widely used to noninvasively treat diseases such as atherosclerosis or aneurisms. Combining computational fluid dynamics models and medical imaging, provides a new perspective to correlate plaque formation and hemodynamics. Therefore, a thorough knowledge of vascular anatomy and hemodynamics would be beneficial for understanding the development and progression of the disease, the therapeutic decision process and follow up [17, 38, 96]. The hemodynamic simulation procedure should be patient specific, but the reproducibility of the arteries is not a trivial task since there is no standard of the geometries or the flow field variables in vivo. Recent researches combining medical imaging modalities and CFD simulations investigated the accuracy and limitations of their CFD methods. J.A. Moore showed that geometry acquisition in particular is the most critical step to lead to accurate results [68]. Other studies have presented that some variables were highly reproducible (up to 90-95%), such as velocity, oscillatory shear index or wall shear stress angle deviation, but other parameters were less reproducible (down to

60%), such as the wall shear stress and wall shear stress gradient [106]. Other recent studies stated that CFD simulations may be a promising tool for studying the relationship between hemodynamics and vascular diseases, however improvements in the precision of image-based CFD models may be required before conventional modeling assumptions [38, 96].

Chapter 3

Uncertainties on Hemodynamic Simulations

In this chapter, we present the different steps of the hemodynamic simulation process. This study has been simplified and done for a steady case where we assumed an incompressible and Newtonian fluid. We then show the verification of our method by performing convergence analysis. The region of interest in this part is the carotid bifurcation. The tools used for this study were the mesh and geometry generation software Gambit and the computational fluid dynamics software FLUENT. Both are commercial products and developed by ANSYS Inc. Along this chapter, we outline the sources of uncertainties that occur during the hemodynamic simulation process.

3.1 Three-Dimensional Reconstruction and Mesh

The traditional procedure of hemodynamic simulations is to reconstruct in 3D the vessel geometry from anatomical data of medical imaging modalities such as Magnetic Resonance Angiography (MRA) or Computed Tomography (CT). Medical images provide information on the shape and functioning of the organs of the human body.

The very first step is to acquire the patient data. The patient is usually lying down on the CT scanner or MRI machine, while a series of images around the region of interest is captured.

In modern machines, the X-ray source rotates around the patient together with the receptors located in front, and whose function is to measure the intensity of radiation after they have partially absorbed during their passage through the body tissues. The data is then processed by a computer, which allows reconstructing cross-sectional views of two-dimensional and three-dimensional views of organs. The contrast of certain tissues can be brought out, particularly blood vessels, by injecting an iodine based contrast agent which has the property of strongly absorb X-rays and thus make very visible tissues where this product is present.

Unlike most medical imaging devices, MRA is a technique based on Magnetic Resonance Imaging (MRI) that does not use X-rays, but the influence of magnetic fields on different tissues. The magnetic fields will position the hydrogen nuclei in the patient's body in a particular state called resonance. The return of the hydrogen atoms in their equilibrium state will result in the formation of a signal in a receiving antenna. During an MRI scan, it is the analysis of this signal by a computer that

provides the images of different parts of the human body. MRA is basically used to visualize the blood vessels to highlight abnormalities such as stenosis, fistulas, aneurysm, etc. MRA may be performed with or without a contrast agent. Gadolinium is the usual contrast agent for MRA; it is injected intravenously in the arm of the patient.

For both of these medical imaging modalities, the computed data is a stack of cross-sectional images along the axis of the neck with an interval varying from 1 to 3 millimeters between each image.

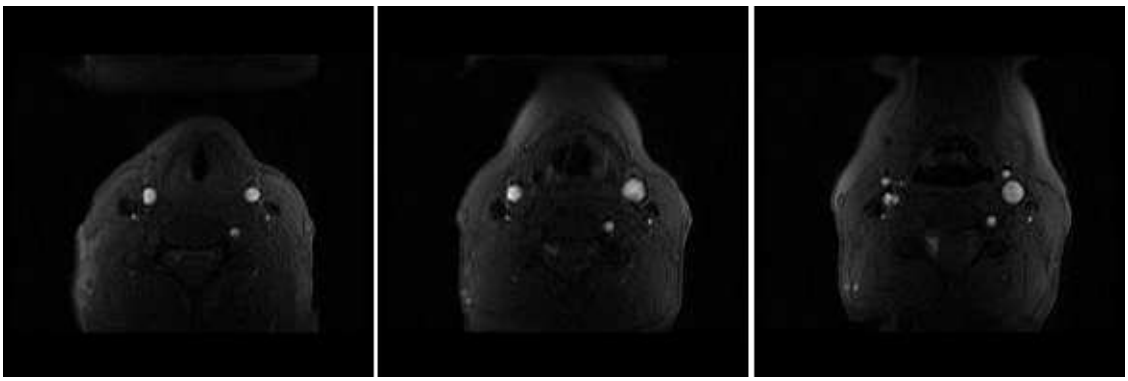

Figure 3.1: MRI images of the two carotid arteries in axial orientation, perpendicular to the axis of the body

From this data set, a segmentation of the contour of the lumen was required in order to be able to rebuild the carotid artery for each patient. We extract the contour of the carotid artery for each slice. By successively performing pre-processing and image segmentation technique on the stack of images, a three dimensional reconstruction of the vessel can be achieved. The segmentation was done through

ImageJ, a multi-platform open source image processing and analysis developed by the National Institutes of Health. It is written in Java and allows the addition of new functionality through plugins and macros [72]. The most common operations in image processing are achievable with ImageJ: visualization and adjustment of the grayscale histogram, denoising, lighting correction, edge detection, direct and invers-Fourier transform, thresholding, and logical operations arithmetic between images, and more generally, any type of linear transformation by defining custom masks. Image processing methods from mathematical morphology are also available such as erosion/dilation, skeletonization, etc... We would like to kindly thank Dr. Christof Karmonik, from the Methodist Hospital Research Institute, for providing patients data and helping us with the image segmentation. The figure 3.2 shows the results of the segmentation of the carotid artery.

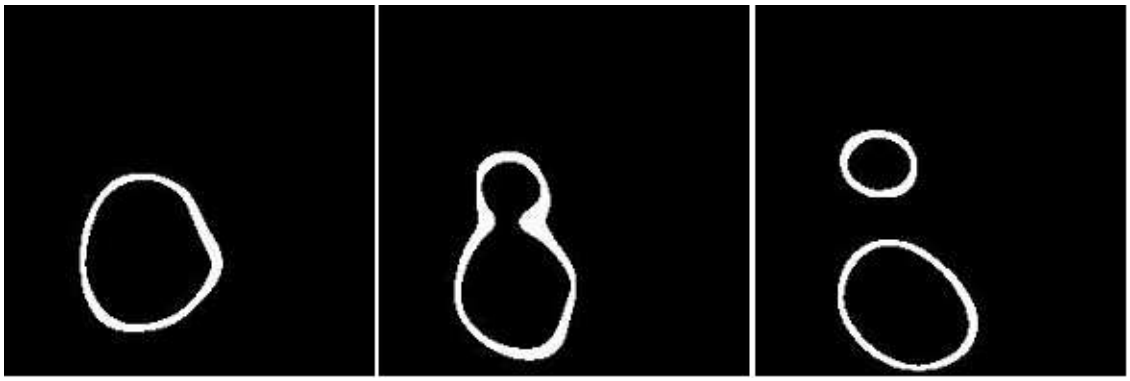

Figure 3.2: Segmentation of the carotid artery using ImageJ [72]

The data acquisition and image segmentation phase can be sources of errors. Indeed, the medical imaging modalities can be compared to sensors. So, there is a step

where the signal has to be converted from analog to digital. In principle, an analog signal contains an infinite number of continuous values while a digital signal has only a finite number of values [101]. The conversion of the signal is usually performed by an analog to digital and digital to analog converters embedded in the imaging devices. This analog/digital conversion is often the step that limits the resolution of the image. Medical imaging is limited in precision. A digital image is a mosaic constituted of elementary cells called pixels, short term for picture elements. In general, an analog image is shrunk into a series of digital values stored in the memory of the computer in a matrix form. The dimension of the matrix is generally $2^n x 2^n$, it is given by the resolution of the imaging device. Each element of this matrix is identified by its geometrical coordinates, i^{th} row and j^{th} column. Each pixel is associated with a digital information representative of the information contained in the corresponding element of the analog image. This information depends on the function of the medical imaging modalities such as an optical density for X-Ray and a density of protons for MRI. Each pixel is represented by a number of bits. The analog/digital conversion consists of representing the matrix, which contains the analog information, by a grayscale or color scale. This step is called quantization. Color scale is hardly used in medical imaging except in nuclear medicine. Most medical digital images have 12 bits (4096 grey levels). Not enough bits leads to quantization artifacts and loss of resolution. The main uncertainty of digital images is that they are dependent on the quantization. At the same time, matrices composed of different numerical values can represent the same reality. The conversion of an analog signal to digital form causes loss of information [15].

Other uncertainties arise at this early stage because data from medical imaging modalities provide only an average position of an anatomic structure at the acquisition time, but the human body is constantly in motion. For example, during medical imaging tests such as MRI or CT, the patient may be asked to hold his breath for a short period of time in order to limit the motion of the body, since motion affects the images. Image segmentation also has its limitations. Images related problems have to be handled carefully to get the best output: noise, intensity, etc. A review of different segmentation techniques, as well as their limitations, for medical images can be found in [83]. The three main classes of medical imaging segmentation are thresholding, classification (Fuzzy K-mean clustering) and deformable models (Active contours).

The second step is the reconstruction of the artery in three dimensions. During the segmentation stage, we traced the contours of the volume of the carotid artery in each slice where it appears. In order to perform the 3D reconstruction from 2D image, we used a geometry and mesh generation software named Gambit which is developed by ANSYS Inc. The basic idea is to connect points or vertices of two consecutive contours and to create a surface between those contours. The creation of the mesh was a tedious procedure. First of all, the contour coordinates of the arterial wall for each slice have been extracted and then stored into files by using our code implemented in MatLab. Figure 3.3 shows the carotid artery of one of the patient after the extraction of the contour points.

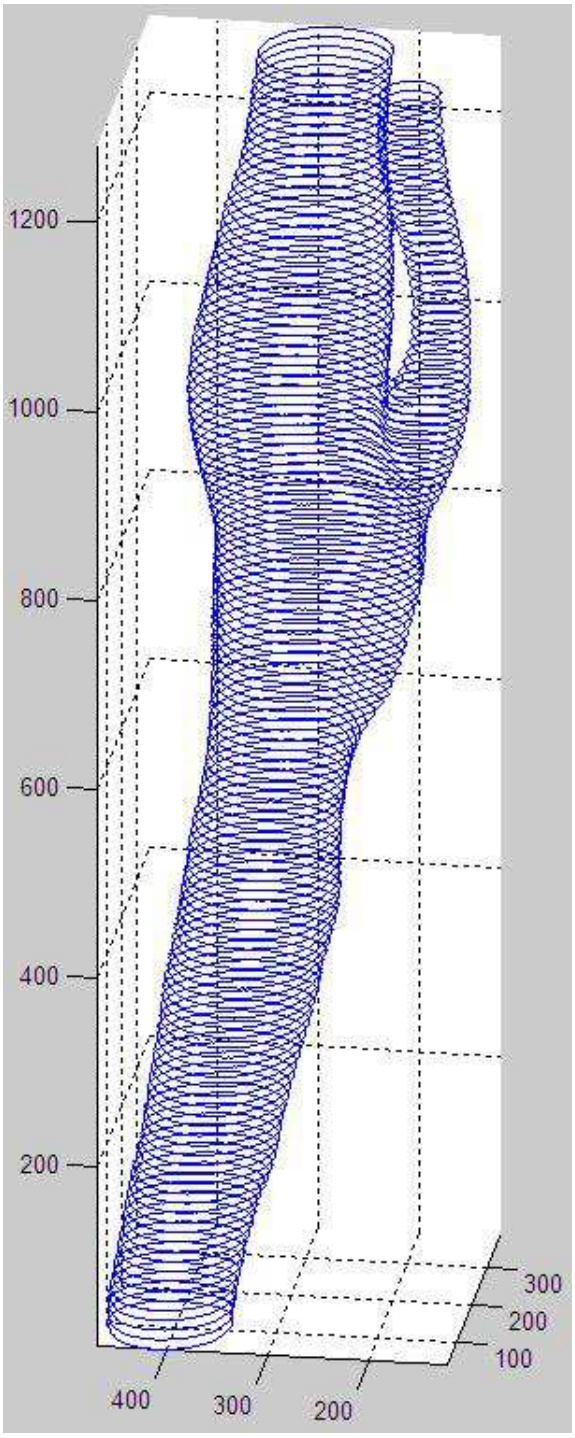

Figure 3.3: Extraction of contour points using MatLab

Subsequently, we wrote a journal file to interpret the set of coordinates in Gambit. A journal file is an executable list of Gambit commands. They can be either created automatically by Gambit from the Graphic User Interface (GUI) and Text User Interface (TUI), or edited externally by a text editor. The list of commands that we edited in the journal was impletemented by a small routine in MatLab and it is given by the following pseudo code:

- Import the set of coordinates of each slice

  import vertexdata $filename_slice#

- Create edges to recover the contour of each slice

  edge create straight strfmt("vertex.%%d",$i)

  strfmt("vertex.%%d",$i-1)

- Create edges between two consecutive contours

  if (i=last_vertex_slice)then

  edge create straight strfmt("vertex.%%d", $i)

  strfmt("vertex.%%d",$first_vertex_next_slice)

  endif

  if (i=middle_vertex_slice)then

  edge create straight strfmt("vertex.%%d", $i)

  strfmt("vertex.%%d",$middle_vertex_next_slice)

  endif

- Create surface of each slice

  for i=1:number_of_edge

face create wireframe ("edge.%d",i)

end

- Create surfaces between two consecutive contours

  face create skin ("edge.%d",$edge_between_contours)

  ("edge.%d",$edge_closing_surface)

- Create volume between two consecutive contours

  volume create stitch ("face.%d",$face_bottom_contour)

  ("face.%d", $face_top_contour)

  ("face.%d", $faces_between_contour)

The main difficulty encounters in this process was the creation of a volume at the bifurcation of the carotid artery. Since there was no technique in Gambit that can automatically create a volume from one inlet surface and two outlet surfaces, this task was manually achieved. In order to complete this task, we divided the last slice before the bifurcation to be able to connect the two branches of the artery.

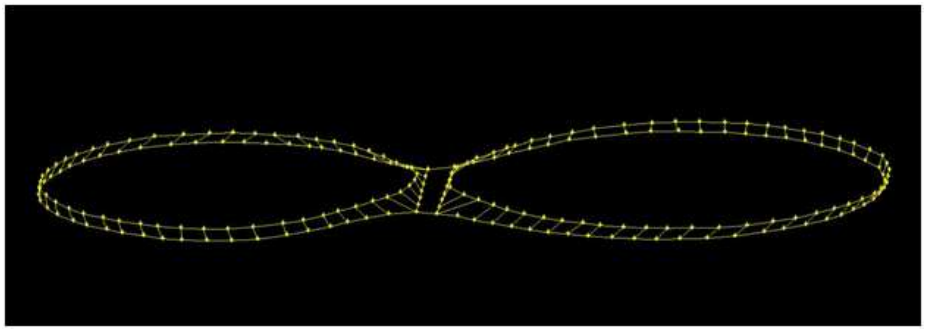

Figure 3.4: Reconstruction step of the carotid bifurcation in Gambit

From there, the creation of surfaces and volume at the bifurcation was possible, thanks to the Volume Merge option in Gambit.

volume merge volume1 volume2 [volume3 ...]

Finally, the entire volume of the carotid artery was completed by merging all the volumes (volumes between slices and volume at the bifurcation). The figure 3.5 shows the reconstruction of the carotid bifurcation of three different patients using our method.

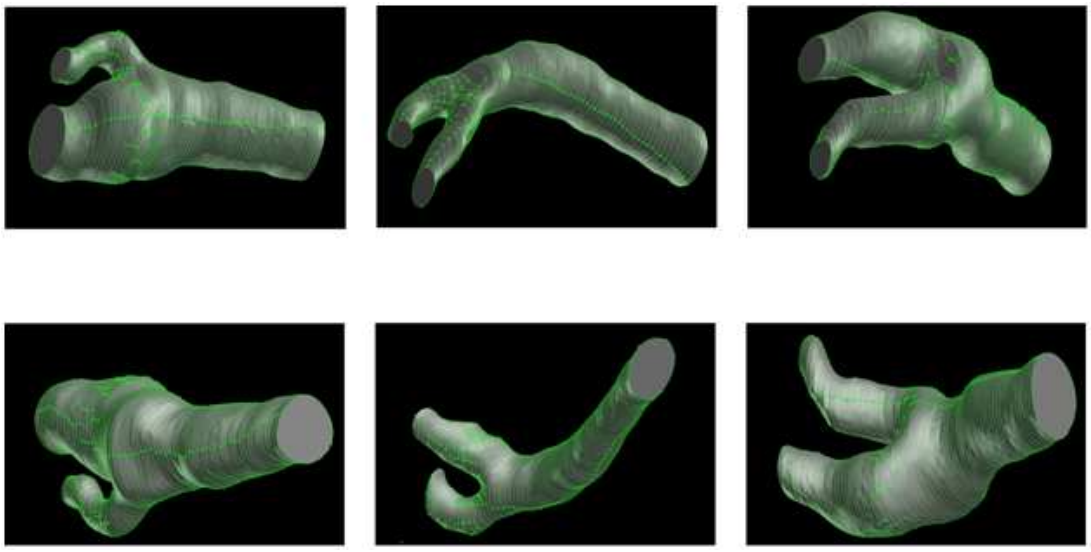

Figure 3.5: 3D reconstruction models of carotid bifurcation artery using software Gambit

The figure above suggests the broad variety of possible geometric differences between patients, and justifies that hemodynamic simulation should be patient specific.

Another source of errors comes from the segmentation of 3D structures from 2D images. The acquired data for the carotid artery are usually taken from an axial orientation or transverse plane (perpendicular to the axis of the body) or from a sagittal orientation (vertical planes oriented from front to rear, that separate the body into a right and left halves). In general, for a reconstruction in three dimensions from 2D medical images, the axial orientation is preferred. However, when we try to recover the desired shape of the artery, it is not said that the direction of medical imaging slices is aligned with the axis of the vessel.

Afterwards, as we presented earlier, in order to compute the Navier-Stokes equation inside the artery model, we needed to discretize its volume. The method for discretization that we used is the finite volume method. It consists of creating a computational mesh for the model. To do so, the volume of the artery model underwent discretization process via Gambit. A mesh is the spatial discretization of a continuous medium, or in other terms, a geometric model of a domain by a proportioned and well defined finite number of elements. The purpose of a mesh is a simplification of a problem by a model that represents the system and possibly its environment, in the context of computational simulations. In our case, the fluid domain has been discretized into small control volumes. Due to the complex geometrical structure of the carotid bifurcation model, the choice of tet/hybrid elements was required. Tet/hybrid mesh specifies that the mesh is composed primarily of tetrahedral elements but may include hexahedral, pyramidal, and wedge elements where appropriate [49]. The figure 3.6 depicts the mesh generation for a patient carotid artery model using tet/hybrid mesh and containing around a million elements.

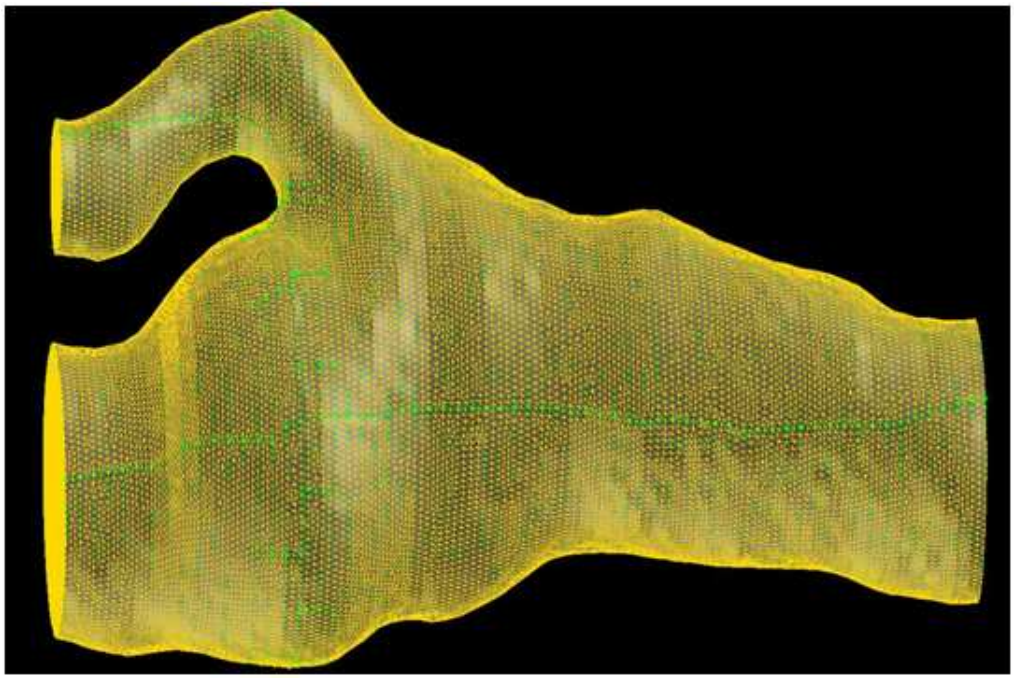

Figure 3.6: Generation of the mesh for the 3D models of carotid artery

The reconstruction in 3D of the carotid artery is a very slow and tedious process. It requires time more than computation power. The procedure for one model will take no less than 5 hours.

The next step in the hemodynamic simulation process is to define boundary conditions prior the simulation. The set of Navier-Stokes equations is indeed incomplete since initial conditions and boundary conditions have not been specified yet.

3.2 Boundary Conditions

Hemodynamic simulations require numerous parameters or boundary conditions in order to reproduce, at best, the blood flow in vessels. The evolution of the hemodynamic and the resulting forces do not depend only on the geometry of the model. The rheology of the fluid and the boundary conditions imposed at the entrance and the exit during experiments may also play an important role. Because of the non-linearity of the Navier-Stokes equations, computational fluid dynamics has always considered initial conditions and boundary conditions to start the iterative process that solves the differential equations. Therefore, boundary conditions, like inlet and outlet conditions, need to be properly parameterized in order to compute accurately the Navier-Stokes equations and the conservative equations.

The two main techniques used to measure arterial hemodynamics are the Doppler Ultrasound and the phase contrast MRI. Defining a good simulation depends not only on a good model, but also on accurate boundary conditions.

After importing the carotid artery model into the fluid flow solver FLUENT, we specified the flow to a steady-state and then assigned a face to a type of boundary conditions. In our case, we had the following boundary conditions to define:

- In fluid mechanics, it is traditional to assume that the tangential velocity at a solid surface is zero, i.e. that the fluid does not slip on the solid surface. So the wall of our model was set as solid with a no-slip condition, which means zero velocity relative to the wall.

- Since our scenario implicates the vascular system, the studied fluid is obviously

blood. It has been widely show that blood can be assumed as a viscous incompressible and Newtonian fluid [80]. The different properties of the fluid have to be specified, so the density and viscosity of the fluid were given as follows:

$$\rho = 1050 km/m^3$$
$$\mu = 0.004 kg/m.s$$

- For the inlet, due to the viscous effect and the no-slip condition at the wall, we know that when a fluid enters a pipe, it will take time and a certain length for the flow to reach a fully developed profile. In order to avoid wasting this entrance of region, there are several methods to achieve that. We can either extend the length of the carotid at the inlet or to impose a fully developed profile at the inlet.

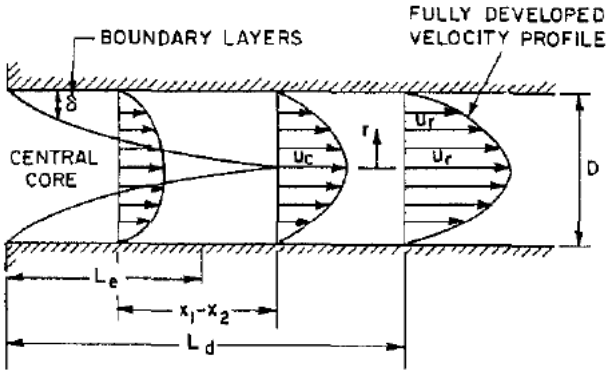

Figure 3.7: Fully developed velocity profile of a fluid entering a pipe given by [1]

Because we restrict ourselves to steady flow, the inlet boundary condition of

the model is easy to implement. We simply use a Poiseuille developed flow computed for the corresponding cross section.

The Poiseuille law, also called the Hagen-Poiseuille law, describes the laminar flow of a viscous and incompressible liquid in a cylindrical pipe. Generally Poiseuille law states a theoretical relationship between the flow rate and viscosity of the fluid, the gradient of pressure at the ends of the pipe, the length and radius of the pipe. The forces applying on the pipe, due to the gradient of pressure between the extremities of the pipe is expressed by:

$$F_p = \Delta p \pi r^2 \tag{3.1}$$

where πr^2 denotes the area of the two extremities of the pipes.

Otherwise, a shearing force is acting on the fluid along the pipe and can be written as follows:

$$F_\tau = -\mu(2\pi r L)\frac{du}{dr} \tag{3.2}$$

where $2\pi r L$ corresponds to the area of outer face of the pipe.

As the flow is assumed steady, there is no acceleration so that the two forces are balanced:

$$\Delta p \pi r^2 = -\mu(2\pi r L)\frac{du}{dr} \tag{3.3}$$

By solving this equation in terms of gradient of velocity, we find that:

$$\frac{du}{dr} = -\frac{\Delta p r}{2\mu L} \tag{3.4}$$

The integration of the equation 3.4 gives the velocity u in terms of r, the distance relative to the center of the pipe [**76**]. Consider that $u = 0$ at $r = R$,

we obtain:

$$u(r) = -\frac{\Delta p R^2}{4\mu}(1 - \frac{r^2}{R^2}) \tag{3.5}$$

The flow rate can be computed by integrating the equation 3.5:

$$Q = -\frac{pi\Delta p R^4}{8\mu L} \tag{3.6}$$

where Δp is the gradient of pressure between the two extremities of the pipe, R correponds to the radius of the pipe, L is the length of the pipe and μ is the dynamic viscosity of the fluid. Poiseuille developed flows, specific to our models, have been implemented into a User Defined Function (UDF). A UDF is a routine in C that codes that are integrated into FLUENT to overcome the limitations of the software for specific applications. Therefore, at the inlet surface, we impose the velocity flow to have a Poiseuille profile according to the inlet cross section.

- One condition that is hard to define is the outlet condition. The carotid bifurcation presents two distinct outlets. It is hard to know the exact distribution among the two branches. The measurement of the velocity upstream the bifurcation might be done by phase contrast MRI or Doppler Ultrasound but it is not a trivial task [39]. The distribution of the flow among the two branches is very much related to the resistance that the network downstream presents, but is not necessarily correlated to the area of the two outlet cross section branches that are reconstructed. It is not said that the branch with the larger diameter will have more flux than the other one. The condition for the two outlets was set to "Outflow". The outflow condition for the outlets was relevant in our

case, since this condition is used to model the fluid outlets which the details of the velocity and pressure at the outlet are not known a priori. If the conditions are unknown at the outflow boundaries, then FLUENT will extrapolate the required information from the interior [4]. Additionally, this condition is not appropriate for the following computations: if the problem involve a condition of type pressure inlet; if the flow is compressible; if the problem is transient or unsteady with variable density. The outflow condition gives us the possibility to model multiple exits or outlets. The distribution among the outflow boundaries is managed by a weigh parameter called the Flow Rate Weighting (FRW). The figure 3.8 illustrates the outflow condition in a case of multiples exits.

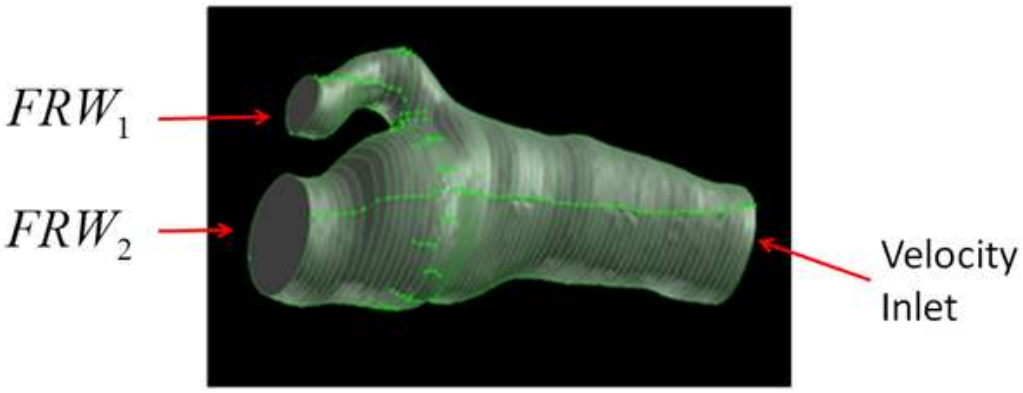

Figure 3.8: Specification of inlet and outlet boundary conditions in FLUENT

The FRW for each outflow boundary is given by the following equation:

$$m_i = \frac{FRW_i}{\sum_i FRW_i} \tag{3.7}$$

A drawback of the outflow condition is that the exact distribution of blood among the carotid artery branches is not known in advance and depends on each patient.

Based on the fluid domain mesh and the corresponding boundary conditions, it is now possible to solve the governing equations for flow motion after choosing the numerical scheme for the solution method and indicating a convergence criterion. In FLUENT, the flow variables, such as velocity, pressure or temperature, that are stored in the center of the cell, must be interpolated to the faces of the control volume and between the values of the neighbor control volumes. It is possible to choose between different discretization schemes for the convective terms of the governing equations. We presented earlier some of the numerical scheme largely used in CFD. FLUENT presents a broad variety of solution methods: first-order upwind scheme, second-order upwind scheme, QUICK scheme, power law scheme. The second-order upwind scheme was the most adequate for our study; it offers us good accuracy and a reasonable computation time. Once the relation between control volumes is set, iterative methods can solve the solution. An iterative solver for a CFD problem seeks to balance the conservation equations of mass, momentum and energy. Starting from an initial solution (boundary conditions), the solver makes it evolve towards a final solution that best respects the various equations. Residuals are defined as a measure of the deviation from a perfect solution. Residuals are the deviation of the value of a variable (pressure, velocity ...) between two consecutive iterations. To confirm that the solution converges properly, the monitoring of the residual is necessary. In FLUENT, the user can specify the convergence criterion of the calculation which is

the criterion that must be checked to stop the calculation. One can either impose a number of iterations or request that the calculation continues to iterate until residuals have not reached a certain value. The convergence criterion by default in FLUENT is underestimated, residuals are all set under 10^{-3}. In our study, we pushed the computation to 10^{-6} precision.

This study was our very first attempt of computational fluid dynamics simulation where we investigated the influence of the size of the mesh on our CFD model in order to provide verification to our method. The computation time for a hemodynamic simulation using our method with a dual core CPU of 2.10 GHz and 4.00 GB RAM will typically take between 15 minutes and 4 hours, depending on the mesh size.

3.3 Results and Convergence Analysis

In the two previous sections, we reconstructed the carotid artery models and defined the boundary conditions in order to solve the flow motion. To achieve this, we used the commercial computational fluid dynamics software FLUENT that can compute a Navier-Stokes flow in the vessel. This software has been previously used to study the blood flow around simplified models of plaque in the carotid artery [45]. The outputs of the CFD simulation provide information on hemodynamic factors not given by medical imaging, such as the pressure and shear stress at the wall.

An important concept in CFD simulations is the verification and validation process. The AIAA Guide provides general procedures for conducting verification and validation in CFD [2]. Oberkampf [73] provides an extensive review of methods and

procedures in assessing verification and validation.

With respect to mathematics, verification aims to analyze the numerical solution of a numerical model while validation, in relation to physics, is to analyze the ability of models to represent a real physical problem. In other words, verification can be seen as a process that intents the correct resolution of equations, while the validation is primarily related to the choice of equations to reproduce a physical phenomenon [86]. The figure 3.9 illustrates the different steps of modeling and simulation and the role of verification and validation.

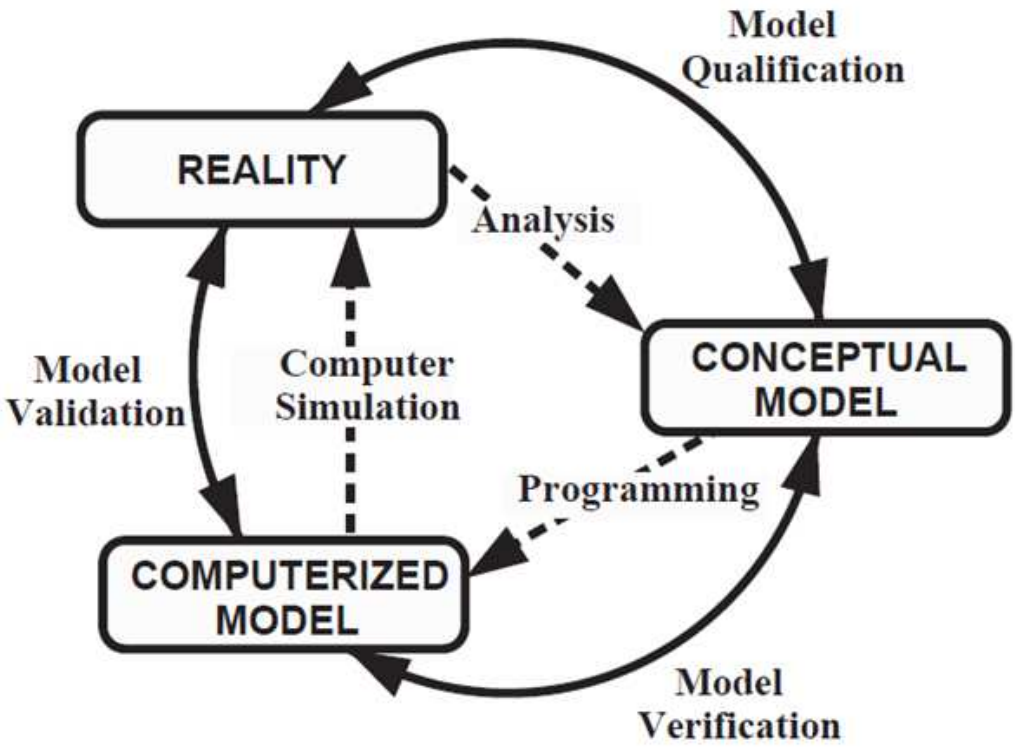

Figure 3.9: Verification and validation process in the implementation of a model given by [89]

Verification is the process that determines whether the implementation of a model and associated numerical methods accurately represents the conceptual description and its solution. The basic strategy of verification is the identification, quantification and error reduction in the numerical model and its solution. Validation is the process that determines the degree to which the model provides an accurate representation of a physical problem. It is therefore to compare precise numerical solutions with experimental or theoretical results.

The main aspect in verification of the solution is to estimate the numerical errors that have three main sources: rounding errors, iterative algorithms errors and discretization errors. The first is due to the finite precision of computers. Errors from iterative algorithms can be due to insufficient convergence. The estimation of discretization errors is performed a posteriori, once the numerical simulation solutions known. A CFD code can only be validated on a set of applications for which experimental data are available. Thus, we rather validate a model, a set of models and simulations rather than code in its entirety.

Some uncertainties come from the numerical solutions of the hemodynamic simulation. For instance, all discretization schemes introduce errors on the solution due to the approximate nature of the polynomial interpolation on which they are based. Errors also appear since there is no exact solution to the Navier-Stokes equations. Nevertheless the accuracy of the computed solution depends deeply on the refinement of the mesh. In principle, a tighter mesh provides a more accurate solution which more closely represents the "true" solution but more resources will be needed for the computer to perform the calculations. The Richardson extrapolation method

explained this perspective [85]. It is based on the systematic refinement of the mesh and the time step for specific problems and assumes that the discretization errors tend asymptotically to 0 when discretization in space and time tend to 0.

In order to verify at least that the numerical computation is reasonable, we did a convergence analysis which is often done in hemodynamic work. This analysis consists of taking fluid flow simulations with uneven number of elements or meshes to study whether or not the results depend on the mesh size. Since we do not know what the exact solution for Navier-Stokes equations is, we take as reference for "true" solution the finest mesh that the computer can manage, and then compare it to coarse meshes in order to plot the error. In our case, the finest mesh contains 1000000 elements.

The comparison of mesh grids with different number of elements cannot be directly performed. As discussed earlier, the flow variables are stored in the center of each control volume. Within this scope, a control volume from a fine mesh will not necessarily coincide with a control volume from a coarse mesh. Such comparison is only possible if the two grids can be described in the same reference space. To achieve that, we used a higher order interpolation tool to project all solution variables at the same point. The most rigorous test for verification of a code is the order of convergence that determines whether or not the discretization error is as expected. The order of convergence can be computed locally in the domain or using a standard error of discretization. Norms L_∞, L_1 and L_2 absolute or relative errors are generally used.

$$\|E\|_1 = \sum_{i=1}^{N} |f_{exact} - f_i| \tag{3.8}$$

$$\|E\|_2 = \sqrt{\frac{1}{N} \sum_{i=1}^{N} |f_{exact} - f_i|^2} \tag{3.9}$$

$$\|E\|_\infty = max_{i=1..N} |f_{exact} - f_i| \tag{3.10}$$

where f_{exact} corresponds to the solution of the finest grid and f_i is the solution of a coarse grid.

p, the observed order of convergence, can be written as follows [97]:

$$p = \frac{ln(\frac{f_3 - f_2}{f_2 - f_1})}{ln(r)} \tag{3.11}$$

where f_1, f_2, f_3 are solutions calculated over grid spacing h_1, h_2, h_3 respectively and r is the grid refinement ratio, $r = \frac{h_2}{h_1}$ or $r = \frac{h_3}{h_2}$.

Therefore, we have realized a convergence study of our simulations with a family of mesh grids with finer and finer mesh size, starting from 100 thousands to one million elements. In the following we will do all comparisons at a cross section of the vessel, immediately before the bifurcation, since this is a rather critical area for flow separation. Figure 3.10 shows an error estimate on the amplitude of the velocity in that cross section with Reynolds number 500, using a mesh grid with 1 million elements as the reference solution.

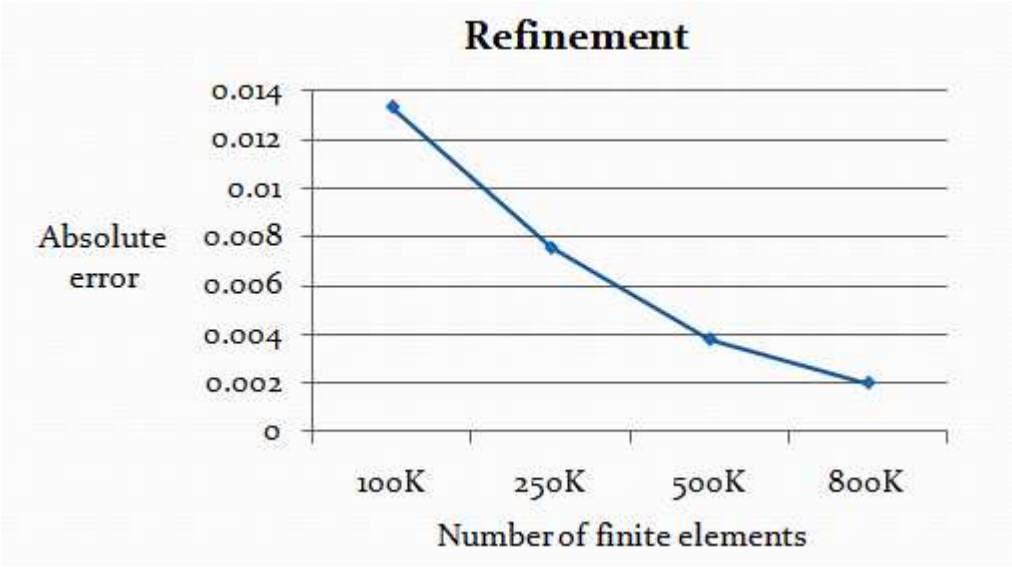

Figure 3.10: Convergence study on the velocity as a function of mesh elements

We observed that the method converge with a nearby second order convergence, which is in agreement with the expectation for the Finite Volume element we chose. This numerical error is relatively small, and confirms that the one million grid solution is satisfactory beyond what is typically used in the literature for such problem. Figure 3.11 shows that the velocity flow profile in the carotid is rather sensitive to the Reynolds number as well as the outlet flow distributions. We have shown here the cross-sectional results of each branch immediately following the bifurcation.

Let us now compute an error estimation on the WSS, notably in the cross section defined above, where the variation of the WSS at the wall is particularly large. All comparisons are now done on a close one dimensional curve that is the boundary of that cross section. We have computed the relative error in the L_2 norm and in

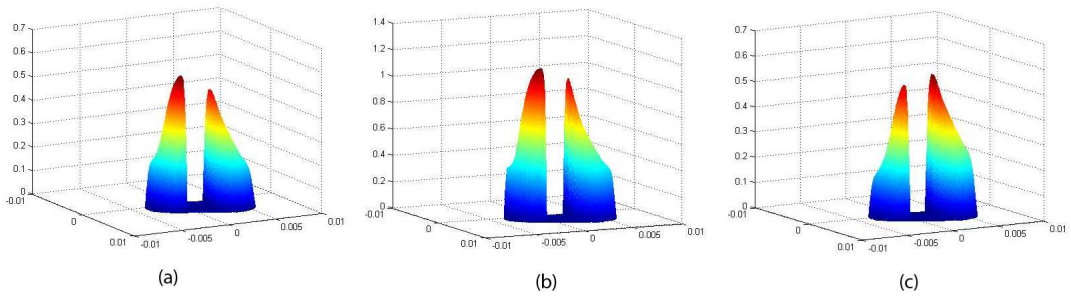

Figure 3.11: Velocity profile with Reynold number 500 for (a) and (b) and 1000 for (c); outlet flow distribution is even for (a) and (c) but uneven with ratio 1/3-2/3 for (b)

the L_∞ norm of the WSS on a section close to the bifurcation, between the selected mesh of reference which is one million elements, and the other meshes. We project the fine grid solution for the WSS on a coarse grid via second order interpolation. The L2 norm relative error for our test cases which are 100K, 200K, and 500K vary from 9% to 3%. The following table 3.1 summarizes our results.

	100K	**250K**	**500K**
L_2 **norm Error**	0.084	0.0422	0.0286
L_∞ **norm Error**	0.7763	0.6029	0.444

Table 3.1: L_2 and L_∞ norm error depending on the number of mesh elements

However, figure 3.12 shows that local errors on the shear stress can be much larger. We intentionally chose a very moderate Reynolds number to present the result, knowing the fact that Reynolds number in carotid can go up a thousand or more in order to show the significant numerical error that one get if the mesh is not fine enough. Since a simulation on a quad core modern PC, with 4 GB of main memory, took

15 minutes for the 100 K elements versus 4 hours for the one million meshes, one should definitively decide to take the time to verify the Finite Element solution with the finest mesh that the PC can handle, which in this case was one million elements. On the other hand, boundary specific layer meshes must be used for larger Reynolds numbers in order to capture correctly the near wall flow variations.

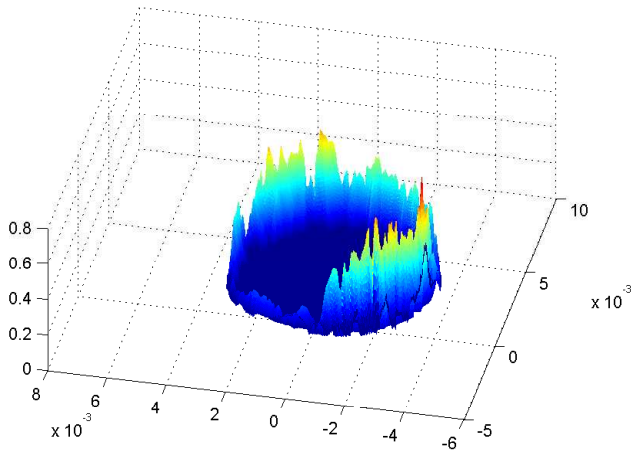

Figure 3.12: Absolute error between 1M and 100K elements

Part III

Dynamic Blood Flow Simulation

Advances in imaging and computer algorithms are developed for the benefit of numerical applications in the vascular system, with the sole intention to determine the real biomechanics. On one hand, the boundary conditions can be derived from medical imaging and are therefore quite realistic. On the other hand, numerical models, more and more sophisticated, provide access to extremely accurate calculations in a reasonable time. The models and methods dedicated to solve the problem of a fluid with surrounding structure have made considerable progress but not yet found the optimal analysis. The question that is often asked is to know whether or not the coupling between fluid and structure occurs. The medical imaging among these methods is then essential. As discussed earlier, fluid-structure problems involve the coupling of fluid dynamics and solid mechanics, which means that the expertise in the two domains is required. Currently the simulation of the human vascular system faces two challenges: the ability to simulate complex structures and their interactions, and the ability to represent the reality in a sufficiently precise manner. There is a particular difficulty specific to fluid-structure interaction problems, which lies in the inadequacy of the description methods for the two sub domains. As explained in the previous chapter, for the solid, we use generally a Lagrangian description, while in the fluid domain the Eulerian approach is better suited. The typical method to handle fluid-structure interaction is to use a Finite Element method called Arbitrary Lagrangian Eulerian (ALE). This method combines the strengths of two conventional approaches. It allow the nodes of the computational domain to move with the material points as in a Lagrangian description or to stay fixed in an Eulerian approach,

but also to be following an arbitrary motion. Several studies have used the ALE approach to study fluid-structure interaction in cardiovascular scenario. For instance, Zhi-Yong Li [58] investigated the blood flow-plaque interaction by implementing the Navier-Stokes equations in the ALE formulation. Other examples of fluid-structure with ALE approaches can be found in [32, 81]. The major drawback of ALE is that remeshing can be necessary in order to guarantee the compatibility fluid-structure interaction. Remeshing is a costly and error prone procedure. In this part, we implemented a technique to handle fluid-structure interaction based on the immersed boundary method from [37].

Chapter 4

Body Motion and Hemodynamic Simulation

We have observed with ultrasound imaging experiments that wall motion is quite unevenly distributed in a carotid bifurcation, due either to non-homogeneous stiffness of the carotid wall in the presence of plaque, or the role of supporting tissue that limit the wall displacement at the internal side and external side differently. In this chapter, we examined the influence and the impact of the wall motion on WSS in the situation of a healthy superior femoral artery that is a much simpler situation to analyze. The method we used to manage fluid-structure interaction was the immersed boundary technique.

The first section focuses on the motion of the arterial wall due to blood pressure. We combined ultrasound imaging and computational fluid dynamics in order to study the blood flow inside patient's superficial femoral artery. The method used to compute

the flow inside the artery is the immersed boundary method. The next section provides an approach to estimate the WSS during the bending motion of the knee. We proposed a simplified model of the superficial femoral artery and solve the Navier-Stokes equations using a fluid flow solver.

4.1 Arterial Wall Motion due to Blood Pressure

One of the limitations of CFD regards the boundary conditions. Until recently, the CFD analyzes were generally confined to blood vessels with rigid walls, based on the assumption that the elasticity of the wall has only a minor effect on the distribution of shear stress [108]. However, the blood vessels are elastic structures that deform under the pressure of blood. This can be modeled by the implementation of fluid-structure interaction. Numerous researches focused on improving the quality of the fluid-structure interaction simulations, correlated with the constitutive law of the artery wall and its surrounding tissue. The compliance of the artery wall plays an important role in regulating the pressure and flow at the tissue level. Integrating the wall compliance into the numerical models does not depend only on accurate fluid-structure solvers but also on the vessels wall properties [46, 50].

Working on MRA images, like presented in the previous chapter, is rather a standard where the use of high definition images to reconstruct the model in 3 dimensions with some accuracy is necessary. The drawback of this technique is that it is quite expensive and takes a long time to perform. Another imaging modality that is more practical is ultrasound, because it is inexpensive and good definition real time 2D

images of vessels can be produced from this medical imaging modality. We showed that in the most simple situation, i.e. a straight section of a SFA monitored by Ultrasound imaging, fluid structure interaction with the artery wall is difficult to predict and will impact the WSS computation significantly. We approached the problem with a two-dimensional approximation that showed the longitudinal cross section of the SFA in a plane perpendicular to the skin to demonstrate our point. Figure 4.1 shows the monitoring of a SFA by ultrasound imaging.

Figure 4.1: Snap shot of an ultrasound image acquisition of a superficial femoral artery

This data set provides a video that shows in-vivo asymmetric motion of the wall, and gives an accurate idea of the time scale and space scale of wall motion. Using an image segmentation procedure that combines image filtering and contrast enhancement followed by an open snake fitting of the wall, we reconstructed the wall motion. Figure 4.2 shows the reconstruction of the internal external walls motion from ultrasound imaging.

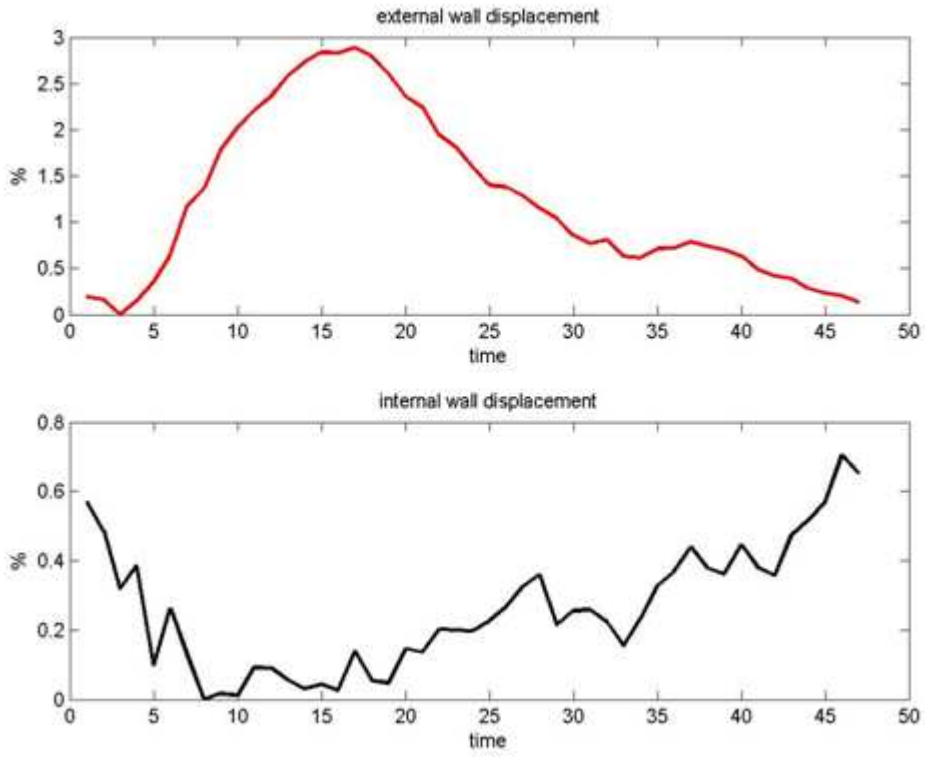

Figure 4.2: Reconstruction of the internal wall (black curve) and external wall (red curve) motion from ultrasound imaging

In this data set the support tissue surrounding the SFA is such that the wall closest to the skin, i.e. the "external wall" has the largest motion while the opposite wall, i.e. the "internal wall" moves very little. Nevertheless, we have observed symmetric wall motion with other SFA ultrasound monitoring data from a different patient. Our preliminary conclusion is that this wall motion is difficult to predict in the absence of an extensive study of the tissue distribution and its material properties. It is however, doubtful that this level of detailed information would be available in routine clinical practice.

Our objective was to investigate the influence of that asymmetrical wall motion on the WSS. Assuming linear elasticity, the input wave form of blood depends linearly on the diameter change. This approximation might be acceptable because of the small displacement observed.

The numerical method used to solve the equation of motion is a domain decomposition technique with immersed boundary conditions adapted to the problem of long vessel structure with time dependent image acquisition such as ultrasound. This technique is a generalization of an image based L_2 penalty method applied to Navier-Stokes [3, 37] and it was applied on the superficial femoral artery. We used the immersed boundary technique in order to compute the shear stress at the wall of a simplified model, a straight pipe, that has wall motion given by figure 4.2, and pulsatile flow accordingly. The pulsatile flow was derived from the analytical Womersley solution [103], which is the function that describes the best the pulsations of the heart. Figure 4.3 shows the velocity profile that was input in our code.

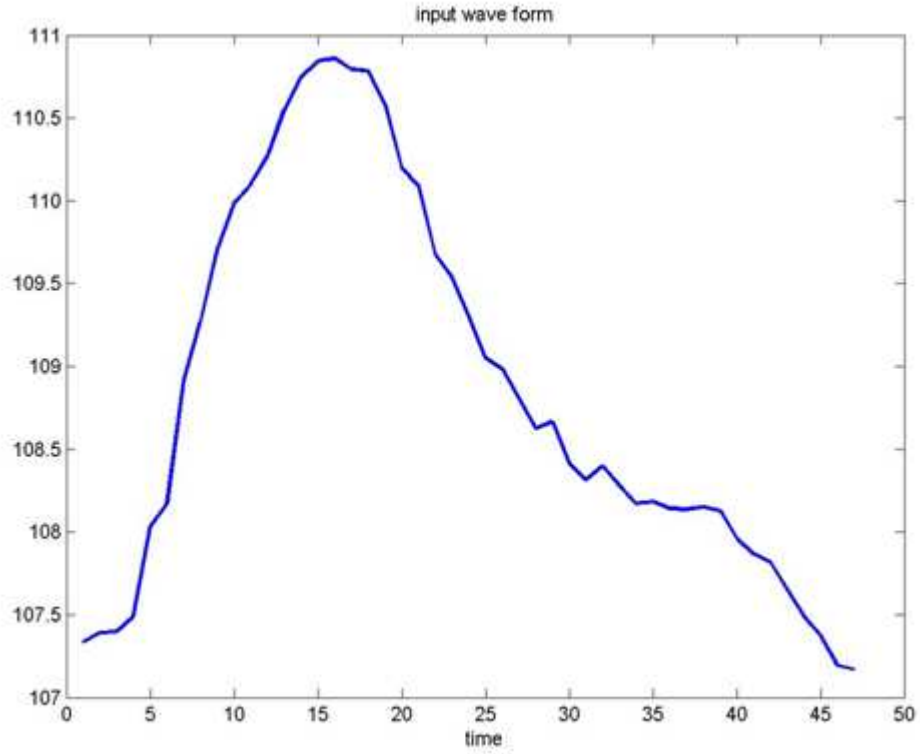

Figure 4.3: Input waveform of the inflow boundary condition that uses an analytical Womersley solution

Beforehand, we checked that the numerical error of our method to compute the WSS with no wall motion is about 2%. Assuming that the wall has uniform motion longitudinally, our results showed a 11% change on the shear stress computation between the external wall and internal wall, which was much larger than the percentage of the relative wall motion. Figure 4.4 depicts the shear stress of the external and internal walls depending on the time.

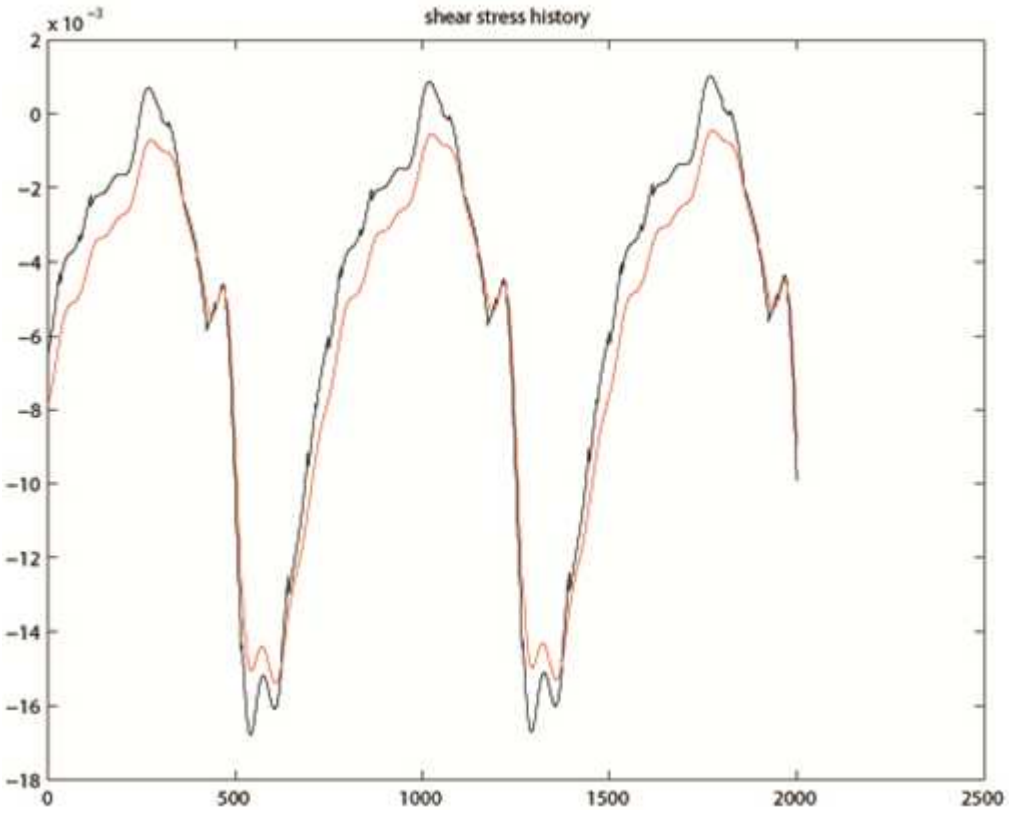

Figure 4.4: Time dependent wall shear stress on internal (black curve) and external wall (red curve) based on the ultrasound video clip

Since the ultrasound clip video monitors only a small portion of the artery, we did the same computation on a longer pipe. With a fixed inlet/outlet size of a 4 cm section of the SFA, the difference on wall shear stress between both walls rose to 16%. The figure 4.5 shows the results of the WSS computation in that situation.

While we restrict ourselves to two dimensional image acquisition and simulation, we speculate that our error estimate would apply to three dimensions. Our conclusion

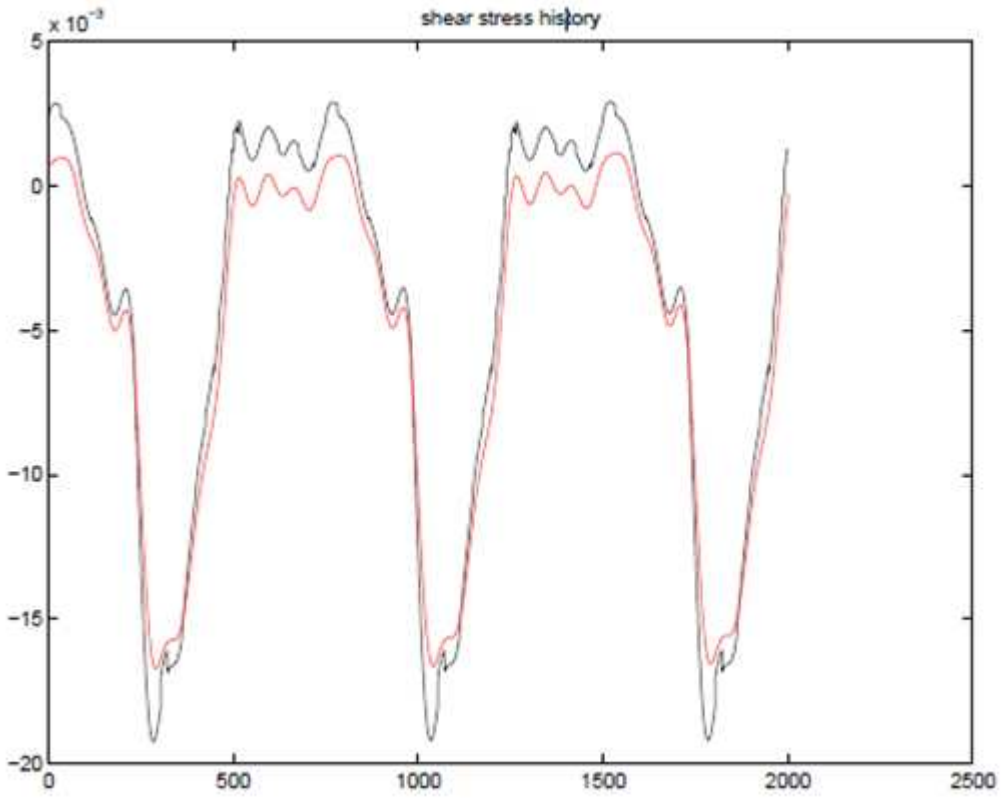

Figure 4.5: Time dependent wall shear stress on internal (black curve) and external wall (red curve) for a 4 cm section of the SFA

is that the level of numerical uncertainties on WSS is significant in the simplest situations that consider a quasi straight section of an artery. Our current work looks at variations of WSS during a physical exercise, such as cycling, which definitively alters the flow properties even further. However, ultrasound imaging in such conditions becomes extremely challenging.

4.2 Bending Motion in FLUENT

As discussed previously, physical exercise is beneficial for cardiovascular health, because it regulates the good functioning of the endothelial cells by stimulating them. The procedure of hemodynamic simulations is usually performed on patients that are in a static position, usually laid down in MRI machine, but the human body is always in motion, even at rest. Although the previous section was investigating the influence of the wall motion due to blood pressure on the WSS calculations, we were interested, in this study, by the impact of the external mechanical forces that apply on the blood vessels. The superficial femoral artery runs through the thigh and connects the popliteal artery behind the knee joint. Therefore, by bending the knee a variety of mechanical forces acts on the SFA such as compression, elongation, and torsion [55]. Figure 4.6 illustrates the diversity of forces that apply on the SFA.

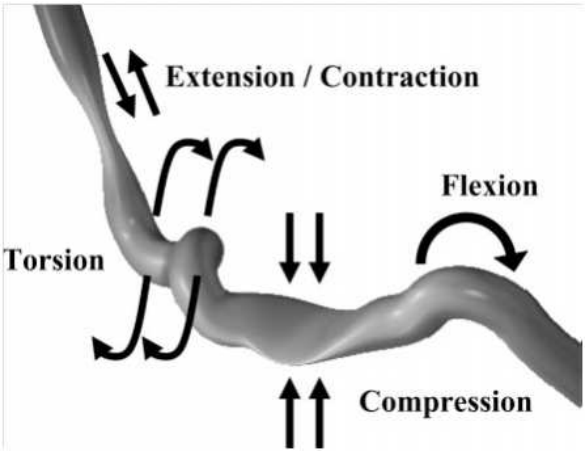

Figure 4.6: The variety of external mechanical forces exerted on the femoropopliteal segment given by [55]

We worked on a simplified model of the superficial femoral artery that was represented by a straight two-dimensional pipe that bends in its middle. When the bending reaches its maximum, the entrance and outlet elevate at 45 degrees. The creation of the bending motion was implemented with MatLab. During the bending motion of the pipe, a compression or pinch was artificially created. Figure 4.7 illustrates the position of the pipe at different steps of the bending motion.

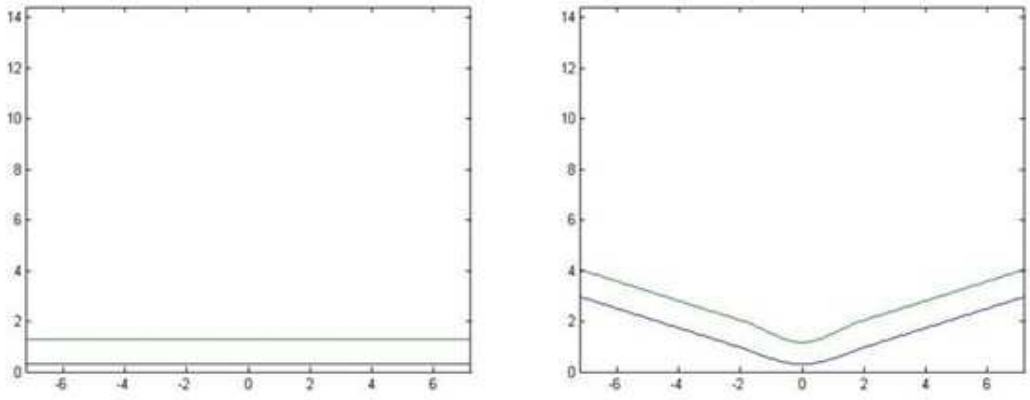

Figure 4.7: Position of the pipe at different steps of the bending motion

At first, we had to ensure that the pipe followed the laws of conservation of volume for each time step. The volume that enters the pipe must emerge. We then studied the flow inside the moving pipe, using the immersed boundary method as seen in the previous section. Our interest in this project was to focus on the calculation of the wall shear stress and to examine the influence of wall motion on these calculations. This scenario presents a domain that has moving boundaries over time. The biggest complication in this problem is the need to have software allowing the flow to move

in such computational domains. Besides the possibility to take into account complex geometries, the mesh that is attached to the model has to be adapted with the deformation of the domain. This mesh adaptation is called remeshing. There are two aspects in the remeshing procedure: the generation of a new mesh and the repair/modification of an existing mesh. This procedure can be performed using software designed for this purpose (Gambit, ICEM), but the procedure is cumbersome and often decisive in the choice of the method of calculation. It is also possible, in simple configurations, to keep the same mesh and only change the coordinates of the points to take into account the deformation of the domain, which is often the case in finite elements applied to the problems of solid mechanics (structural deformation) or fluids dynamics (confined flow). In extreme cases, the mesh can present such distortions due to deformation of the computational domain, that it loses precision or even numerical stability.

Dynamic mesh is mainly used in fluid mechanics when one or more domain boundaries are subject to displacement over time. It is therefore necessary to adapt the mesh to monitor internal nodes of the mesh. Software products known to enable dynamic mesh are FLUENT, Star-CD and OpenFOAM.

The first two are commercial software while the third is open source. It was chosen to use the software FLUENT in order to compute a dynamic mesh for the bending pipe problem. The use of dynamic mesh in FLUENT requires the introduction of user-defined functions (UDF). In our model, the update of the volume mesh is performed at each time step and its generation is dependent on the new positions of the nodes. FLUENT proposes predefined macros to define UDFs that control the behavior of a

dynamic mesh. These macros are: DEFINE_CG_MOTION, DEFINE_GEOM, and DEFINE_GRID_MOTION. The function that was the most appealing to us was the DEFINE_GRID_MOTION because it offered the most freedom for the displacement of the domain. It allows the user to move any nodes belonging to the fluid zones or to the boundary zones. The general syntax for the DEFINE_GRID_MOTION macro is described in the UDF Manual as follows [5]:

$$\text{DEFINE\_GRID\_MOTION}(name, d, dt, time, dtime)$$

where the arguments used are given by the table 4.1:

Argument Type	**Description**
char *name*	UDF name
domain **d*	Pointer to domain
dynamic thread **dt*	Pointer to structure that store the dynamic mesh attributes that are specified or that are calculated by FLUENT
real *time*	Current time
real *dtime*	Time step

Table 4.1: Declaration of the predefined DEFINE_GRID_MOTION macro given by [5]

The approach of this study can be summarized by these following points:

- In Gambit, we create a straight pipe that corresponds to the resting position and attach a mesh to it.
- In MatLab, we create a similar pipe with the according grid at resting position. Then, we apply the bending motion to this pipe. At each time step, the grid

nodes got new positions that are defined by their coordinates (x, y). Subsequently, our MatLab code creates a file that stores the coordinates of all the nodes for that particular time step.

- In FLUENT, at time step n, we read the position of a node and find its corresponding position in the MatLab file. We can then assign the new position of the node based on the MatLab file at time step $n + 1$.

For the last part, a UDF was implemented in order to modify the boundary conditions and manage the dynamic mesh. In order to identify a mesh point position, we used FLUENT macros for node position variables to extract its (x, y) coordinates. Table 4.2 shows the macros for node coordinates.

Macro	**Argument Types**	**Returns**
NODE_X(node)	Node *node	Real x coordinate of node
NODE_Y(node)	Node *node	Real y coordinate of node

Table 4.2: Declaration of the macros NODE_X and NODE_Y given by [5]

Since we did not notice any particular order on how FLUENT loops on the nodes of the grid, for a given time step, we had first to recover the node position variables in order to find a match by browsing in the MatLab file.

As shown on the right graph of figure 4.7, the inlet surface is moving vertically over time which can become an issue if the boundary conditions are not defined accurately. For instance, with the use of a UDF, we had to make sure that the flow at the inlet remained along the pipe direction. Moreover we gave to the flow a parabolic and pulsatile profile. The figure 4.8 describes the pulsatile waveform of the flow.

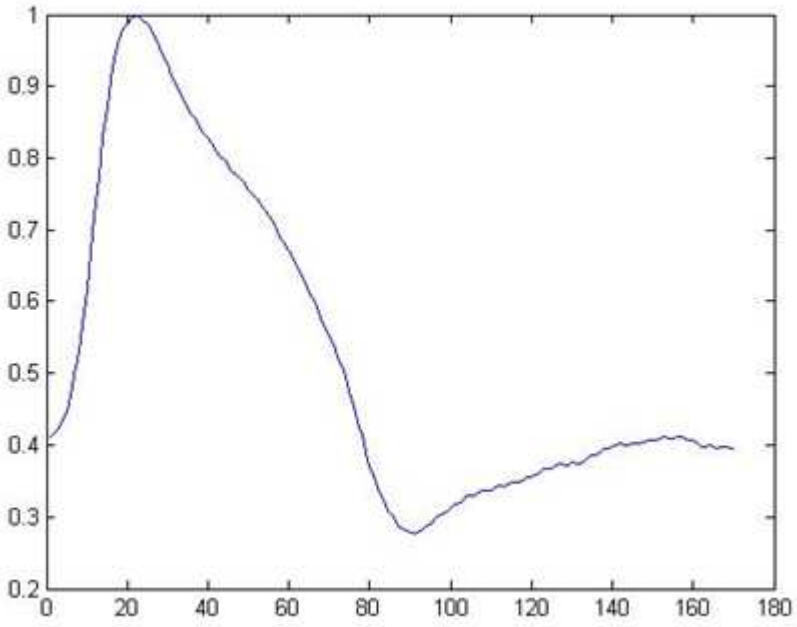

Figure 4.8: Pulsatile input waveform for the inlet boundary condition implemented in UDF

In order to manipulate the parameters for the velocity at the inlet, another macro was modified in our UDF. DEFINE_PROFILE that allows the user to custom a boundary condition profile that varies as a function of spatial coordinates or time. Once the UDF code is written, it can be either interpreted or compiled for use in Fluent. The UDF is then linked to the FLUENT code through the extra commands on the GUI. An interpreted UDF is compiled during the simulation iterations, while a compiled UDF is first built and then loaded in a library ahead of time. Both interpreted and compiled UDFs have their advantages and drawbacks, however FLUENT has some

restrictions on the macro DEFINE_GRID_MOTION: UDFs that are defined using DEFINE_GRID_MOTION can be executed only as compiled UDFs [5].

During this study, we played with the numerical and physical parameters of the bending pipe model. Concerning the physical parameters, the Reynolds number, the speed of the bending oscillation, the pulsatile inlet as well as the narrowing of the pinch can be modified before running simulation. The substantial parameter known as the "Reynolds number" is used to identify and predict different types of flows. The Reynolds number is the ratio of inertial forces and viscous forces and it quantifies the relative importance of these two types of force. A laminar flow is present when the Reynolds number is low, while the viscous forces are dominant, and is characterized by a soft, fluid motion constant. The turbulent flow is dominated by inertial forces, and is present when the Reynolds number is high. The Reynolds number can be written as follows:

$$Re = \frac{\rho u L}{\mu} \tag{4.1}$$

where μ is the dynamic viscosity, ρ is the density of the fluid, L is a characteristic linear dimension (diameter or length), u is the average velocity of the fluid.

For the numerical parameters, different discretizations in space or in time have been studied. However, the numerical scheme for all set of simulations remained the second-order upwind scheme. The properties of the fluid as well as the convergence criterion were defined as in the previous chapter. Figure 4.9 shows the velocity field inside the moving pipe at different time steps.

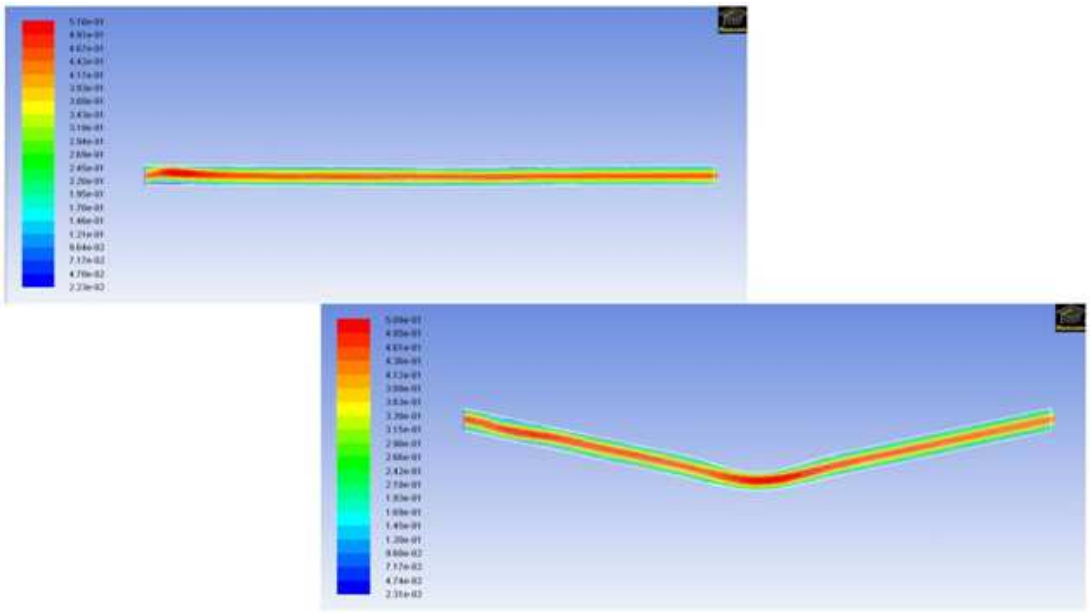

Figure 4.9: Screenshots of the velocity amplitude inside the bending pipe at different time steps, using FLUENT

4.3 Discussion and Conclusion

The goal of this project is to investigate the influence of the bending motion on the computation of the WSS. Our approach was to compare results of two types of simulations: one with a pipe that remains a slightly bended position over time and the other where the bending motion of the pipe takes place. The fixed pipe has its inlet and outlet elevated at 30 degrees. Both simulations were set up as transient or unsteady (time-dependent) since a pulsatile flow has been assigned at the inlet boundary. During simulations in FLUENT, the automatic export of flow variables, like velocity and shear stress, was selected for each time step. The format file of the export was chosen to be Data Explorer because it allows the user to pick from an

extensive list which variables to store and also the delimiters in the created file were convenient for a post-processing. In this way, the WSS values were tracked all along the bottom and top wall of the pipe. The bending motion entailed that the top wall was subject to a stronger flexion than the bottom wall. The computation of WSS results of both simulations are shown in the two following figures 4.10, 4.11.

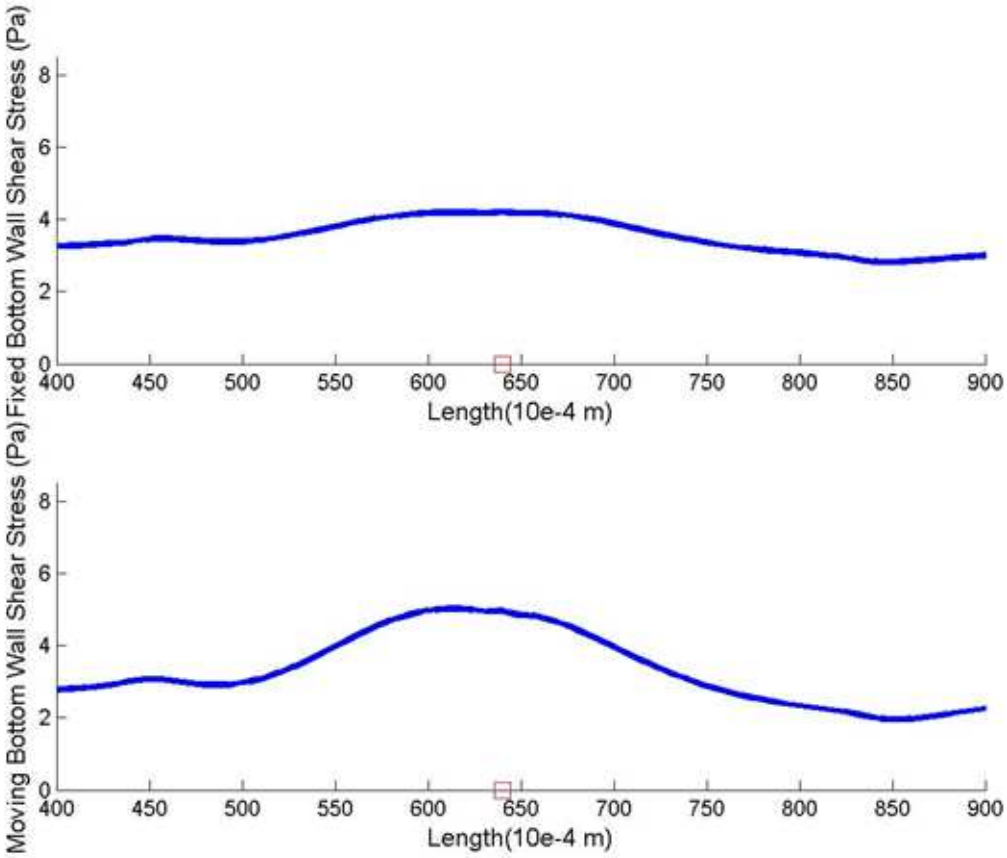

Figure 4.10: Shear stress profile of the bottom wall at the bending joint, upper graph represents the simulation of a fixed pipe while lower graph gives the WSS profile for the moving pipe

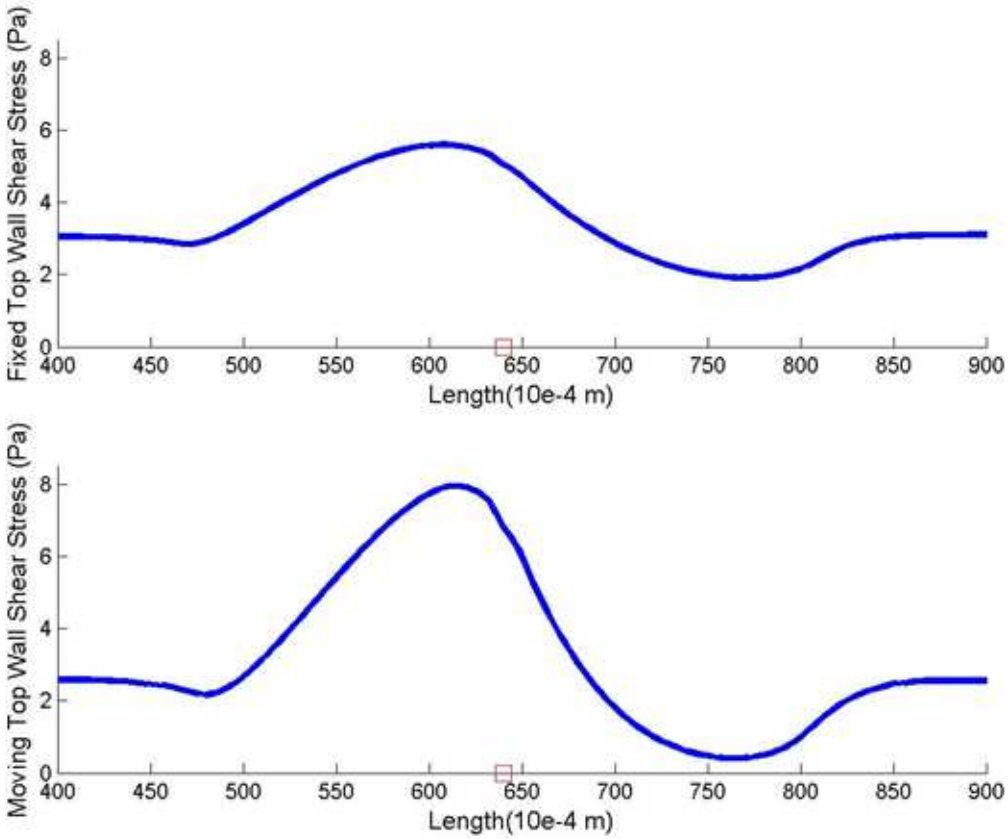

Figure 4.11: Shear stress profile of the top wall at the bending joint, upper graph represents the simulation of a fixed pipe while lower graph gives the WSS profile for the moving pipe

These two figures represent the shear stress amplitude at the two walls in a fixed pipe and a moving pipe. The post-processing of the data has been achieved in MatLab where the FLUENT output files needed to be sorted and compared. We focused our analysis on the region around the bending joint. Based on the WSS profile of the two walls, we calculated the relative errors.The following table (table 4.3) summarizes

some of the results:

Maximum Relative Error	$\alpha = 0°$	$\alpha = 22°$	$\alpha = 45°$	$\alpha = 22°$	$\alpha = 0°$
Bottom Wall	0.42	0.23	0.65	0.32	0.43
Top Wall	0.53	0.28	0.73	0.41	0.54

Table 4.3: Relative error between a fixed pipe and a moving pipe at different angle of elevation

We noticed that depending on the oscillation of the pipe and the input cardiac cycle, the relative error was significant especially at the bending point and the zone right after it, where the shear stress is low.

We observed, in this part, the importance of the body motion on the computation of the WSS with two simple hemodynamic benchmark problems that correspond to important problems in endovascular diseases. These studies emphasize that hemodynamic simulation should be time dependent and consider the motion of the body in the process.

Part IV

Blood Flow Simulation and Particles Tracking

With the improvements of computational tools and the advances in numerical methods, it is nowadays possible to study, in a more rigorous way, the flow of a fluid at a particle level. This analysis can be modeled by multiphase flow as discussed previously. The dynamics of dispersed multiphase fluid is involved in a variety of processes, such as industrial (thermal power plant, fluidized bed reactors...), environmental (dispersion of pollutants, problem of advancing sand dune...), or medical (deposition and migration of cells...). In this context, the numerical experiment is used to analyze a diverse number of problems such as the distribution of particles and their behavior in the vicinity of an interface or a wall. The analysis of particles trajectories belongs to the techniques of visualization. These visualization techniques provide only qualitative information and no quantitative information on the velocity field. In contrast, to visualize flow through the structures (zones of recirculation, vortices, shock waves ...) is very useful for understanding of the phenomena and their modeling. Hence, this is often a prerequisite for a quantitative measure of velocity. As explained previously, we know that the shear stress generated by the blood flow on the vessel wall influences endothelial cell biology. Indeed, around regions of strong curvatures or bifurcation points, where the blood flow is disturbed and the shear stress is weak, the morphology of the endothelium alters, presenting a loss of cell orientation and changes in cell shape. However, in arteries where the flow is laminar and the shear stress is normal, endothelial cell morphology is elongated as if the cells are adapting to the shear forces between them and the circulating blood [24].

In this research, we were interested to study the flow and fluid particles in the problem of vein graft failures. Angioplasty and vein bypass grafting are common procedures to treat occlusive diseases in the lower limbs even if they are known to have shortcoming issues. Restenosis is the most frequent complication after these surgical procedures. This chapter presents the study of the vein graft of several patients that went under surgery to alleviate their occlusive disease. The computational tools used to examine the particles was the Discrete Phase Model (DPM) in FLUENT.

Chapter 5

Vein Graft Study

In this chapter, we present the vein graft study where we used the fluid flow solver FLUENT to compute particles trajectories. We first give a background on the vein graft failures and the restenosis process. The second section introduces the vein graft study and the method used to track particles. Finally the last section discussed about the results of the large set of simulations.

5.1 Vein Graft Failure

As discussed previously, bypass vein grafting is an invasive surgical procedure to revascularize the superficial femoral artery. The bypass consists of deriving the blood by inserting a conduit between arteries located on either side of the affected artery. This tube may be a piece of vein (saphenous vein) taken from the patient or a prosthetic graft. In the lower limbs, the vein graft failures can be divided into three

temporal phases [61, 75]:

- During the first postoperative month, it is the early phase that depends on the surgery. During this phase, a thrombotic occlusion can occur inside the graft (which happens in $5 - 10\%$ of cases) due to either technical errors or endothelial damage related to graft manipulation during its collection, which will cause deposits of fibrin and platelets responsible for a local thrombosis.

- Between the third and twelfth month after operation, it is the intermediate phase. Lesions of fibro muscular hyperplasia occur during this period of adaptation of the vein graft to his new position. This proliferative process may be exaggerated and lead to stenosis of the graft.

- Finally, the late phase that occurs after the first postoperative year occurs as a progressive intimal fibrosis. The development of atherosclerotic plaques in the wall of the vein will gradually lead to thrombosis of the degenerated bypass.

The figure 5.1 illustrates and explains the different steps that lead to the vein graft failure.

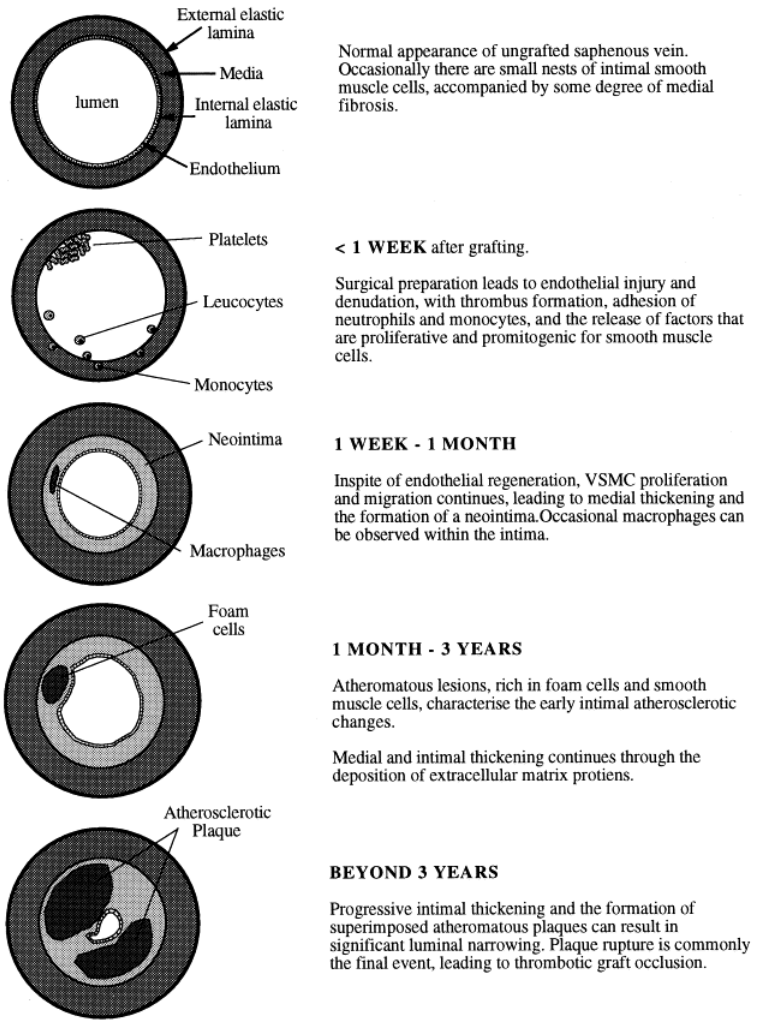

Figure 5.1: Mechanism of vein graft failure by [64]

This intervention has shown an initial satisfactory success rate with a low risk of complications. However, restenosis and occlusion can still occur in the time frame of months to years [31]. Restenosis is the re-narrowing of the artery that occurs in some patients who underwent angioplasty or bypass vein grafting. Restenosis happens when an artery narrows again due to overgrowth of scar tissue on the inner wall

of the artery. This overgrowth of scar tissue appears in some individuals during the process of healing of the artery. The proliferation of scar tissue may form at the site of intervention and appears in some patients within six months after treatment. Two aspects are predominant in the mechanism of restenosis, one resulting from intimal hyperplasia at the dilated site (by migration and proliferation of smooth muscle cells from the media to the intima associated with an increased production of extracellular matrix), the other comes from a constrictive remodeling of all structures of the arterial wall contributing to the reduction of late global caliber of the artery.

Vascular remodeling is a fundamental mechanism of adaptation of the vessels. It is often beneficial in the development of atherosclerotic process by delaying the reduction of vascular diameter. It sometimes exceeds its role by participating essentially in the restenosis after angioplasty or bypass procedures. To date, the mechanisms of vascular remodeling are poorly understood. Considering enlargement or narrowing, the remodeling is primarily a change in the structure of the vessel. Schwartz [90] conducted a study on the pathophysiology of restenosis and the leading causes of restenosis: vascular remodeling, thrombosis, and intimal hyperplasia. It has also been shown in [42] that hemodynamic forces such as wall shear stress and wall tension have been recognized as major factors impacting vein graft remodeling. Other researches approach the problem of intimal hyperplasia by studying the blood particle stasis and blood particle deposition. It is in this perspective that we started our vein graft study.

5.2 Presentation of the Study

This study has been initiated in the scope of understanding the development of restenosis and the events leading to vein graft failures. Patients who had a revascularization surgery are generally followed clinically. The purpose of the follow-ups is to ensure the graft patency to limit the risk of amputation. Strict control of cardiovascular risk factors is essential to prevent restenosis and limit the progression of atherosclerosis. Continual smoking after revascularization is the major risk factor for occlusion of bypass and triples the risk for vein graft as well as for prosthetic grafts [102]. The clinical exam is essential for surveillance and to assess the functional activity of the patient. It consists of pulse palpation and measurements of the pressure at the ankle. Although this exam is important, it does not guarantee the absence of stenosis or pseudoaneurysm of the bypass [67]. In this case, it is not uncommon to highlight, with ultrasound Doppler, lesions of the anastomosis upstream and downstream that could threaten graft patency. Other diagnostic tools, such as MRI and CT, provide detailed information to detect early stenosis.

Our vein graft study gathers a total of 23 patients that went under bypass vein grafting surgery of the femoral artery and had postoperative monitoring. The frequency of the clinical follow-up examinations was established to 1 week, 1 month, 6 months and 12 months. However, the data for the examination at 12 months were not accurate enough to be able to analyze them. During their revascularization surveillance, a series of CT scans have been acquired for each patient. Ultrasound Doppler examination has also been performed in order to record flow information. Hence, the flow rate at the inlet of the vein graft is known for each patient. The

segmentation and the reconstruction of the three-dimensional models of the femoral artery have been completed using the Vascular Modeling Toolkit (VMTK) software [7] and stored in STL (STereoLithography) files which contains information on the model surface. All these data have been kindly provided by Dr. Berceli's group, from University of Florida. The figure 5.2 shows some of the 3D vein graft models that have been reconstructed.

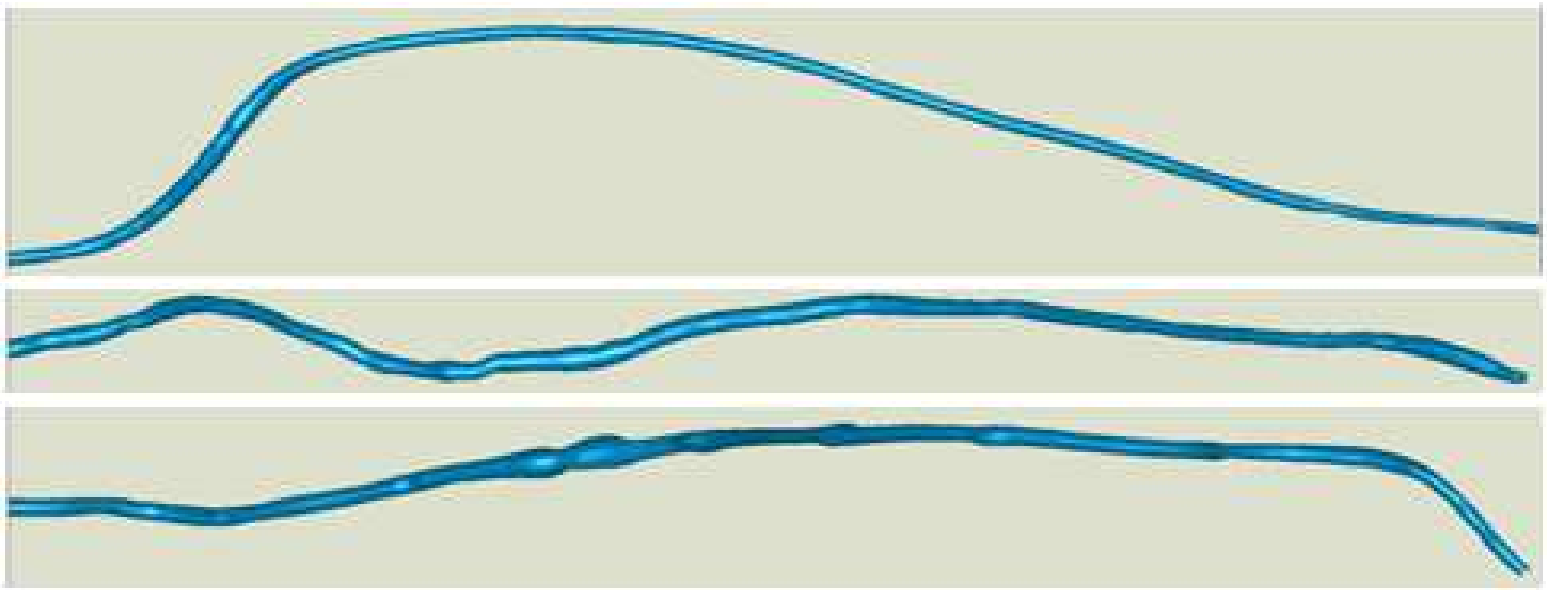

Figure 5.2: 3D reconstruction of vein graft models based on specific patient data

The whole set of vein graft models has been preprocessed in VMTK and MatLab in order to derive features that would be useful for the output analysis. This includes the extraction of the skeleton or centerline of vein grafts and the creation of cross-sectional surfaces normal to the centerline. The predefined function to compute centerlines in VMTK is vmtkcenterlines. This script takes as argument a surface and estimates centerlines. The following code is an example of the usage of the vmtkcenterlines script applied on the grafts of our study.

vmtkcenterlines -ifile vein_graft1.stl –pipe vmtkcenterlinesmoothing -i @vmtkcenterlines.o -iterations 100 -factor 0.05 –pipe vmtkcenterlineresampling -i @vmtkcenterlinesmoothing.o -length 1 -ofile vein_graft1_centerline_... vmtk.dat

The surfaces normal to the centerline have been then determined in MatLab based on the vein graft data and centerlines coordinates. The first step was to extract the face and vertex data from the STL files. Then, the MatLab code computed the normal vector to the centerline direction at each particular point of the centerline.

Another preprocessing step was the creation of inlet and outlet extensions for easy implementation of the boundary conditions. Inlet and outlet were extended by straight tubes that were depending on the shapes of the surfaces.

Some studies have focused on the flow residence time, in particular the particle residence time, in thrombus formation, especially near the arterial walls [9, 84]. By obtaining cross-sectional surfaces of the vein grafts, we aim to study locally the

change in area, the WSS and the deposition of particles, between the clinical follow-up examinations.

5.3 Simulation with Particle Tracking, Discrete Phase

As explained previously, FLUENT has the capability to model particles movement through multiphase flow. In this model, the fluid phase is treated as a continuous phase approximated by Euler-Euler method by solving the equations of Navier-Stokes whereas for the dispersed phase, a number of particles, bubbles or droplets, is followed by a Lagrangian description. DPM can simulate the exchange of energy, mass and momentum between the dispersed phase and the fluid. In flows in which the volume fraction of the dispersed phase is less than or equal to 10%, DPM is the appropriate model.

The dispersed phase consists of particles of spherical shape. In this study, we were interested to release around 10000 particles from the inlet surface and to track particles along the vein graft. We chose this large number to study how the particles flow and behave in the continuous phase. Releasing only few particles would not have a significant meaning for this study.

In order to track particles in the continuous phase, they need to be injected inside the computational domain. FLUENT offers several ways to create injections of particles. The different types of injections are: single, group, cone, surface, etc. They are all described thoroughly in [4]. However each type of injection presents some

disadvantages. In our first attempt, we used the surface injection type to release the particles at the inlet surface. With this approach, we were limited on the number of particles since the number of released particles is dependent on the number of mesh elements there are at the specified surface (particles are injected at the centroid of mesh element). If the distribution of the injection cannot be described by the different kinds of injection, FLUENT has the possibility to read external files that contain particle initial conditions such as position, velocity, diameter, temperature, and mass flow rate, to overcome the limitations of the injection types. In this perspective, we created a file containing the necessary information to release about 10000 particles at the inlet surface of the vein graft.

First, we had to make sure that all the inlet surfaces of all the vein graft models were aligned in the (x, y) plane. We performed this task by using the volume align option in Gambit (figure 5.3).

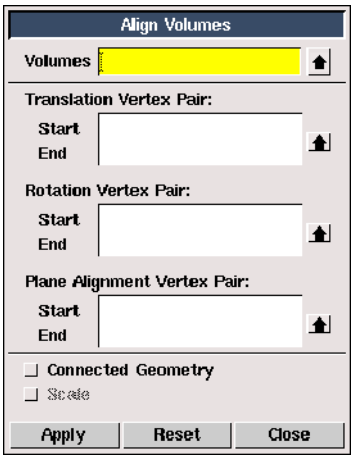

Figure 5.3: Screenshot of Gambit window for aligning volumes where the translation, rotation and plane alignment should pair a vertex from the intlet surface to a vertex on a the (x, y) plane

This preliminary step was completed in order to simplify the problem of the injection file by restricting the position of injected particles to a 2D (x, y) plane. By extracting the new position of the inlet surfaces, we created the coordinates positions of release points for the particles. Therefore, based on the position of the injection release points and the patient information, we created files containing the particle initial conditions. The following lines of code give an example of the kind of files created:

((positionX positionY positionZ velocityU velocityV velocityW diameter temperature mass-flow)name_injection:#_particles)

((-7.491436e-004 1.292297e-003 5.000000e-004 0.000000 0.000000 1.060000 0.000002 293.000000 1.136341e-002)injection0:0)

((-7.491436e-004 1.324835e-003 5.000000e-004 0.000000 0.000000 1.060000 0.000002 293.000000 1.136341e-002)injection0:1)

((-7.491436e-004 1.357373e-003 5.000000e-004 0.000000 0.000000 1.060000 0.000002 293.000000 1.136341e-002)injection0:2)

We noticed that Gambit and FLUENT do not have the same precision. When we imported a Gambit mesh into FLUENT, some uncertainties occurred on the position of surfaces. The most notable case was the alignment of the inlet surfaces of the vein grafts. When the alignment procedure in Gambit was completed, the inlet surfaces were only defined in (x, y) plane which means that all points that belong to the inlet surfaces have their z-coordinates, $z = 0$. However, when the same models are then imported into FLUENT, the inlet surfaces appear to have their z-coordinates varying between $\pm 5e^{-8}$. This uncertainty problem can lead to particle issues because if the release point of a particle is outside of the domain, the particle is considered lost and

is not taken into account in the computation of the discrete phase. In order to not lose too many particles at the inlet surfaces, we specified the release points of the injections, not at the exact inlet surface, but inside the inlet extensions.
A new type of boundary condition becomes available for the discrete phase when using DPM model. By enabling DPM in FLUENT, the interaction of particles with the computational domain walls can be set up. The behavior of a particle that hits the walls can be defined as:

- Reflect. The particle rebounds on the wall with a certain angle that is customizable by the user. In general, the angle of the rebounds will depend on the trajectory of the particle before it bounces on the wall.
- Escape. When a particle encounters a wall that has the "escape" boundary condition, it vanishes and the trajectory calculations for that particle are terminated. This "escape" condition is assumed by default for all flow outlets.
- Trap. If a particle hits a wall, the particle will stick to it, and the computation of the particle trajectory is terminated.

We chose the "trapped" option for the discrete phase boundary condition since we want to investigate the impact of the particle deposition on the WSS computation. However, this "trapped" condition is a very simplistic approach and does not relate the reality. Red blood cells, white blood cells, or platelets usually do not stick to the arterial walls as soon as they touch them, but rather roll along them. That is why an expertise in that field is necessary to be able to model accurately the behavior of blood cells in the vicinity of the walls.

5.4 Discussion and Conclusion

With the large numbers of simulations to run and the extensive amount of data resulting from these simulations, we came up with a concept of a spreadsheet.
This document gathers:

- all the information of the patients:
  - Patient identification
  - Frequency of the clinical follow-up examination: 1 week, 1 month, 6 months
  - Mean velocity at the inlet
- all the preprocessing data
  - Length of the vein grafts (computed from the centerline of the grafts)
  - Cross-sectional area along the vessels
  - Curvature of the vein graft skeletons
- all the outputs of the CFD simulations
  - Wall shear stress
  - Particle residence time
  - Particle velocity (minimum, maximum, average)
  - Counts of particles for different status (escaped, incomplete and trapped)

The purpose of a bypass vein grafting and angioplasty procedures is to reestablish the flow in or around a constricted or obstructed vessel of the vascular system. The clinical follow-up examinations aim to identify differences in the vascular remodeling over time. Mechanical forces play an important role in the vascular remodeling. Our current study focuses on the analysis of the WSS computation, the changes in cross-sectional area along the vein grafts, and the particles deposition in order to find a correlation between them.

We started to investigate the data and gave a global analysis.We were particularly interested in singular phenomena where particle rate deposition and shear stress are disconnected.

We divided the vein grafts into segments of one centimeter in order to study locally WSS, area and particle deposition related. We looked first for segments where there was high particle rate and an average wall shear stress (figure 5.4).

From the selected particles, we then highlighted the relation between wall shear stress and area. Our hypothesis is that early sign of vein graft failures has multi-factorial origins: our goal is to construct a statistical indicator of early sign of vein graft failures, with no a priori further assumption, from an extensive database that gathers anatomic reconstructed from CT and fluid dynamic data obtained by standardized Navier-Stokes flow simulation. It should be a step by step process that selectively adds those additional measures that improve prediction. Eventually biological lab data that are accessible in the clinic will be considered.

We can extract from the 3D reconstruction, the skeleton of the vein graft, its main

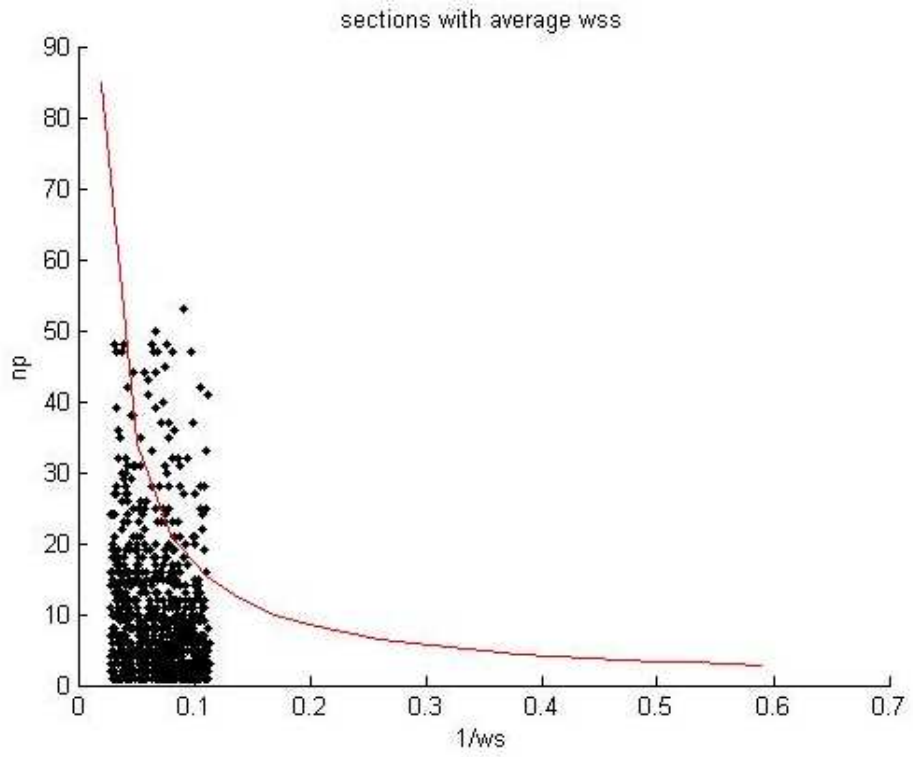

Figure 5.4: Behavior of the wall shear stress depending on the number of trapped particles for selected vein graft sections

curvature, and each cross-sectional area. Computational fluid dynamics simulations were performed and some massless particle tracking was done to track trajectories. We have computed standard output such as pressure, main velocity, and wall shear stress, as well as a large data set of particle trajectories.

For the later, we have computed the distribution of particle residence time in each vein graft section as well as the particle rate deposition.

To be more specific, the vein grafts have been divided into small segments of 1 centimeter in order to study locally the flow and the particle deposition. The whole set

of vein graft models has been preprocessed in VMTK and MatLab in order to derive features that would be useful for the output analysis. As mentioned earlier, this includes the extraction of the skeleton or centerline of vein grafts and the creation of cross-sectional surfaces normal to the centerline.

Overall we did not intend to compute realistic hemodynamic in the vein graft that would reflect the exact flow condition in the vein graft. In fact all simulations are performed in steady state, with inlet boundary conditions that correspond to ultra sound measurement for each patient during the clinic exam, and free outlet boundary condition. The point is that such simulation should show how anatomy translates into mean flow conditions through the Navier-Stokes operator: our hypothesis is that failure of vein graft should be correlated to multiple CFD indicators in a non-trivial way, and that we can recover the best possible correlation with the proper optimization method.

In the following, we will review step by step the preliminary results we have obtained from this perspective.

But let us first do some observations of the dynamic of the anatomy of the vein graft we have collected.

As a first attempt to understand where the vein graft failures occur, we analyzed local and global remodeling of the grafts. Figure 5.5 shows the global remodeling depending on the local remodeling for the different vein grafts.

The global remodeling considers the average change in area while the local remodeling takes into account the stronger stenose of the vein graft.

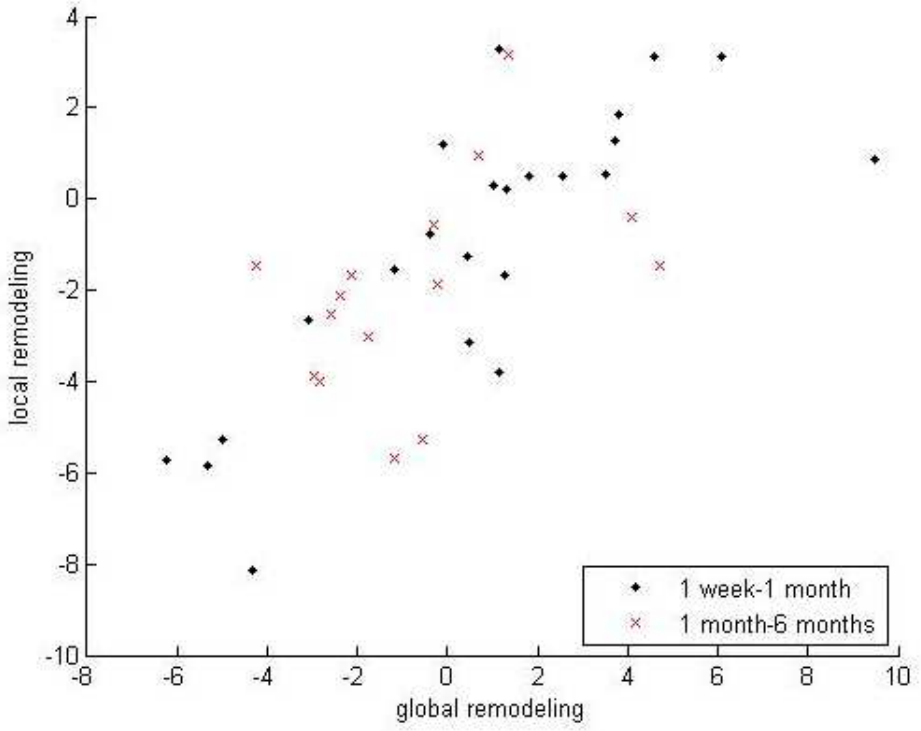

Figure 5.5: Global remodeling versus local remodeling for early stage (1 week to 1 month) and transient plasticity (1 month to 6 months)

From this data, we computed two statistical indicators, the coefficient of determination and the correlation coefficient.

The first coefficient is a measure by which to judge the quality of a single or multiple linear regressions. On a value between 0 and 1, it measures the match between the model and the observed data.

The correlation coefficient is a statistical coefficient to highlight a connection between two types of data sets. It is the square of the coefficient of determination [23, 95]. Although the correlation coefficient is a powerful tool in statistics, it has also its

limitations. The data may be described by a curve more complicated than a straight line, but this will not show up in the calculation of R. Outliers strongly influence the correlation coefficient. If we see any outliers in our data, we should be careful about what conclusions we draw from the value of R.

In the following we will define as early stage the clinical outcome at 1 week and 1 month. We will call transient plasticity the change from 1 month to 6 month.

Therefore, we computed first the indicators for early stage, between the 1 week and 1 month follow up examinations. We observed a strong relation between parameters, R^2 or coefficient of determination gives a 0.6411 and R or coefficient of correlation equals 0.8007.

The computation of the coefficients for "transient" plasticity, between 1 month and 6 months follow up examinations is shown as follows:

- R^2 or coefficient of determination = 0.1886
- R or coefficient of correlation = 0.4343

These numbers indicate a rather weak relation between parameters.

From these results, we observe that at early stage, the vascular remodeling happens on a global scale but later on the vascular remodeling should occur at specific location of the vein grafts.

We are now going to report on the method we have use to take advantage of CFD indicators versus vein graft failure.

The interpretation of the correlation coefficient is given by the following table 5.1:

Correlation	Negative	Positive
Weak	-0.5 to 0.0	0.0 to 0.5
Strong	-1.0 to -0.5	0.5 to 1.0

Table 5.1: Range and interpretation of the correlation coefficient value

5.4.1 Methods

The outputs of the CFD simulations, that we consider, are the Wall Shear Stress (WSS), the area of each section and the number of particles that are trapped by the wall.

We built a matrix that gathers this information. The goal is to statistically analyze the results on flow simulation / particle deposition for the vein grafts regarding the vein graft remodeling.

Our method can be divided into the following main parts:

1. Computation of the WSS and the number of particles for each segment, for each vein graft and for each time point.

2. Segment of vein graft are treated as independent data sets.

3. Use a parameterized non linear model in rational form $\frac{1+\alpha x}{\beta+\gamma x}$ to take into account a saturation effect.

4. Optimize the fit of the non linear model in order to get the best correlation with data: we use R, the coefficient of correlation, as criterion.

In order to improve the fitting, we further investigate if the data set should be decomposed in several characteristic sub sets or not. Therefore, we proceed as follows:

5. Cluster the data sets (WSS, number of particles and area) with respect to WSS or WSS and number of particles, or all.

6. Compare the best fit for early remodeling or transient remodeling with the corresponding cluster provided by 5.

The information given for each cluster is: the position of the centroid of the cluster (5), the number of elements in a cluster and the best fit for the coefficient of correlation (6). Eventually we can use other models or other parameters as well as different distance for clustering.

The analysis can focus on the early plasticity (between 1 week and 1 month), the "transient" plasticity (between 1 month and 6 months) or on the overall. Two parameterized models have been implemented in order to find the best fitting of the data set. Both models are non linear function. The first model takes only into account the WSS, while the second model takes into account WSS and number of particles.

The first non linear model to fit the data set considers only the wall shear stress. It is given by:

$$x = \frac{1 + \alpha_2 \overline{WSS}}{\alpha_1 + \alpha_3 \overline{WSS}} \tag{5.1}$$

where $\overline{WSS} = \frac{WSS_{local}}{Max(WSS)}$.

The second model estimates the best fitting by regarding WSS and the number of trapped particles. It is defined as follows:

$$x = \frac{1 + \alpha_2 \overline{WSS}}{\alpha_1 + \alpha_3 \overline{WSS}} \cdot \frac{1 + \alpha_4 \overline{NP}}{1 + \alpha_5 \overline{NP}} \tag{5.2}$$

where $\overline{NP} = \frac{NP_{local}}{Max(WSS)}$, NP represents the number of particles trapped by the wall.

5.4.2 Results

1. Non linear or linear fitting for early and transient plasticity do not make much difference.

	Linear	Non linear
Early remodeling	$R = 0.5303$	$R = 0.5325$
Transient remodeling	$R = 0.4253$	$R = 0.4324$
Overall	$R = 0.4317$	$R = 0.4426$

Table 5.2: Values of R for linear and non linear model at different time points

2. Taking into account the number of particles for early stage makes no difference.

Linear	Non linear with WSS	Non linear with WSS and NP
$R = 0.5303$	$R = 0.5325$	$R = 0.5363$

Table 5.3: Considering early remodeling, values of R for different non linear models, the first one takes into account only WSS while the second regards WSS and the particle deposition rate

3. For transient plasticity:

Linear	Non linear	Non linear Cluster 1	Non linear Cluster 2	Non linear Cluster 3
$R = 0.4253$	$R = 0.4324$	$R = 0.8940$	$R = 0.7629$	$R = 0.3713$
# elements = 663	# elements = 663	# elements in cluster = 8	# elements in cluster = 69	# elements in cluster = 586

Table 5.4: Considering transient remodeling with fitting model based on WSS and particle deposition rate, values of R for the 3 clusters of different sizes

First of all, we can see that good correlation between mechanic properties, such as WSS and number of trapped particles, and vascular remodeling is missed in the transient plasticity as well. It is even slightly worst than in early stage. Clustering the data set should pinpoint the local character of remodeling.

Cluster 1 shows good correlation however the number of elements is very low but it also corresponds to the artifact on the particle deposition. As a matter of fact, the inlet boundary condition is build using a straight pipe extension of the vein graft upstream. Unfortunately this extension set a singularity on the curvature at the junction with th evein graft. While this is a standard technique for velocity and pressure that does not suffer from that defect, particle deposition rate at the wall, is indeed very sensitive to that local curvature singularity.

The cluster analysis alows us to take out from our data sample, automaticaly those artifacts of the method.

Cluster 2 gathers 69 particles and the fitting criterion improves significantly. This cluster seems to collect automaticaly those set of data where interaction between WSS and particle deposition is significant.

As for the cluster 3, it presents similar results to the all data set with no clustering. These data points seem to provide a fairly random distribution of WSS versus particle deposition.

Once again, it is interesting to notice that the cluster analysis automatically selects those segments of the vein graft where a multi-factorial analysis that takes into account both WSS and particle deposition rate makes a difference.

The graph below is representing the best fit non linear model for the cluster 2.

Further we observe that the best fitted model for the interesting cluster 2 does exhibit indeed a threshold effect on shear stress dependency (figure 5.6).

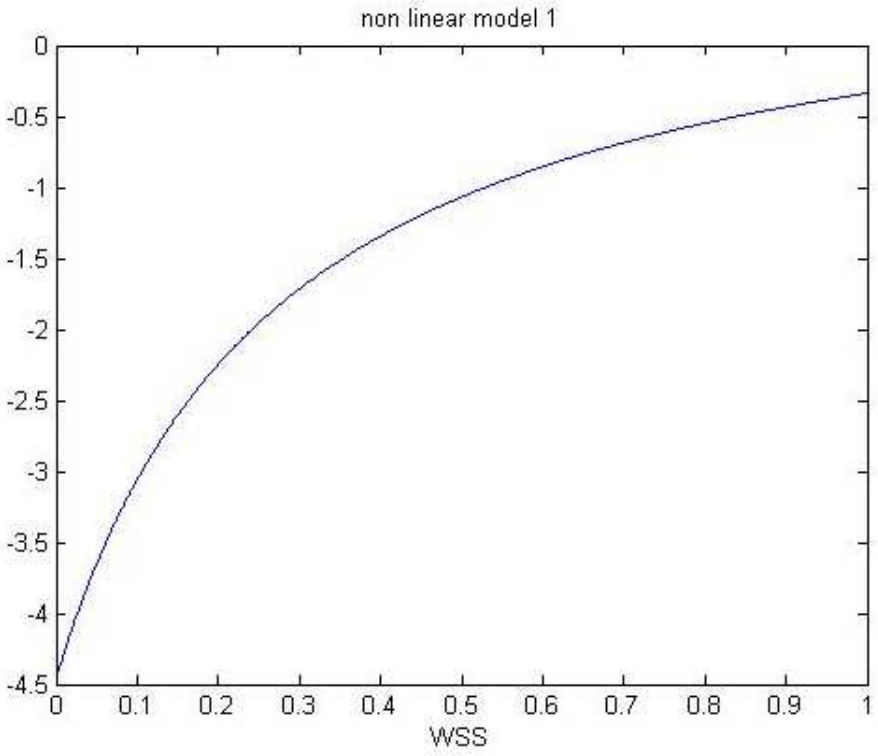

Figure 5.6: Best fitted non-linear model for the cluster 2

However we remark that the model does not take into account the positive remodeling.

The following graph represents the 3 differents clusters. Their wall shear stress is shown accordingly to the number of particles. Clusters 1,2, and 3 appear respectively in red, black, and blue. As discussed previously, cluster 2 (black squares) presents a

strong correlation of the data set but also shows a broad range in WSS values with a high number of trapped particles.

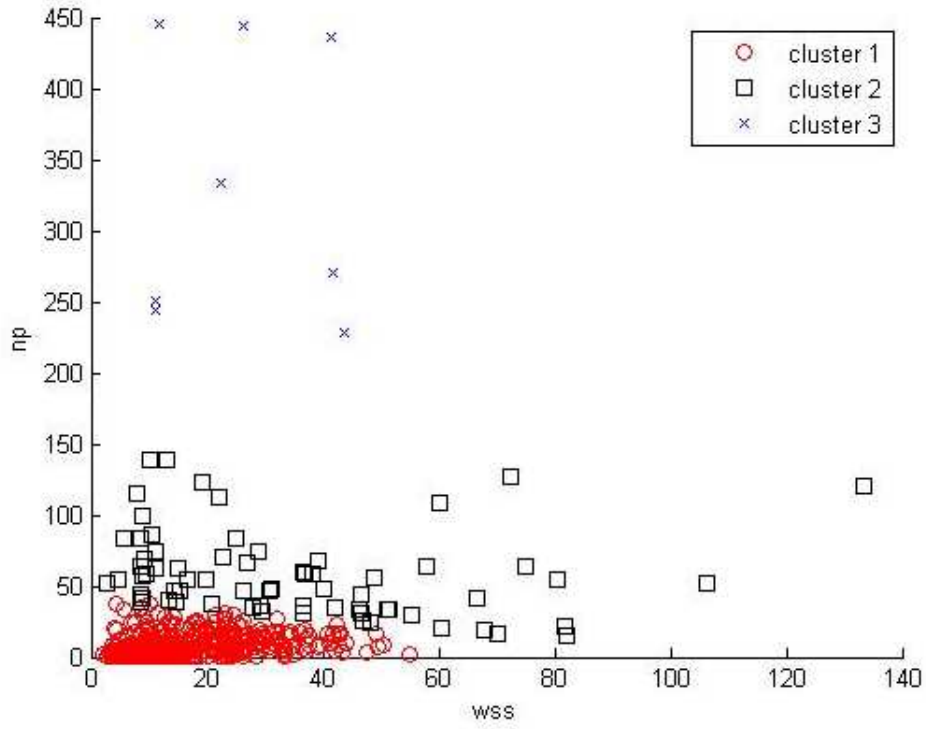

Figure 5.7: K-mean clustering technique for the patients data set

4. The following graph shows for each vein graft with normalized coordinates in the longitudinal direction.

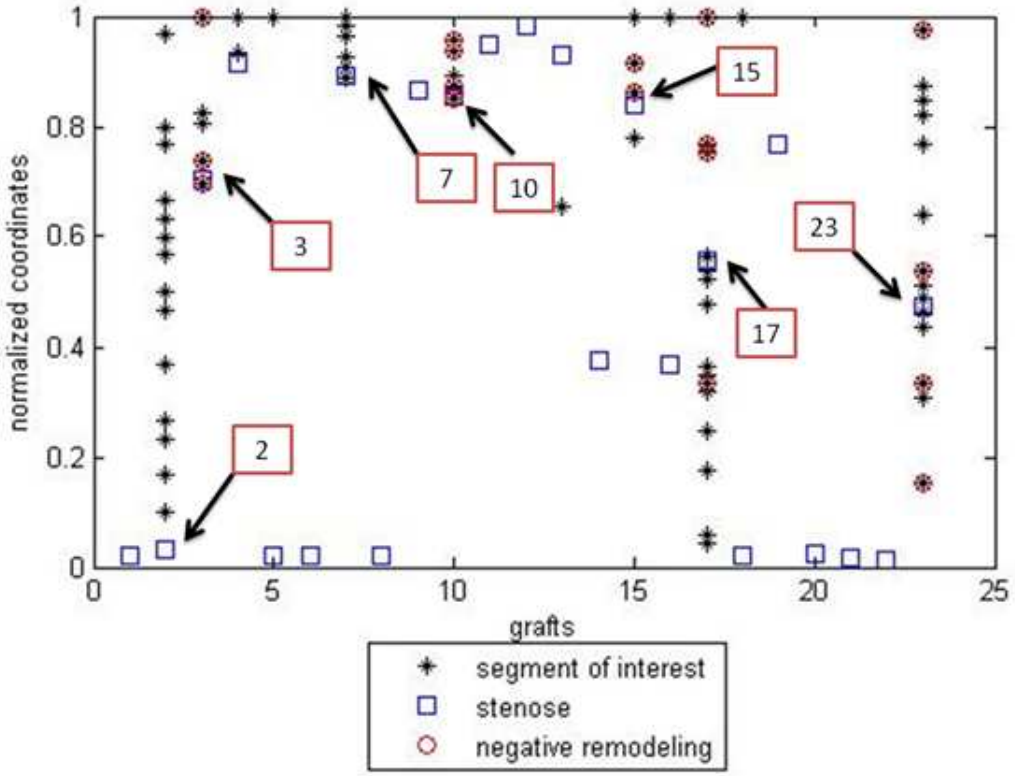

Figure 5.8: Predictive model of negative remodeling for the different vein grafts

The blue square denotes the position of the local stenose. We notice that 10 out of 23 have the most pronounced local stenose near the outlet (9 out of 10) or possible the outlet (1 out of 10). We should exclude these from our analysis since they may have obeyed very different mechanism than the others.

10 vein grafts have segments that belong to cluster 2. We eliminate vein graft 5 and 16 that have only segments of cluster 2 next to the inlet. 6 out of these 8 vein graft present negative remodeling, i.e. the worst local stenose gets more

pronounced after month 6 than one month.

For 6 of the vein grafts out of 8, we can see a good prediction of our model at the local stenose.

Out of those, 7 grafts present in the cluster of interest with the best non linear model, 5 of them presents a "failure", which is what we consider as negative remodeling (figure 5.8). The model presents an accurate prediction for 3 vein grafts (#3, #10, and #15). While the vein graft #17 is strongly missed by the model, the #23 is missed by only a couple of centimeters.

To check if we can improve the performance of the model, we are going now to consider the residence time of particles as an additional possible feature that can add information.

Thanks to Fluent and how it handles multiphase flows, the average particle residence time and its standard deviation were variables derived from the CFD simulations. The time of a particle is recorded at the entrance of each segment of the vein grafts. In our program, we read and compute the residence time of all particles for all segments. By doing this, we obtain the distribution of residence time for any segment. To give a more compact set of information, we consider the average residence time of particles and the standard deviation as a significant description of the distribution.

Later on we may look at the deviation of these distributions from a normal law: this might be interpreted as local flow disturbance that are away from Poiseuille. The following figure (figure 5.9) shows the mean residence time depending on the standard deviation where a k-mean clustering have been performed in order to classify the vein graft segments.

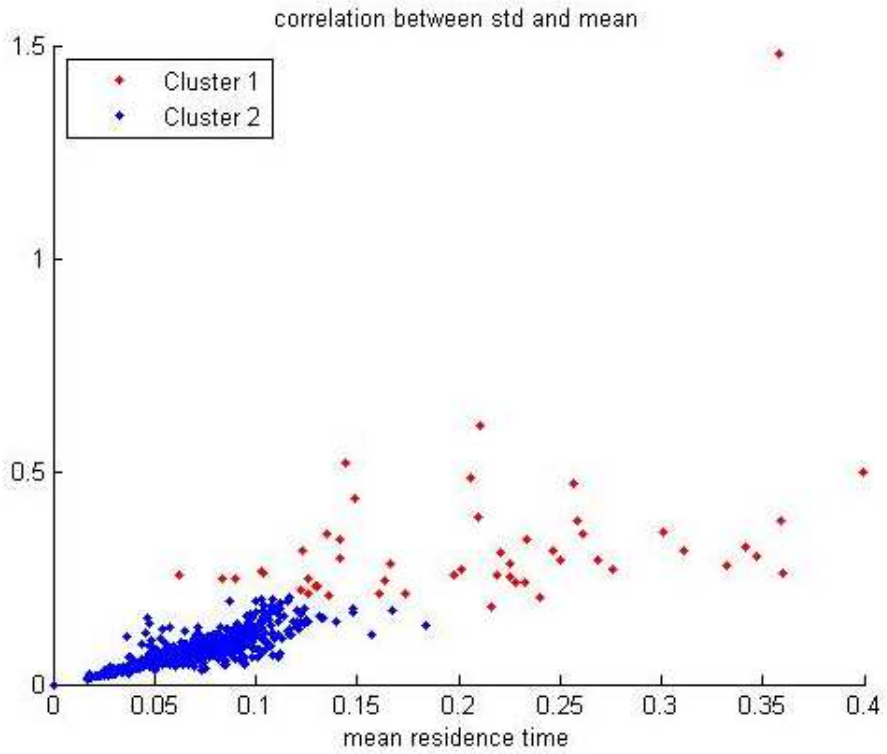

Figure 5.9: Average particle residence time as a function of standard deviation of particle residence time

Some studies have focused on the flow residence time, in particular the particle residence time, in thrombus formation, especially near the arterial walls. It is in this perspective that we add the mean residence time and the standard deviation of particle residence time to our statistical analysis.

5. Taking into account the mean residence time (MRT) for early stage makes no difference.

Linear	Non linear with WSS	Non linear with WSS and MRT
$R = 0.5303$	$R = 0.5325$	$R = 0.5392$

Table 5.5: Considering early remodeling, values of R for different non linear models, the first one takes into account only WSS while the second regards WSS and the average particle residence time

6. For transient plasticity with fitting based on WSS and mean residence time of particles:

Linear	Non linear	Non linear Cluster 1	Non linear Cluster 2	Non linear Cluster 3
$R = 0.4253$	$R = 0.4354$	$R = 0.9377$	$R = 0.7733$	$R = 0.3792$
# elements = 663	# elements = 663	# elements in cluster = 8	# elements in cluster = 69	# elements in cluster = 586

Table 5.6: Considering transient remodeling with fitting model based on WSS and average particle residence time, values of R for the 3 clusters of different sizes

By using a fitting based on WSS and mean residence time of particles, we see that the results do not improve or change significantly the coefficient of correlation in comparison with our first run 3 where we used a fitting based on WSS and the number of trapped particles. We conclude that at this coarse level of detail of our statistical analysis, particle residence time and particle deposition rate play a similar role.

5.4.3 Conclusion

On the manipulation with transient plasticity, the vein grafts showing stenoses close to their entrances were excluded in the analysis. Therefore 14 grafts were part of

the clustering procedure. Our model gave results for 7 vein grafts. 8 additional vein grafts with negative remodeling did not make it to this cluster. 3 out of these 8 vein graft left out had significant negative remodeling.

In conclusion, we can say that our method shows good prediction on the vein grafts where a failure occurs for those vein graft that automatically selected by the cluster analysis. It can detect 3 out of 5 vein grafts.

More analysis needs to be done. Our main result is still this apparently new methodology that has shown some potential rather than a definitive true indicator of vein graft failure. We should now add one by one any measure either from in silico simulation such as Navier-Stokes or lab exam, to improve or very preliminary indicator of vein graft failure

Part V

Dissertation Review

Chapter 6

Conclusion and Future Work

The primary goal of this dissertation was to develop an efficient computational framework for hemodynamic simulation. This has been accomplished with the development of a set of techniques which allow to reconstruct, to edit, to analyze and to discretize 3D models of vasculature from CT and MRI images and successively to post-process the results of CFD analysis. We were able to streamline efficiently hemodynamic simulations for main arteries (carotid artery and femoral artery) in order to produce database for clinical studies. We provided some good confidence estimate on numerical results in part I. We extended the state of the art of clinical study by including motion and particles analysis. With the advances in numerical method and the progress in technology, CFD has been increasingly used as a simulation tool for blood flows. However, there exists a gap between the advances in technology and the actual application into the clinical world. From the literature cited in the first chapter about the techniques and methods used so far, we have

identified several sensitive issues in area of expertise. Indeed, the methods used are not yet able to significantly represent the physiological reality. The development of imaging techniques is very important and facilitates the acquisition of morphological and functional data. Mathematical models must be able to handle the resolution performances, in terms of space and time, provided by the new imaging techniques. Therefore, the information contained in medical imaging is the working basis for realistic and patient-specific calculations obtained by CFD. The clinical motivation for this work is that accurate hemodynamic simulation may lead to better understanding of the development and progression of atherosclerosis than the current diagnostic techniques that are based solely on the degree of stenosis. In this chapter, we present the conclusion of our work. In section 6.1 the conclusion derived from the accuracy assessment study on the carotid artery bifurcation is presented. The conclusion from the dynamic blood flow simulation is presented in section 6.2. This is followed up in section 6.3 by the conclusion from the vein graft study. Finally, in section 6.4 are detailed the potential for further studies in the area.

6.1 Accuracy Assessment Studies

In chapter 3, we built a workflow for hemodynamic simulations where we had to assess verification and validation. We observed that uncertainties can occur at every step of the workflow, such as medical imaging acquisition, image segmentation, 3D reconstruction, and definition of the boundary conditions. We reconstructed several

carotid artery bifurcations from patients' medical images. We implemented and defined the boundary conditions for the CFD simulations.

Our original contribution in this chapter resides mainly in carotid artery bifurcation initialization and reconstruction approach as well as the establishment of a verification protocol based on higher interpolation. We have observed that our method converge with a nearby second order convergence, which is in agreement with the expectation for the Finite Volume element we chose. In our convergence analysis the L2 norm relative error was varying from 3% to 9%. Nevertheless, local errors on the wall shear stress appeared to be much larger. We have shown in this chapter that a good hemodynamic simulation does not only depend on a good model but also on accurate boundary conditions. The workflow on hemodynamic simulation requires the expertise of different areas.

6.2 Dynamic Blood Flow Simulation Studies

As discussed in chapter 4, the ability to simulate complex structures and their interactions, and the ability to represent the reality in a sufficiently precise manner are the two main challenges to simulate the human vascular system. For instance, the displacement of the vessel wall should determine the conditions for the flow. This argument leads us to think that we should not make mistakes on the position of the wall at every moment of the cardiac cycle. Indeed, in our first analysis, depending on the length of the femoral artery section, we observed 11% to 16% of change on the shear stress computation between the external wall and internal wall, which was

much larger than the percentage of the relative wall motion. A sequence of image segmentation techniques has been employed for the extraction of the wall motion, while we implemented an immersed boundary method based on the L2 penalty method for the computation of the WSS.

In the second part, we investigated the influence of the bending motion of the knee on the computation of the WSS. Our contributions reside in the implementation of a User Defined Function that handles the appropriate boundary conditions as well as the bending motion by remeshing the model at every time step. We noticed that the relative error between a slightly bended pipe and a moving pipe was quite significant, reaching 0.73 in some cases.

We have demonstrated in this chapter that the motion of the human body should be taking into account in hemodynamic simulation and that simulations should be dependent on time.

6.3 Vein Graft Study

In part 4 IV, an original approach for CFD simulation with particle tracking employed on vein grafts was given. First, we coded a UDF in order to inject around 10000 particles that were tracked at every time step of the simulation. Then we ran an extensive set of simulations for the patient data (23 patients at 3 different clinical follow-up examinations: 1 week, 1 month and 6 months) provided by Dr. Berceli from the Department of Surgery at the University of Florida. Besides the initialization of the simulations and the definition of the proper boundary conditions,

our contributions consist of analyzing the post-processing data. Numerous studies have demonstrated the correlation between WSS and endovascular diseases. In this work, our primary goal was to investigate if the particle deposition rate could provide additional information to those studies. We developed non linear models to fit the data set based on WSS only, and on WSS and number of trapped particles. A k-mean clustering method was used to identify the local character of remodeling. Our method gives a good prediction on the vein grafts where a "failure" occurs for those vein grafts that were automatically selected by the cluster analysis. It was able to detect 3 out of 5 vein grafts.

6.4 Future Work

We presented a workflow in hemodynamic simulation where we observed the importance of the body motion on the WSS computation. In a computational surgery context, the expertise of different fields is necessary to model and simulate real biomechanics. For instance, arterial wall motion is difficult to predict in the absence of an extensive study of the tissue distribution and its material properties. A better knowledge on a medical point of view would be beneficial for this work. We saw in the vein graft study that it happens that, during the procedure, surgeons used several vein grafts, instead of just one graft, to reconstruct the femoral artery, which could lead to uncertainties.

Several improvements and further possibilities are offered on the basis on the present work. The study of the bending motion could be extended of a 3D model. Indeed,

our remeshing method can be used in 3D as long as the wall motion is well defined. In the vein graft study, a parameter that needs to be investigated is the near-wall particle residence time. At last, a combination of the moving mesh method and particles tracking could be a good approach to simulation blood flows and understand the development and progression of atherosclerosis.

Bibliography

[1] S.A. Al-Nassri and T. Unny. Developing Laminar Flow in the Inlet Length of a Smooth Pipe. *Applied Scientific Research*, 36:313–332, 1981.

[2] American Institute of Aeronautics and Astronautics. *Guide for the Verification and Validation of Computational Fluid Dynamics Simulations*, 1998.

[3] P. Angot, C.H. Bruneau, and P. Fabrie. A Penalisation Method to Take into Account Obstacles in Viscous Flows. *Numerische Mathematik*, 81:497–520, 1999.

[4] ANSYS FLUENT 12.0. *Theory Guide*, April 2009.

[5] ANSYS FLUENT 12.0. *UDF Manual*, 2009.

[6] ANSYS Inc. ANSYS. `http://www.ansys.com`, 2013.

[7] Luca Antiga. vmtk.org. `http://www.vmtk.org/`, 2012.

[8] Bartleby.com. Gray's anatomy of the human body. `http://www.bartleby.com/107/`, 2000.

[9] C. Basciano, C. Kleinstreuer, S. Hyun, and E. A. Finol. A Relation Between Near-Wall Particle-Hemodynamics and Onset of Thrombus Formation in Abdominal Aortic Aneurysms. *Annals of Biomedical Engineering*, 39(7):2010–2026, 2011.

[10] C. Bekdemir, L.M.T. Somers, and L.P.H. de Goey. First Application of the Flamelet Generated Manifold (FGM) Approach to the Simulation of an Igniting Diesel Spray. *Int. Multidim. Engine Modeling Users Group Meeting*, 2009.

[11] Bharat Bhushan, Ravindra Kumar, and Shruti Mishra. Analysis of Pressure and Velocity in Coal Combustion System using DPM Method in FLUENT Software. *International Journal of Engineering Research and Applications (IJERA)*, 2:2885–2889, May-June 2012.

[12] Steven N. Blair, Harold W. Kohl, Carolyn E. Barlow, and et al. Changes in Physical Fitness and All-Cause Mortality: A Prospective Study of Healthy and Unhealthy Men. *JAMA*, 273(14):1093–8, April 1995.

[13] Piero O. Bonetti, Lilach O. Lerman, and Amir Lerman. Endothelial Dysfunction. A Marker of Atherosclerotic Risk. *Arterioscler Thromb Vasc Biol.*, 23:168–175, 2003.

[14] J.R. Buchanan, C. Kleinstreuer, S. Hyun, and G.A. Truskey. Hemodynamics Simulation and Identification of Susceptible Sites of Atherosclerotic Lesion Formation in a Model Abdominal Aorta. *Journal of Biomechanics*, 36:1185–1196, 2003.

[15] Jerrold T. Bushberg. *The Essential Physics of Medical Imaging*. Lippincott Williams & Wilkins, 2011.

[16] Harpal S. Buttar, Timao Li, and Nivedita Ravi. Prevention of cardiovascular diseases: Role of exercise, dietary interventions, obesity and smoking cessation. *Exp Clin Cardiol*, 10(4):229–249, 2005.

[17] C.P. Chang, D. Parker, and C. Taylor. Quantification of Wall Shear Stress in Large Blood Vessels using Lagrangian Interpolation Functions with Cine Phase-Contrast Magnetic Resonance Imaging. *Annals of Biomedical Engineering*, 30:1020–1032, 2002.

[18] Namrata Chhabra. Endothelial dysfunction - A predictor of atherosclerosis. *Internet Journal of Medical Update*, 4(1), January 2009.

[19] Gilwoo Choi, Christopher P. Cheng, Nathan M. Wilson, and Charles A. Taylor. Methods for Quantifying Three-Dimensional Deformation of Arteries due to Pulsatile and Nonpulsatile Forces: Implications for the Design of Stents and Stent Grafts. *Annals of Biomedical Engineering*, 37(1):14–33, 2009.

[20] S. Cloete, S. Johansen, M. Braun, Popof B., and S. Amini. Evaluation of a Lagrangian Discrete Phase Modeling Approach for Resolving Cluster Formation in CFB Risers. In *CSIRO*, 2010.

[21] R.L. Courant. Variational Methods for the Solution of Problems of Equilibrium and Vibration. *Bulletin of the American Mathematical Society*, 49:1–23, 1943.

[22] Paolo Crosettoa, Philippe Reymond, Simone Deparis, Dimitrios Kontaxakis, Nikolaos Stergiopulos, and Alfio Quarteroni. Fluid-Structure Interaction Simulation of Aortic Blood Flow. *Computers & Fluids*, 43:46–57, 2011.

[23] R.B. Darlington. *Regression and Linear Models*. New York: McGraw-Hill, 1990.

[24] Peter F. Davies. Flow-Mediated Endothelial Mechanotransduction. *Physiol Rev.*, 75(3):519–560, July 1995.

[25] Jean Davignon and Peter Ganz. Role of Endothelial Dysfunction in Atherosclerosis. *Circulation*, 109:III–27 – III–32, 2004.

[26] M. E. DeBakey, G. M. Lawrie, and D. H. Glaeser. Patterns of Atherosclerosis and their Surgical Significance. *Ann Surg*, 201(2):115–31, 1985.

[27] J.J. Derksen. The Lattice-Boltzmann Method for Multiphase Fluid Flow Simulations and Euler-Lagrange Large-Eddy Simulations. *Multiphase Reacting Flows: Modelling and Simulation, CISM International Centre for Mechanical Sciences*, 492:181–228, 2007.

[28] C. Ross Ethier and Craig A. Simmons. *Introductory Biomechanics, From Cells to Organisms*. Cambridge University Press, 2007.

[29] Ulrich Förstermann and Thomas Münzel. Endothelial Nitric Oxide Synthase in Vascular Disease. From Marvel to Menace. *Circulation*, 113:1708–1714, 2006.

[30] C.A. Felippa, K.C. Park, and C. Farhat. Partitioned analysis of coupled mechanical systems. *Comp. Method. Appl. Mech. Eng.*, 190:3247–3270, 2001.

[31] Chessy M. Fernandez, Darin R. Goldman, Zhihua Jiang, C. Keith Ozaki, Roger Tran-Son-Tay, and Scott A. Berceli. Impact of Shear Stress on Early Vein Graft Remodeling: A Biomechanical Analysis. *Annals of Biomedical Engineering*, 32(11):1484–1493, November 2004.

[32] Nenad Filipovic, Srboljub Mijailovic, Akira Tsuda, and Milos Kojic. An Implicit Algorithm within the Arbitrary Lagrangian-Eulerian Formulation for Solving Incompressible Fluid Flow with Large Boundary Motions. *Computer Methods in Applied Mechanics and Engineering*, 195:6347–6361, 2006.

[33] Rodney O. Fox. Large-Eddy-Simulation Tools for Multiphase Flows. *Annual Review of Fluid Mechanics*, 44:47–76, 2012.

[34] Stuart Ira Fox. *Human Physiology*. W.C. Brown, 1998.

[35] Andreas O. Frank, Peter W. Walsh, and James E. Moore Jr. Computational Fluid Dynamics and Stent Design. *Artificial Organs*, 26(7):614–621, 2002.

[36] Dai Fukumura, Takeshi Gohongi, and Ananth Kadambi. Predominant role of endothelial nitric oxide synthase in vascular endothelial growth factor-induced angiogenesis and vascular permeability. *PNAS*, 98(5):2604–2609, February 27 2001.

[37] M. Garbey and F. Pacull. A Versatile Incompressible Navier Stokes Solver for Blood Flow Application. *Int. J. for Numerical Methods in Fluids*, 54:473–496, 2007.

[38] F.P. Glor, Q. Long, A.D. Hugues, A.D. Augst, B. Ariff, S.A. McG Thom, P.R. Verdonck, and X.Y. Xu. Reproducibility of Magnetic Resonance Image-based Computational Fluid Dynamics Prediction of Carotid Bifurcation Flow. *Annals of Biomedical Engineering*, 31:142–151, 2003.

[39] Harald C. Groen, Lenette Simons, Quirijn J.A. van den Bouwhuijsen, E. Marielle H. Bosboom, and et al. MRI-based Quantification of Outflow Boundary Conditions for Computational Fluid Dynamics of Stenosed Human Carotid Arteries. *Journal of Biomechanics*, 43:2332–2338, 2010.

[40] C. W. Hirt and B. D. Nichols. Volume of Fluid (VOF) Method for the Dynamics of Free Boundaries. *J. Comput. Phys.*, 39:201–225, 1981.

[41] G. Hou, J. Wang, and A. Layton. Numerical Methods for Fluid-Structure Interaction - A Review. *Commun. Comput., Phys.*, 12:337–377, 2012.

[42] Minki Hwang, Scott A. Berceli, Marc Garbey, Nam Ho Kim, and Roger Tran-Son-Tay. The dynamics of vein graft remodeling induced by hemodynamic forces: a mathematical model. *Biomech Model Mechanobiol*, 11:411–423, 2012.

[43] Borja Ibañez, Juan J. Badimon, and Mario J. Garcia. Diagnosis of Atherosclerosis by Imaging. *Am J Med*, 122:S15–S25, 2009.

[44] Mamoru Ishii. *Thermo-Fluid Dynamics of Two-phase Flow*. Eyrolles, 1975.

[45] Absaar Ul Jabbar, Rana Usman Ali, Khalid Parvez, and Umar H. K. Niazi. Three-Dimensional Numerical Analysis of Pulsatile Blood Flow around Different Plaque Shapes in Human Carotid Artery. *International Journal of Bioscience, Biochemistry and Bioinformatics*, 2(5):305–308, 2012.

[46] F. Kabinejadian and D. N. Ghista. Compliant model of a coupled sequential coronary arterial bypass graft: Effects of vessel wall elasticity and non-Newtonian rheology on blood flow regime and hemodynamic parameters distribution. *Medical Engineering & Physics*, 34:860–872, September 2012.

[47] C. Kassiotis, A. Ibrahimbegovic, and H. Matthies. Partitioned solution to fluid-structure interaction problem in application to free-surface flows. *European Journal of Mechanics - B/Fluids*, 29:510–521, 2010.

[48] Seinosuke Kawashima and Mitsuhiro Yokoyama. Dysfunction of Endothelial Nitric Oxide Synthase and Atherosclerosis. *Arterioscler Thromb Vasc Biol*, 24:998–1005, 2004.

[49] Sameer Ali Khan, A.V. Deshpande, and A. K. Tak. Heat And Fluid Flow Analysis Of Argon- Ferrocene Mixture In A High Temperature Reactor Used For Producing Carbon Nanotubes. *International Journal of Engineering Research and Applications*, 3:1011–1016, 2013.

[50] Young-Ho Kim, Jong-Eun Kim, Yasushi Ito, Alan M. Shih, Brigitta Brott, and Andreas Anayiotos. Hemodynamic Analysis of a Compliant Femoral Artery Bifurcation Model using a Fluid Structure Interaction Framework. *Ann Biomed Eng.*, 36(11):1753–63, 2008.

[51] Christoph Kloss, Christoph Goniva, Georg Aichinger, and Stefan Pirker. Comprehensive DEM-DPM-CFD Simulations - Model Synthesis, Experimental Validation and Scalability. In *Proceedings Seventh International Conference on CFD in the Minerals and Process Industries, CSIRO, Melbourne, Australia*, 2009.

[52] Kozic, S. Ristic, M. Puharic, and B. Katavic. Comparison of Euler-Euler and Euler-Lagrange Approach in Numerical Simulation of Multiphase Flow in Ventilation Mill-air Mixing Duct. In *Proceedings Third Serbian (28th Yu) Congress on Theoretical and Applied Mechanics, Vlasina lake, Serbia*, 2011.

[53] David N. Ku. Blood Flow in Arteries. *Annu. Rev. Fluid Mech.*, 29:399–434, 1997.

[54] David N. Ku, Don P. Giddens, Christopher K. Zarins, and Seymour Glagov. Pulsatile Flow and Atherosclerosis in the Human Carotid Bifurcation Positive Correlation between Plaque Location and Low and Oscillating Shear Stress. *Arterioscler Thromb Vasc Biol.*, 5:293–302, 1985.

[55] J.R. Laird. Limitations of Percutaneous Transluminal Angioplasty and Stenting for the Treatment of Disease of the Superficial Femoral and Popliteal Arteries. *Journal of Endovascular Therapy*, 13(Supplement II):II–30 – II–40, 2006.

[56] Thomas F. Lüscher and Matthias Barton. Biology of the Endothelium. *Clin. Cardiol.*, 20:II–3 – II–10, 1997.

[57] Huige Li and Ulrich Förstermann. Prevention of Atherosclerosis by Interference with the Vascular Nitric Oxide System. *Current Pharmaceutical Design*, 15(27), 2009.

[58] Zhi-Yong Li and Jonathan H. Gillard. Simulation of the Interaction between Blood Flow and Atherosclerotic Plaque. *EMBS*, pages 1699–1702, 2007.

[59] Peter Libby, Paul M. Ridker, and Attilio Maseri. Inflammation and Atherosclerosis. *Circulation*, 105:1135–1143, 2002.

[60] Y. Liu, A. Nagaraj, A. Hamilton, K. Liu, LiJing Yan, D.D. McPherson, and K.B. Chandran. Alteration in Fluid Mechanics in Femoral Arteries with Atheroma Development. *Engineering in Medicine and Biology*, 2:1287–1288, 2002.

[61] Joseph Loscalzo. Vascular Matrix and Vein Graft Failure. Is the Message in the Medium? *Circulation*, 101:221–223, 2000.

[62] A.B. Lumsden and et al. Peripheral Arterial Occlusive Disease: Magnetic Resonance Imaging and the Role of Aggressive Medical Management. *World J Surg*, 31:695–704, 2007.

[63] Mikko Manninen and Veikko Taivassalo. On the mixture model for multiphase flow. *VTT publications 288*, pages 1–67, 1996.

[64] Dheeraj Mehta, Mohammed B. Izzat, Alan J. Bryan, and Gianni D. Angelini. Towards the prevention of vein graft failure. *International Journal of Cardiology*, 62:S55–S63, 1997.

[65] C. Michler, S.J. Hulshoff, E.H. van Brummelen, and R. de Borst. A Monolithic Approach to Fluid-Structure Interaction. *Computers & Fluids*, 33(5-6):839–848, March 2003.

[66] Rajat Mittal and Gianluca Iaccarino. Immersed Boundary Methods. *Annu. Rev. Fluid Mech.*, 37:239–61, 2005.

[67] Gregory L. Moneta and John M. Porter. Repair and Follow-up of Leg Arteries With Vein Grafts. *WJM*, 159(6), December 1993.

[68] J. A. Moore, D. A. Steinman, D. W. Holdworth, and C. R. Ethier. Accuracy of Computational Hemodynamics in Complex Arterial Geometries Reconstructed from Magnetic Resonance Imaging. *Annals of Biomedical Engineering*, 27:32–41, 1999.

[69] Yoichiro Mori and Charles S. Peskin. Implicit Second-Order Immersed Boundary Methods with Boundary Mass. *Comput. Methods Appl. Mech. Engrg.*, 197:2049–2067, 2008.

[70] Jonathan Myers. Exercise and Cardiovascular Health. *Circulation*, 107:E2–E5, 2003.

[71] National Heart, Lung, and Blood Institute. What Is Atherosclerosis. `http://www.nhlbi.nih.gov/health/health-topics/topics/atherosclerosis/`, 2011.

[72] National Institutes of Health. ImageJ. `http://rsb.info.nih.gov/ij/`, 2013.

[73] William L. Oberkampf and Timothy G. Trucano. Verification and Validation in Computational Fluid Dynamics. *Aerospace Sciences*, 38:209–272, 2002.

[74] D.R. Owen, A.C. Lindsay, R.P. Choudhury, and Z.A. Fayad. Imaging of atherosclerosis. *Annu Rev Med*, 62:25–40, 2011.

[75] Christopher D. Owens, Karen J. Ho, and Michael S. Conte. Lower extremity vein graft failure: a translational approach. *Vascular Medicine*, 13:63–74, 2008.

[76] T.G. Papaioannou, E.N. Karatzis, M. Vavuranakis, J.P. Lekakis, and C. Stefanadis. Assessment of vascular wall shear stress and implications for atherosclerotic disease. *International Journal of Cardiology*, 113:12–18, 2006.

[77] Theodoros G. Papaioannou and Christodoulos Stefanadis. Vascular Wall Shear Stress: Basic Principles and Methods. *Hellenic J Cardiol*, 46:9–15, 2005.

[78] Vijayajothi Paramasivam, Kanesan Muthusamy, and Mohammed Rafiq Abdul Kadir. Application of Computational Fluid Dynamics in Assessing the Hemodynamics in Abdominal Aortic Aneurysms. *IEEE EMBS Conference on Biomedical Engineering and Sciences*, 1:32–37, 2010.

[79] R.R. Pate, M. Pratt, S.N. Blair, and et al. Physical Activity and Public Health: A Recommendation from the Centers for Disease Control and Prevention and the American College of Sports Medicine. *JAMA*, 273:402–7, 1995.

[80] T.J. Pedley. *The Fluid Mechanics of Large Blood Vessels*. Cambridge University Press, 1980.

[81] Ian Owens Pericevic and Moji Moatamedi. Application of the penalty coupling method for the analysis of blood vessels. *Revue Européenne de Mécanique Numérique (European Journal of Computational Mechanics)*, 16(3-4):537–548, 2007.

[82] C.S. Peskin. The Immersed Boundary Method. *Acta Numerica*, 11:1–39, 2002.

[83] Dzung L. Pham, Chenyang Xu, and Jerry L. Prince. Current Methods in Medical Image Segmentation. *Annu. Rev. Biomed. Eng.*, 2:315–37, 2002.

[84] V. L. Rayz, L. Boussel, L. Ge, J. R. Leach, A. J. Martin, M. T. Lawton, C. McCulloch, and D. Saloner. Flow Residence Time and Regions of Intraluminal Thrombus Deposition in Intracranial Aneurysms. *Annals of Biomedical Engineering*, 38(10):3058–3069, October 2010.

[85] L.F. Richardson and J.A. Gaunt. The Deferred Approach to the Limit. *Transactions of the Royal Society of London, Series A: Mathematical and Physical Sciences*, 226:299–361, 1927.

[86] P.J. Roache. Quantification of Uncertainty in Computational Fluid Dynamics. *Annu. Rev. Fluid. Mech.*, 29:123–60, 1997.

[87] Marco Roffi, Debabrata Mukherjee, and Daniel G. Clair. Carotid artery stenting vs. endarterectomy. *European Heart Journal*, 30:2693–2704, 2009.

[88] R. Ross. Atherosclerosis - An Inflammatory Disease. *The New England Journal of Medicine*, 340:115–126, 1999.

[89] S. Schlesinger. Terminology for model credibility. *Simulation*, 32(3):103–4, 1979.

[90] Robert S. Schwartz. Pathophysiology of Restenosis: Interaction of Thrombosis, Hyperplasia, and/or Remodeling. *Am J Cardiol*, 81(7A):14E–17E, 1998.

[91] Akram M. Shaaban and André J. Duerinckx. Wall Shear Stress and Early Atherosclerosis: A Review. *AJR*, 174(6):1657–1665, 2000.

[92] A. Sokolichin and G. Eigenberger. Dynamic numerical simulation of gas-liquid two-phase flows EulerEuler versus EulerLagrange. *Chemical Engineering Science*, 52:611–626, 1997.

[93] Detlef Stolten and Bernd Emonts. *Fuel Cell Science and Engineering: Materials, Processes, Systems and Technology*, volume 1. John Wiley & Sons, May 21 2012.

[94] Charles A. Taylor, Thomas J.R. Hughes, and Christopher K. Zarins. Effect of Exercise on Hemodynamic Conditions in the Abdominal Aorta. *J Vasc Surg*, 29:1077–89, 1999.

[95] Richard Taylor. Interpretation of the correlation coefficient: a basic Review. *JDMS*, 1:35–39, 1990.

[96] J.B. Thomas, J.S. Milner, B.K. Rutt, and D.A. Steinman. Reproductibility of Image-Based Computational Fluid Dynamics Models of the Human Carotid Bifurcation. *Annals of Biomedical Engineering*, 31:132–141, 2003.

[97] David E. Thompson. Verification, Validation, and Solution Quality in Computational Physics: CFD Methods applied to Ice Sheet Physics. Technical report, NASA/TM-2005-213453, NASA, Ames Research Center, 2005.

[98] James N. Topper, Jiexing Cai, Dean Falb, Michael A. Gimbrone, and JR. Identification of vascular endothelial genes differentially responsive to fluid mechanical stimuli: Cyclooxygenase-2, manganese superoxide dismutase, and endothelial cell nitric oxide synthase are selectively up-regulated by steady laminar shear stress. *Proc. Natl. Acad. Sci.*, 93:10417–10422, 1996.

[99] Oren Traub and Bradford C. Berk. Laminar Shear Stress: Mechanisms by Which Endothelial Cells Transduce an Atheroprotective Force. *Arterioscler Thromb Vasc Biol.*, 18:677–685, 1998.

[100] VascularWeb. Peripheral Artery Disease (PAD). `http://www.vascularweb.org/Pages/default.aspx`, 2004.

[101] B.S. Verma and I.K. Indrajit. Advent of Digital Radiography: Part 1. *Indian J Radiol Imaging.*, 18(2):113–116, 2008.

[102] E.M. Willigendael, J.A.W. Teijink, M.L. Bartelink, and et al. Smoking and the patency of lower extremity bypass grafts : A meta-analysis. *J Vasc Surg*, 42:67–74, 2005.

[103] J.R. Womersley. Method for the Calculation of Velocity, Rate of Flow and Viscous Drag in Arteries when the Pressure Gradient is known. *J. Physiol.*, 127:553–563, 1955.

[104] C. Wood, A. J. Gil, O. Hassan, and J. Bonet. A Partitioned Coupling Approach for Dynamic Fluid-Structure Interaction with Applications to Biological Membranes. *Int. J. Numer. Meth. Fluids*, 57:555–581, 2008.

[105] World Health Organization. Cardiovascular disease. `http://www.who.int/cardiovascular\_diseases/en/`, 2013.

[106] H.F. Younis, M.R. Kaazempur-Mofrad, R.C. Chan, and et al. Hemodynamics and Wall Mechanics in Human Carotid Bifurcation and its Consequences for Atherogenesis: Investigation of Inter-Individual Variation. *Biomechan Model Mechanobiol*, 3:17–32, 2004.

[107] Duan Z. Zhang, W. Brian VanderHeyden, Qisu Zou, and Nely T. Padial-Collins. Pressure calculations in disperse and continuous multiphase flows. *International Journal of Multiphase Flow*, 33:86–100, 2007.

[108] S.Z. Zhao, X.Y. Xu, A.D. Hughes, S.A. Thom, A.V. Stanton, B. Ariff, and Q. Long. Blood Flow and Vessel Mechanics in a Physiologically Realistic Model of a Human Carotid Arterial Bifurcation. *Journal of Biomechanics*, 33:975–984, 2000.